Pentamethylcyclopentadienyl Aminoborole Complexes of Hafnium

Thesis by Andrew F. Kiely

In Partial Fufillment of the
Requirements for the Degree of
Doctor of Philosophy

Division of Chemistry
and Chemical Engineering

California Institute of Technology
Pasadena, California

1997
(Submitted August 20, 1996)

For My Parents

Acknowledgments

First and most importantly, I would like to thank John Bercaw for the support, encouragement, and opportunities that he has given me over the course of my studies at Caltech. I have been very fortunate to have been able to learn chemistry from someone who is a fine and generous person as well as a great scientist, and I am very grateful to him.

I am also grateful to Bill Schaefer, Larry Henling, and Mike Day for performing all the crystallographic work that is reported in this thesis. I appreciate all their good humor and patience despite my (occasional) impatience and (more occasional) ignorance. I've really enjoyed hiking with Bill and playing outfield with Larry as well.

The students and post-docs in the Bercaw group have been friends as well as coworkers. Over the years, people in the Bercaw group have been generous with their time, advice and friendship. When I was getting started in the group, Donny Cotter, Bryan Coughlin, and Roger Quan were never too busy to answer my questions or to set me straight. I'm especially grateful to Roger, who helped me to learn vacuum line techniques when I was starting on the aminoborole project. Eric Kelson, the Bercaw group guru of things electrochemical, helped me with the E-chem measurements reported in chapter 1. Bob Blake endured the joys and sorrows of Ru chemistry with me, and has a great talent at explaining things. I always enjoyed working with Bob, who, along with Roger and Gerrit Luinstra, contributed to my education in many ways, not least by showing me that there are genres of pop music that I just don't appreciate. Sharad Hajela is a founding member of the Bercaw mafia, who, when he makes an offer you can't refuse, means the Ath. Tim Herzog has been a terrific classmate. He's a great scientist and has been an incredible source of information about Z-N chemistry. I think I've had more useful discussions with him than with any other member of the group. He's also a supportive coworker (meaning he mixes a great margarita) and we have shared many of the high and low points of grad school together. Mike Abrams is a man who appreciates the finer things of life (Diver Cocktails™), was a great linemate, and is as generous as he is discreet (he never complained when I neglected to wait at the top of the ridge for him, and he even retrieved my hat for me coming down that *@#% pass). Shannon Stahl has fine scientific judgment and I've had interesting conversations on many matters with him, but sometimes he is just too optimistic (he's a Cubs fan).

Susan Brookhart was a great coworker who always had a ready wit and a ready laugh. Cory Nelson and Antek Wong-Foy, when they weren't turning triple plays, were my coworkers on the ABo project and always kept me on my toes scientifically. Steve Miller was a great source of information about preparing group IV Cp complexes. The first years, Jeff Yoder, Deanna Zubris, Chris Brandow, and Paul Chirik, couldn't pick a Christmas tree to save their lives but it has been great getting to know them.

The post-docs in the Bercaw group have also been very supportive and friendly. Guy Bazan started the ABo project, and I've had many helpful conversations with him. David Lyon set a remarkable pace in Hogball. Jon Mitchell was a great coworker and a great teammate at trivia quizzes. His generosity and friendliness are exceeded only by his sartorial flair. Eugene Mueller impressed me with his knowledge and how quickly he learned organometallic chemistry. David Antonelli was a great synthetic organometallic chemist and gave me much good advice. Jim Gilchrist was an amazing scientist and an amazing character. Antonio Pastor was kind enough to give me some of his zirconium compounds for spectroscopic characterization. Matt Holtcamp and Cyrille Loeber have been fun working with and playing outfield with. Dario Veghini, besides being a babe magnet, has invited me to wonderful dinners at his apartment.

I would also like to thank several people outside the Bercaw group. Teri Longin provided a cheerfully bitter perspective that I always thoroughly appreciated. Chris Kenyon and Michael Murray (along with Bob) provided me with opportunities to make a fool of myself. Bill Connick has been a great roommate and along with Eva Birnbaum and Harry Gray, helped me understand more about spectroscopy.

Abstract

The tricyclophosphate ligand, $(P_3O_9)^{3-}$, was investigated as an oxidation resistant ligand for ruthenium chemistry. The silver salt of tricyclophosphate, $Ag_3(P_3O_9).H_2O$, was found to be a useful synthon in the preparation of organic soluble tricyclophosphate salts. The complex $[(P_3O_9)Ru(C_6H_6)]^-$ was prepared and characterized. In water, it was found that the tricyclophosphate ligand dissociated from the $[(C_6H_6)Ru]^{2+}$ dication. Cyclic voltammatry in acetonitrile shows only a small irreversible oxidation at 0.95 V (Vs ferrocene). The rhenium carbonyl complex $[(P_3O_9)Re(CO)_3]^{2-}$ was also investigated as a precursor to high valent tricyclophosphate rhenium complexes. Based on these results as well as related work by Klemperer and coworkers, it is concluded that the tricyclophosphate ligand is an exceptionally hard one that binds only weakly to transition metals.

The preparations of chloro and allyl derivatives of pentamethylcyclopentadienyl aminoborole hafnium complexes are described. The chloro derivative, $Cp^*[C_4H_4BN(CHMe_2)_2]HfCl{\cdot}LiCl$, is prepared by treatment of Cp^*HfCl_3 with $Li_2(THF)\{C_4H_4BN(CHMe_2)_2\}$. The structures of the chloro derivatives $Cp^*[C_4H_4BN(CHMe_2)_2]HfCl{\cdot}LiCl(Et_2O)_2$ and $\{Cp^*[C_4H_4BN(CHMe_2)_2]HfCl{\cdot}LiCl\}_2$ were determined by single crystal X-ray analysis. Treatment of $Cp^*[C_4H_4BN(CHMe_2)_2]HfCl{\cdot}LiCl$ with allyl magnesium bromide yields $Cp^*[C_4H_4BN(CHMe_2)_2]Hf(\eta^3\text{-}C_3H_5)$, whose structure was determined by X-ray analysis. The allyl species was active for the polymerization of ethylene, but not for the polymerization of α-olefins. Addition of ligands to the allyl derivative results in the formation of $Cp^*[C_4H_4BN(CHMe_2)_2]Hf(C_3H_5)(L)$ (L = PMe_3, pyridine, CO). The structure of $Cp^*[C_4H_4BN(CHMe_2)_2]Hf(\eta^3\text{-}C_3H_5)(CO)$ was determined. Treatment of $Cp^*[C_4H_4BN(CHMe_2)_2]Hf(\eta^3\text{-}C_3H_5)(CO)$ with PMe_3 results in the formation of the dieneolate complex $Cp^*[C_4H_4BN(CHMe_2)_2]Hf(OCHCHCHCH_2)(PMe_3)$. The electronic spectra of several aminoborole complexes were investigated and the low energy transitions assigned as borole-metal LMCT transitions. The amphoteric complex $Cp^*\{\eta^5\text{-}C_4H_4BN(CHMe_2)_2\}HfCl{\cdot}LiCl$ heterolytically cleaves H-X bonds to form $Cp^*\{\eta^5\text{-}C_4H_4BNH(CHMe_2)_2\}HfCl(X)$ (X = Cl, CCR). $Cp^*\{\eta^5\text{-}C_4H_4BNH(CHMe_2)_2\}Hf(CCTMS)_2$ is prepared from $Cp^*\{\eta^5\text{-}C_4H_4BN(CHMe_2)_2\}Hf(\eta^3\text{-}C_3H_5)$ and two equivalents of (trimethylsilyl)acetylene. Methyl iodide reacts with $Cp^*\{\eta^5\text{-}C_4H_4BN(CHMe_2)_2\}HfCl{\cdot}LiCl$ to form $Cp^*\{\eta^5\text{-}C_4H_3MeBNH(CHMe_2)_2\}HfClI$. Control experiments using deuterium labelled substrates show heterolysis occurs with no incorporation of deuterium into the 2,5 positions of the borole heterocycle. The X-ray structure determinations of $Cp^*\{\eta^5\text{-}C_4H_4BNH(CHMe_2)_2\}HfCl_2$, $Cp^*\{\eta^5\text{-}C_4H_4BNH(CHMe_2)_2\}HfCl(CCTMS)$, and $Cp^*\{\eta^5\text{-}C_4H_3MeBN(CHMe_2)_2\}HfClI$ are reported.

Table of Contents

List of Figures

List of Tables

Chapter 1

Ruthenium Tricyclophosphate Complexes

Abstract

The search for new oxidation catalysts is hampered by the ease with which most ligands commonly employed in inorganic and organometallic are themselves oxidized. The tricyclophosphate ligand, $(P_3O_9)^{3-}$, was investigated as an oxidation resistant ligand for ruthenium chemistry. The silver salt of tricyclophosphate, $Ag_3(P_3O_9).H_2O$, was found to be a useful synthon in the preparation of organic soluble tricyclophosphate salts. The complex $[(P_3O_9)Ru(C_6H_6)]^-$ was prepared and characterized. In water, it was found that the tricyclophosphate ligand dissociated from the $[(C_6H_6)Ru]^{2+}$ dication. Cyclic voltammatry in acetonitrile shows only a small irreversible oxidation at 0.95 V (Vs ferrocene). Attempts to chemically oxidize the $[(P_3O_9)Ru(C_6H_6)]^-$ complex failed. Other efforts to prepare ruthenium complexes in both low and high oxidation states were unsuccessful. The rhenium carbonyl complex $[(P_3O_9)Re(CO)_3]^{2-}$was also investigated as a precursor to high valent tricyclophosphate rhenium complexes. Attempts to chemically oxidize this complex also failed. Based on these results as well as related work by Klemperer and coworkers, it is concluded that the tricyclophosphate ligand is an exceptionally hard one that binds only weakly to transition metals. Most of the tricyclophosphate complexes that have been prepared have π-acceptor ligands, and it is proposed that this ability to accept π-electron density is important to the stability of the complexes.

1. Introduction

Metal catalyzed oxidation of hydrocarbons is a fundamentally important process that has received widespread attention. The partial oxidation of alkanes is a difficult goal, because the initial oxidation products are usually more reactive than alkanes, so the reaction is driven to CO_2 and H_2O as final products. However, the potential benefits of partial oxidation of alkanes are great; low molecular weight alkanes, such as methane, are naturally abundant, but are difficult and dangerous to store and transport. Thus their value as cheap fuel is limited because of transportation costs. With current technology, it is not economical to convert methane to liquid fuel such as methanol or gasoline. Current fuel cells use H_2 as fuel, rather than liquid hydrocarbons, because there are no electrochemical oxidation catalysts that are efficient for alkanes. Selective partial oxidants are also in great demand in synthetic organic chemistry. Thus there are many areas in science and industry that would benefit from improved oxidation catalysts.

Previous work on oxidation in the Bercaw group focused on the early transition metals, such as Ta and W. Though oxo complexes of tantalum and tungsten do undergo stoichiometric reactions, they were not very strong oxidants.[1] The early transition metals are known to form strong metal-oxo bonds; these strong bonds are often a thermodynamic sink rather than a source of reactivity. This oxophilic nature of the early transition metals has been explained by invoking a resonance structure of the metal-oxo bond in which a lone pair on the oxo donates to the metal, forming a third, dative bond (Fig 1). Some workers have concluded instead that the strong metal-oxo bond formed by the early transition metals is due primarily to the highly ionic nature of this bond.[2] In any case, the strong metal oxygen bonds formed by these elements do not make their complexes likely candidates for oxidation catalysts.

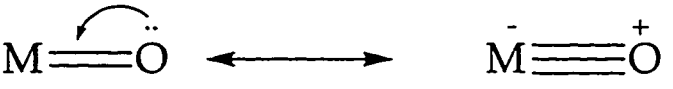

Figure 1: Bonding in Metal Oxides

This rationale for the low reactivity of early transition metal oxo complexes, however, does lead to the expectation that later transition metals should form more reactive metal-oxo bonds. This is indeed the observed periodic trend, and the Fe, Ru, Os triad is the last one for which stable metal oxo complexes have been observed.[3] These elements are well known in oxidation chemistry, particularly the heavier elements ruthenium and osmium. Osmium tetroxide is well-known to be a valuable olefin dihydroxylation catalyst from the work of Sharpless and others,[4] and ruthenium tetroxide is an even stronger oxidant.[5] RuO_4 is such a strong oxidant that it will even oxidize alkanes, though not very efficiently. Many researchers have tried to modify these oxo complexes by ligation, in order to stabilize these highly reactive species and to harness their oxidation potential for more selective oxidations.

The problem of finding good ancillary ligands for oxidation chemistry is a difficult one. Most common organometallic ligands are simply too easily oxidized. Phosphines typify this problem. Trialkyl- or triarylphosphines, PR_3, comprise one of the most widely used class of organometallic ligand, but they are very easily oxidized to phosphine oxides. In general, organometallic ligands are soft ligands, and stabilize lower oxidation states better than higher oxidation states. Thus, in oxidation chemistry, harder ligands[6], such as amines,[7] are more common.

Biological systems have provided many insights into the ligand problem. There are many metalloenzymes which are oxidants, perhaps the best known of these is cytochrome P-450. This protoporphyrin based metalloenzyme is potent enough to oxidize alkanes. Though the mechanism has not been fully elucidated, it is believed to proceed by a hydrogen atom abstraction, radical recombination mechanism (Fig. 2). The solvent-caged alkyl radical may undergo partial epimerization before recombination to alcohol and reduced metalloporphyrin.[8]

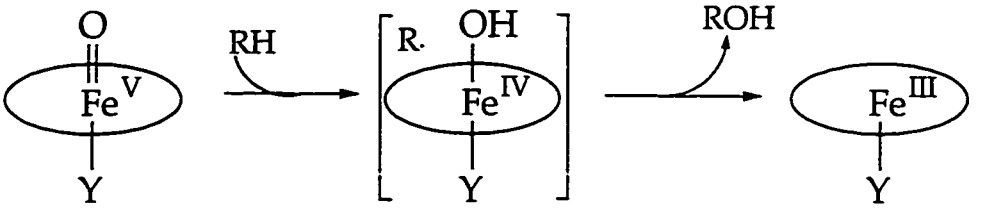

Figure 2: Alkane Oxidation by Metalloporphyrins

Model compounds based on the porphyrin ligand are also good oxidants, and porphyrins have now become one of the most widely used ligands in oxidation chemistry.[9] There are many synthetic variations on the basic porphyrin. Usually, these derivatives have been targeted at correcting one of three problems: oxidative degradation of the porphyrin, dimerization, and substrate selectivity. One of the most serious drawbacks to porphyrins is that they are susceptible to oxidation, particularly at the *meso* positions. Many of the attempts to improve the stability of porphyrins involve substitution at the *meso* position to block this side reaction. Generally, bulky groups at the *meso* position serve both to prevent dimerization and to protect the *meso* carbons from oxidation. Newer porphyrins have halogenated substituents at the meso position, or even halogenation of the porphyrin macrocycle itself.[10] These perhalogenated porphyrins are much more resistant to oxidation than their non-substituted progenitors, but their syntheses can be difficult and often proceed in rather low yield.[11] Furthermore, other decomposition reactions of porphyrin catalysts that do not involve oxidation of the *meso* positions are known. In particular, the so-called N-alkylation reaction is known for metalloporphyrin catalysts (Fig. 3).[12]

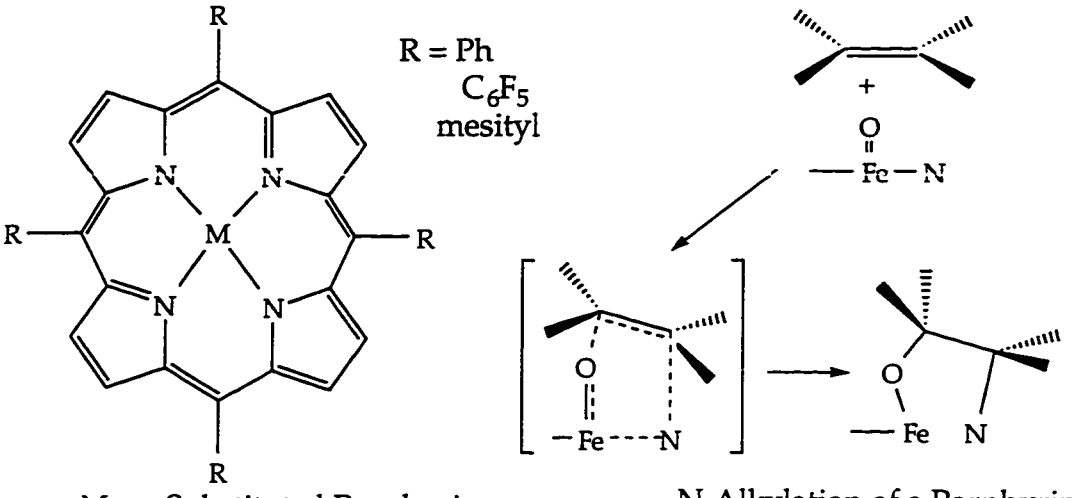

Figure 3: Porphyrin and N-Alkylation Reaction

The problem of ligand oxidation is certainly not limited to porphyrins. The common organometallic ligands cyclopentadienyl, Cp, and pentamethylcyclopentadienyl, Cp^*, undergo both ring-slippage and oxidation reactions. The reaction of $Cp^*_2W(O)$ with oxidants illustrates both of these problems (Fig. 4).[13]

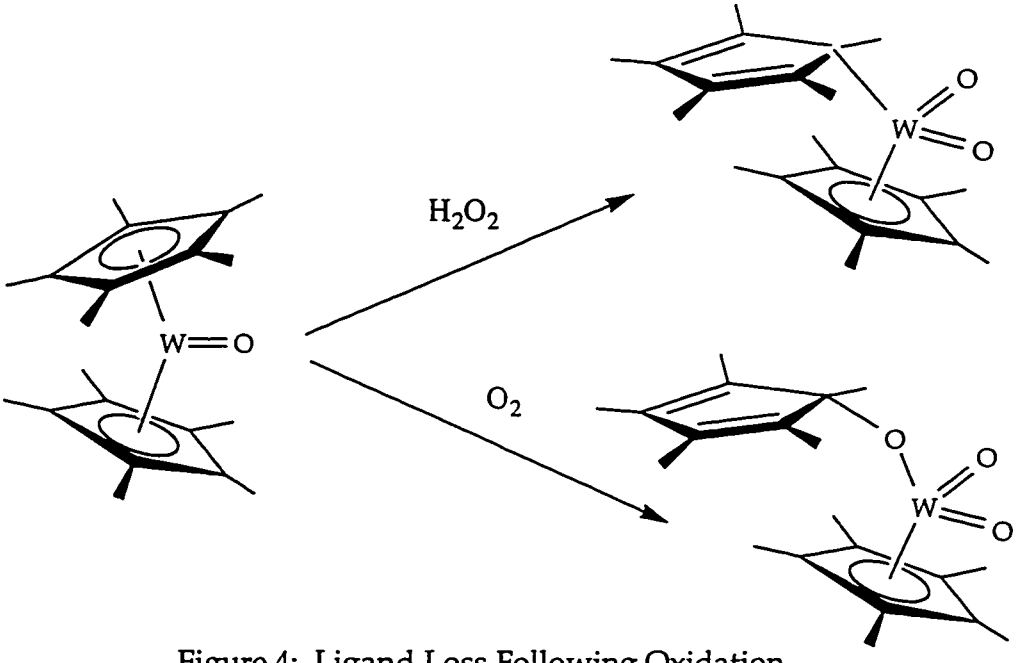

Figure 4: Ligand Loss Following Oxidation

The ring-slippage reactions demonstrate the powerful *trans*-labilizing effect of oxo groups. A good ligand for oxidation chemistry thus needs to be very strongly coordinating to compete with the oxo ligands.

Previous work in the Bercaw group has focused on a cyclopentadienyl tris(phosphito) cobalt complex as an oxidation resistant ligand. The ligand, shown in Fig. 5, was first synthesized by Klaui and co-workers.[14] It is tridentate, coordinating facially via the oxygen atoms. The Klaui ligand is a mono-anionic, five electron donor, and is thus a Cp or Cp^* analogue. It is highly resistant to oxidation, as demonstrated by its ability to coordinate Ce^{4+} ion without being oxidized.[15] Klaui has explored its coordination chemistry, and describes it as a weak-field, hard ligand, similar to fluoride or hydroxide. An interesting feature of this ligand is that its solubility is largely dependent on the organic substituents of the phosphito moieties. The methoxy derivative, [L_{OMe}^-], is soluble only in polar solvents, such as water, alcohols, and CH_3CN. The ethoxy derivative, [L_{OEt}^-], is much more soluble in non-polar organic solvents such as benzene or Et_2O.

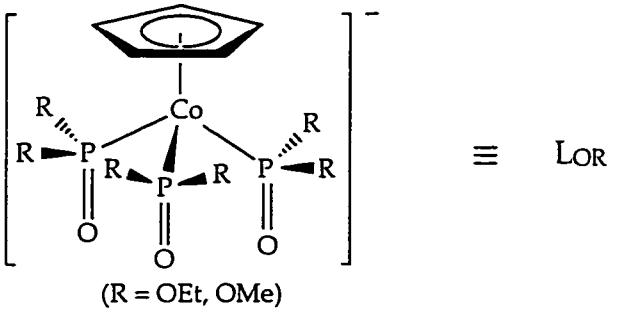

Figure 5: The Klaui Ligand

Using the Klaui ligand, several high-valent ruthenium complexes have been prepared and characterized by the Bercaw group.[16] Two of them, [L_{OR}Ru(OH)(μ-O)]$_2$ and [L_{OR}Ru(O)(μ-O)]$_2$, are of interest because they oxidize alcohols (Fig. 6).[17] These dimers have been found to generally maintain their dimeric core throughout redox reactions, so they are referred to by the oxidation state of the metals, i.e.. as the Ru^V-Ru^V dimer for the [L_{OR}Ru(O)(μ-O)]$_2$ complex and as the Ru^{IV}-Ru^{IV} dimer for the [L_{OR}Ru(OH)(μ-O)]$_2$ complex.

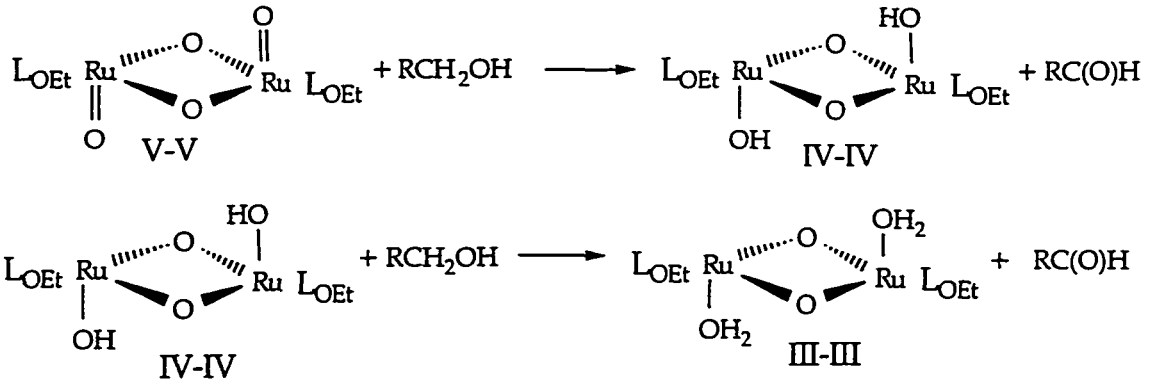

Figure 6: Alcohol Oxidation by Ru Dimers

The Ru^{V}-Ru^{V} dimer and the Ru^{IV}-Ru^{IV} dimer have both been structurally characterized, and a further reduction product, the Ru^{III}-Ru^{III} dimer, has been characterized as the CH_3CN adduct. It is interesting to note that the dimeric core remains unchanged across two redox reactions, since such structural robustness could be useful for oxidation catalysts.

The kinetics of the reaction of the Ru^{V}-Ru^{V} dimer with *sec*-phenethyl alcohol were studied, and found to be first order in catalyst and first order in substrate. The kinetics are complicated because the Ru^{V}-Ru^{V} dimer reacts to produce the Ru^{IV}-Ru^{IV} dimer, which also reacts with alcohol.[18]

The electrochemistry of the Ru^{IV}-Ru^{IV} dimer has also been studied. The Ru^{IV}-Ru^{IV} dimer is an electrocatalyst for the oxidation of methanol. The oxidation potential for the (III-III)/(IV-IV) couple is quite low, ~100 mV vs. SCE at pH 7.[19] Even though the turnover numbers for the electrocatalysis are low, the redox potential is considerably better than those of amine or pyridyl based Ru systems. This result is encouraging, and supports the belief that harder, oxygen donors such as the Klaui ligand stabilize high oxidation states better than nitrogen donors.

However, these studies of the Klaui ruthenium system have also indicated that the Klaui ligand is not completely inert to strong oxidants. This observation is surprising in light of the ligand's purported stability in coordinating Ce^{4+}, which is a very strong oxidant. However, there is definite evidence for the oxidative decomposition of the ligand. In the synthesis of

the Ru^{IV}-Ru^{IV} dimer for instance, RuO_4 is allowed to react with the ligand in 1% H_2SO_4. The yield is about 75%. In this reaction, ruthenium is being reduced from Ru^{VIII} to Ru^{IV}, but it is unclear what the reductant is. It is possible that water is being oxidized, but it is more likely that some of the ligand itself is being oxidized. The isolation of a species which analyzes as $(L_{OR})_2Co$ from the reaction indicates that some of the ligand is being destroyed.[20] The likely problem is that the C-H bonds of the ligand are being oxidized. Other workers have noted that the organometallic complexes of the ligand can participate in dealkylation reactions similar to the Michaelis-Arbuzov reaction noted for alkoxy phosphonium ions, so this is also a possible decomposition route.[21]

These results prompted the search for a ligand that would be completely oxidation resistant, yet still maintain the desirable oxygen donor environment. An entirely inorganic ligand should be more oxidation resistant; the group of Klemperer has recently been investigating small metal oxide clusters, termed polyoxometallates, as ligands for transition metals. Klemperer has also introduced the tricyclophosphate ion, $(P_3O_9)^{3-}$, as a simpler analogue of the polyoxometallate ligands for organometallic chemistry (Fig. 7). Tricyclophosphate ion, also called the tricyclophosphate ion, is a hard oxygen donor ligand. It is a trivalent anion, and should thus stabilize high oxidation states. It is similar to the Klaui and Cp ligands in that it is a tridentate, facially coordinating ligand. One potential drawback to the ligand is that it is slowly hydrolyzed in water, with acids and bases catalyzing the reaction. However, this susceptibility to hydrolysis might be reduced or eliminated upon coordination.

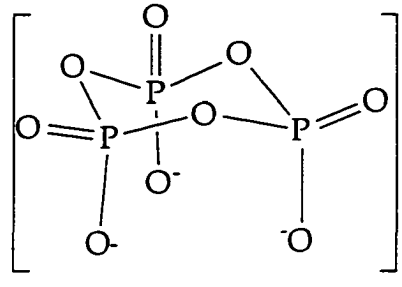

Figure 7: The Tricyclophosphate Ligand

The tricyclophosphate ion has been known for a long time, but only recently has it been used as a ligand in organometallic chemistry.[22]

Klemperer and coworkers have prepared a number of well characterized $(P_3O_9)^{3-}$ complexes of Ir, Rh, Mn, and Re.[23,24,25] The $[(P_3O_9)Ir(cyclooctadiene)]^{2-}$ complex reported by Klemperer is particularly interesting, because it reacts with O_2 to give an oxametallacyclobutane and further oxidation products (Fig. 8) .[26] This result provided encouragement that $(P_3O_9)^{3-}$ would be an a useful ligand in oxidation chemistry.

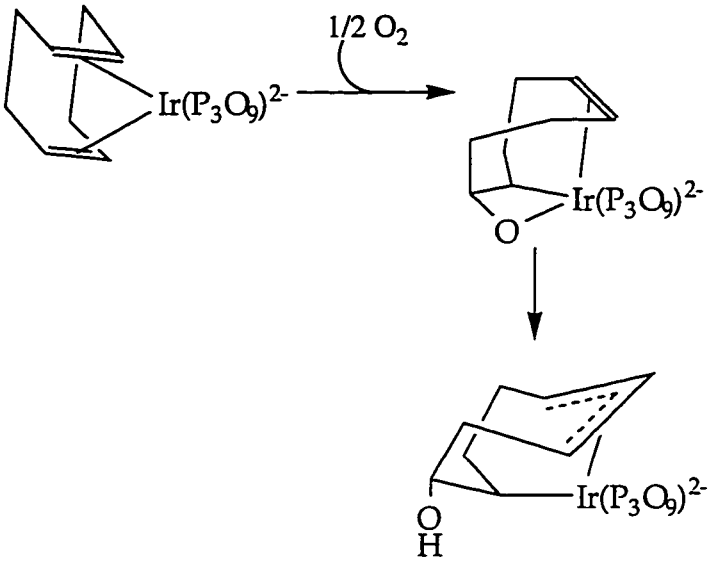

Figure 8: Oxidation of coordinated diene by a $(P_3O_9)^{3-}$ supported metal

In other work, it was found that thermolysis of the $(P_3O_9)MoO_2OEt^{2-}$ complex lead to the formation of acetaldehyde and ethanol as the organic products, presumably via intramolecular oxidation of the ethoxy group.[27]

Thus, based on these results, we undertook an investigation of the chemistry of ruthenium tricyclophosphate complexes. The goal was the preparation of complexes that would be oxidation catalysts with potentials low enough to be useful in electrocatalysis.

2. Results and Discussion

The synthesis of the sodium tricylcophosphate ligand is very straightforward. NaH_2PO_4 is heated to 550°C for six hours, resulting in formation of $Na_3(P_3O_9)$ by condensation reaction.[28] Tricyclophosphate is also available commercially as the hexahydrate salt. The sodium salt is soluble only in water, but Klemperer's group has developed syntheses to tetrabutylammonium, TBA, and bis(triphenylphosphoranylidene)ammonium, PPN, salts that are soluble in organic solvents. The tetrabutylammonium salt, soluble in a variety of organic solvents, is prepared by cation exchange chromatography of the sodium salt. The PPN salt is easier to prepare, since it can be precipitated from aqueous solution, but it is not as soluble in as wide a range of solvents as the TBA salt.

The synthesis of the TBA and PPN salts of tricyclophosphate has been improved through the use of $Ag_3(P_3O_9)\cdot H_2O$. The silver salt readily precipitates when aqueous $AgNO_3$ is added to a solution of $Na_3(P_3O_9)\cdot 6H_2O$ (eq. 1); it is slightly soluble in water, and will undergo halide metathesis even in

$$Na_3(P_3O_9) + 3Ag(NO_3) \longrightarrow Ag_3(P_3O_9) + 3Na(NO_3) \quad (1)$$

organic solvents. Treatment of $Ag_3(P_3O_9)\cdot H_2O$ with (TBA)Br or (PPN)Cl results in formation of the organic cation salts in high yield (eq. 2). This route circumvents the tedious ion-exchange chromatography, and eliminates the need to evaporate the large volumes of solution resulting from it. The yield

$$Ag_3(P_3O_9) + 3M(X) \longrightarrow (M)_3(P_3O_9) + 3Ag(X) \quad (2)$$
$$M = TBA, PPN$$
$$X = Cl, Br$$

is also higher using the silver halide metathesis route, because the product loss due to hydrolysis of $(P_3O_9)^{3-}$ is less with the silver metathesis reaction. Thus, the use of silver tricyclophosphate greatly facilitates the preparation of $(TBA)_3(P_3O_9)\cdot 3H_2O$, and provides a convenient alternate route to the preparation of $(PPN)_3(P_3O_9)\cdot H_2O$. The silver salt has also been used in the synthesis of tricyclophosphate complexes, simultaneously providing a source of the ligand and a halide-abstracting agent.

Synthetic Strategy:

There are two general routes to making high oxidation state complexes. The first is to coordinate the ligand to a metal in a low oxidation state, and subsequently to oxidize it to the desired high valent complex. The second route is to substitute the ligand on to a metal that is already in a high oxidation state. The advantage of the first route is that most syntheses in organometallic chemistry begin with low-valent metals, so there is a much larger literature of possible starting materials; also, it is possible to characterize complexes in a stable, low-valent state before oxidation. The disadvantages of this route are the longer syntheses required, and possible difficulties in oxidizing the low-valent complexes. This can be a serious drawback. For example, the Klaui-ruthenium complex $L_{OEt}Ru(CO)_2Cl$ cannot be oxidized cleanly despite having an oxidation resistant ancillary ligand. It is often possible to prepare metal oxos via oxidation of carbonyls, but in this instance it is not possible even in these favorable circumstances.[29]

The advantage of the high-oxidation state route is that typically, fewer steps are required for the synthesis. The problem is that the relative shortage of high-valent species makes finding a good starting material difficult. Also, many high-valent metal species, such as RuO_4, lack good leaving groups, and thus need to be somehow reduced or activated before substitution can occur.

For this project, the low-valent route was initially chosen. Eventually, a number of ruthenium complexes, both high and low valent, were investigated as possible synthons, but since the low valent route was investigated first, these results will be discussed first. Our anticipation was that the superior oxidation resistance of the ligand would permit low-valent complexes to be oxidized cleanly. Also, since $(P_3O_9)^{3-}$ chemistry was still relatively unexplored, making and characterizing some ruthenium tricyclophosphate complexes would establish a good foundation for further research.

The general criteria for starting materials were ruthenium complexes with two or three halides, and easily oxidized ligands such as carbonyl, water, hydroxide, or nitrile. Tricyclophosphate is similar to the Klaui ligand in that it is a weak-field, hard ligand. It is also trivalent, and so it should be similar

to three halides, which are weak, hard ligands. Thus it seemed that the most straightforward synthesis of $(P_3O_9)^{3-}$ complexes would be from di- or trihalide starting materials. After searching the literature, the ruthenium chloro carbonyl dimer, $Ru_2Cl_4(CO)_6$, a compromise between labile ligands and oxidizible ligands, was chosen as the most likely starting material.

The $Ru_2Cl_4(CO)_6$ dimer is easily synthesized from $RuCl_3{\cdot}3H_2O$. Initial reactions of the dimer with $(PPN)_3(P_3O_9)$ in CH_2Cl_2 were followed by ^{31}P NMR. New peaks downfield from the free ligand grew in, so it was clear that a reaction was taking place. However, the presence of multiple peaks, one of which was a doublet, indicated that the expected $[(P_3O_9)Ru(CO)_3]^-$ was not being formed, or that it was not being formed exclusively. It seemed likely that part of the problem was incomplete substitution of the chlorides, since tricyclophosphate is not a strong nucleophile. The reaction was tried with $AgSbF_6$ to drive the reaction. ^{31}P NMR showed a single peak at -11.7ppm, well downfield of the free ligand. Thus it seemed that the reaction had gone completely to one species. However, the IR spectrum showed six peaks in the metal carbonyl region, indicating that the reaction was not clean. The reaction was very difficult to work up; the products were intractable oils. The simplicity of the NMR spectrum and the complexity of the IR spectrum suggested that NMR silent species were present. Since the ruthenium dimer is d^6, low-spin metal, it was concluded that a redox reaction was taking place to generate some paramagnetic, NMR silent species. Silver ion is known to be a strong oxidant, and the observation of grayish precipitates suggests that silver metal may be forming. Since it was not possible to isolate any pure products, and because it was believed that redox reactions were resulting in a complicated mixture of compounds, the reaction was shelved in favor of other starting materials.

The two most commonly used starting materials for ruthenium oxidation chemistry are $RuCl_3{\cdot}3H_2O$ and $K_2[RuCl_5OH_2]$. Ruthenium trichloride is a poorly defined mixture of ruthenium compounds, and is believed to be mostly Ru^{IV} oxo and hydroxychloride species. $RuCl_3{\cdot}3H_2O$ was heated with $Na_3(P_3O_9){\cdot}6H_2O$ in water. The black solution did not visibly change, and no products could be characterized from the reaction. A variety

of reaction conditions were attempted, but none yielded species that showed any signs of coordinated tricyclophosphate by NMR or IR.

$K_2[RuCl_5(H_2O)]$ is a well-defined starting material that is commonly used in the synthesis of macrocyclic amine and porphyrin complexes of ruthenium. Ruthenium pentachloride, a reddish solid, turns black when heated in water. The hydrolysis products are probably ruthenium trichloride type species. When $K_2[RuCl_5(OH_2)]$ was refluxed with $(TBA)_3(P_3O_9)\cdot 3H_2O$ in CH_3CN, a white solid precipitated as the pentachloride dissolved. The white precipitate was water soluble and contained free $(P_3O_9)^{3-}$ by NMR, so it was concluded that the counterion metathesis had occurred (eq. 3). No reaction occurred upon addition of more ligand.

$$K_2[RuCl_5(H_2O)] + (TBA)_3(P_3O_9) \xrightarrow{\Delta} (TBA)_2[RuCl_5(H_2O)] + 2/3K_3(P_3O_9) + 1/3(TBA)_3(P_3O_9) \quad (3)$$

The failure of the common ruthenium starting materials to react suggested that other ligands were needed to help stabilize the ruthenium tricyclophosphate complexes. The $RuCl_3L_3$ species were chosen as starting materials because they were the simplest molecules with stabilizing ligands that had three chlorides for the pseudo-halide tricyclophosphate to replace.

$RuCl_3(CH_3CN)_3$ failed to react with $(PPN)_3(P_3O_9)\cdot H_2O$ in refluxing methanol over days. Attempts to make cationic species by halide abstraction with silver ion resulted in decomposition of the starting materials to ill-defined mixtures. The other $RuCl_3L_3$ species, $RuCl_3(PhCN)_3$ and $RuCl_3(PPh_3)_3$, were also tried, in the belief that stronger donor ligands might help to stabilize a 17 electron $(P_3O_9)RuL_3$ species. However, neither species reacted with tricyclophosphate, and all attempts generate more reactive ruthenium cations failed. It was surprising how inert the chlorides of the Ru(III) species were; $RuCl_3(PhCN)_3$ was refluxed with $Ag_3(P_3O_9)\cdot H_2O$ for two days in acetonitrile, but only substitution of benzonitrile by solvent was found to occur.

The results with ruthenium(III) complexes suggested that the synthetic problems were due more to the low reactivity of the starting materials than the instability of the products, so more reactive complexes were sought. The ruthenium(II) species $[Ru(H_2O)_6]OTs_2$ and $[Ru(NH_3)_6]Cl_2$ were promising, because as cations they should coordinate strongly to the anionic tricyclophosphate ligand. Reaction of the pink hexaaquo ruthenium(II) cation in water with $Na_3(P_3O_9)\cdot 6H_2O$ resulted in a dark blue, paramagnetic solution that slowly precipitated an insoluble blue-black solid. All attempts to characterize or dissolve the solid failed.

No reaction occurred between hexammine ruthenium(II) and $Na_3(P_3O_9)\cdot 6H_2O$ in water. Heating the mixture resulted only in hydrolysis of the hexammine ruthenium complex.

Another versatile synthon in low valent Ru chemistry is the arene ruthenium dichloride species. The reaction between $(PPN)_3(P_3O_9)\cdot H_2O$ and $\{(C_6H_6)RuCl_2\}_x$ had been tried earlier by another member of our group, but the product had not been characterized.[30] However, the experiment was repeated with both $(TBA)_3(P_3O_9)\cdot 3H_2O$ and $(PPN)_3(P_3O_9)\cdot H_2O$, and the tricyclophosphate ruthenium benzene anion was isolated in good yield (Figure 10). Consistent with the generally observed solubility trends, the TBA salt is more soluble in a wider range of solvents. It is also possible to prepare the arene Ru tricyclophosphate anion via direct substitution of the halides (eq. 4). However, this route necessitates the use of DMSO to dissolve the insoluble $\{(C_6H_6)RuCl_2\}_x$ species, making subsequent isolation and recrystallization of the product more difficult, so the method shown in Figure 10 is the preferred one.

$$\{(C_6H_6)RuCl_2\}x + 2AgOTf \xrightarrow{CH_3CN} (C_6H_6)Ru(CH_3CN)_3^{2+} + 2AgCl$$

$$\downarrow \text{ 1) filter, 2)}(TBA)_3(P_3O_9)$$

$$TBA[(P_3O_9)Ru(C_6H_6)] + 2TBA(OTf)$$

Figure 9: Synthesis of $TBA[(P_3O_9)Ru(C_6H_6)]$

Orange PPN[$(C_6H_6)Ru(P_3O_9)$] was recrystallized from dichloromethane/ether solution. The ^{31}P NMR shows a singlet at -7.81ppm, indicating that the phosphorous atoms are equivalent. Likewise, the proton NMR displays only a singlet for the coordinated arene, and peaks due to the counterion. X-ray quality crystals were grown by slow evaporation of a 1,2 dichloroethane solution of the PPN salt. A single crystal of the complex was selected and an X-ray structure obtained. An ORTEP of the anionic ruthenium complex is shown in Figure 11, and selected bond distances and angles are shown in Table 1.

$$\{(C_6H_6)RuCl_2\}x + (PPN)_3(P_3O_9) \xrightarrow{DMSO} PPN[(C_6H_6)Ru(P_3O_9)] + 2\,PPNCl \quad (4)$$

The molecule crystallized in the space group $P2_1/c$, and there is a molecule of water per anion, hydrogen-bonding to oxygens of tricyclophosphate. The tricyclophosphate ligand is bound to the metal in κ^3-*O*-P_3O_9 fashion, consistent with what Klemperer and coworkers have observed. The Ru-O distances, though similar, are not exactly the same in the solid state, so that the molecule approaches C_{3v} symmetry. Again, this is consistent with what Klemperer has observed for other organometallic complexes of tricyclophosphate.

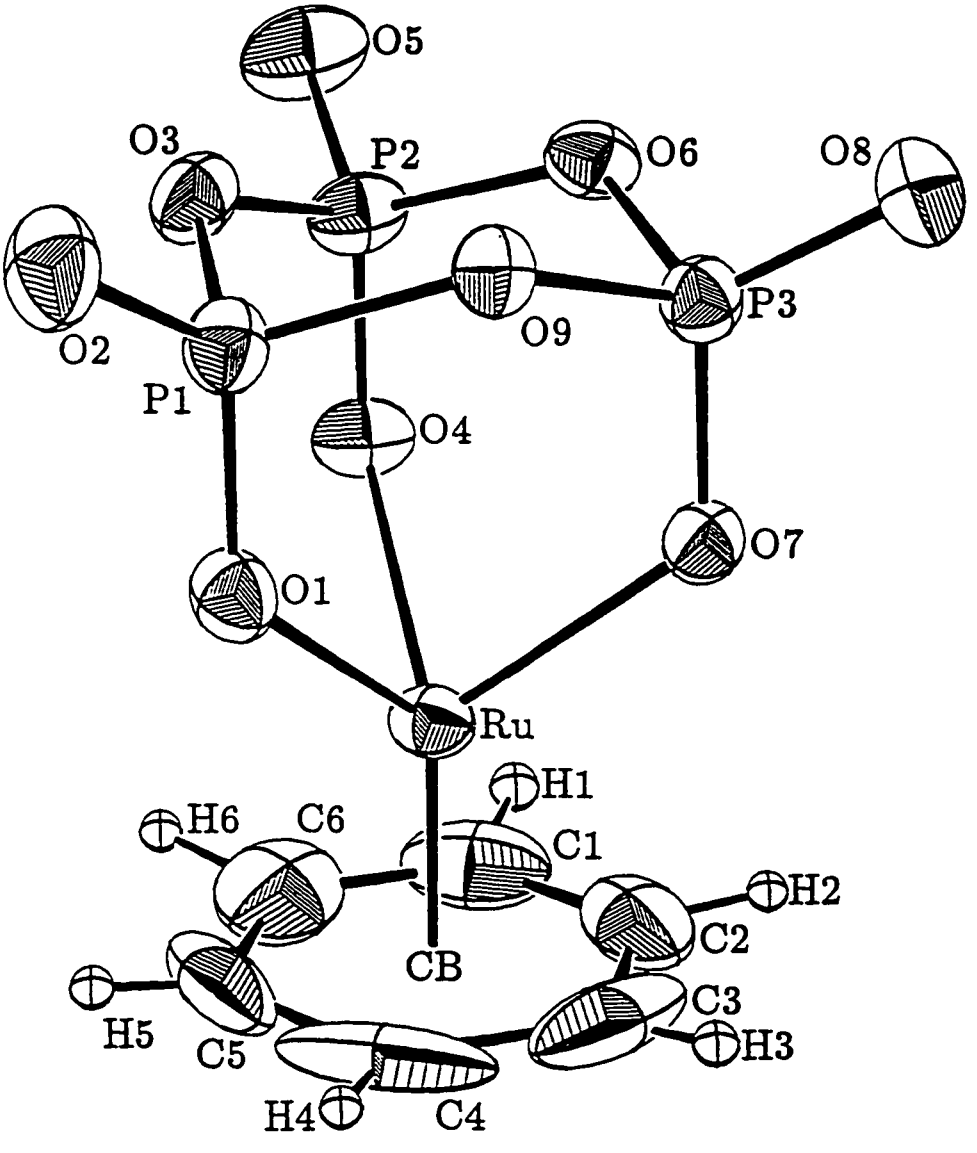

Figure 10: ORTEP Diagram of $(P_3O_9)Ru(C_6H_6)^-$

Table 1: Selected Bond Lengths and Bond Angles for PPN[(P_3O_9)Ru(C_6H_6)]

Ru-O1	2.124Å	P1-O1	1.508Å
-O4	2.120	-O3	1.615
-O7	2.127	-O9	1.611
		-O2	1.450
Ru-C1	2.142		
-C2	2.137	P2-O4	1.507
-C3	2.129	-O3	1.608
-C4	2.133	-O6	1.610
-C5	2.128	-O5	1.459
-C6	2.139		
		P3-O7	1.508
		-O6	1.616
		-O9	1.610
		-O8	1.448
O1-Ru-O4	87.17°	O2-P1-O1	119.33°
O4-Ru-O7	85.44	O5-P2-O4	118.33
O7-Ru-O1	84.87	O8-P3-O7	119.12
Ru-O1-P1	127.08	P2-O3-P1	123.28
Ru-O4-P2	126.19	P3-O6-P2	122.25
Ru-O7-P3	127.31	P3-O9-P1	123.55

$[(P_3O_9)Ru(C_6H_6)]^-$ is apparently unstable in water, as the ^{31}P NMR of the ligand shifts upfield to the resonance for the free ligand when the complex is dissolved in water. This result is quite surprising, because one would expect the electrostatic interaction between the ruthenium dication and $(P_3O_9)^{3-}$ to be quite strong. Addition of water dropwise to an acetonitrile solution of $TBA[(P_3O_9)Ru(C_6H_6)]$ initially resulted in the formation of an orange precipitate. Continued addition of water caused the precipitate to oil out as a drop of viscous orange liquid; the CH_3CN solution lost much of its color. Based on these results, the ligand does not remain coordinated in the presence of water.

The electrochemistry of $[(P_3O_9)Ru(C_6H_6)]^-$ in acetonitrile was examined. The only feature was a small non-reversible oxidation at 0.95V vs. ferrocene/ferrocenium. The small size of the oxidation wave suggests that it could be due to an impurity. Alternatively, it could be due to extremely slow electron transfer from the $[(P_3O_9)Ru(C_6H_6)]^-$ ion. If this is the case, the potential of the oxidation is surprisingly high; one would expect an anion to be oxidized more readily. Thus, this result is puzzling and somewhat discouraging, since the complex was expected to be much more susceptible to oxidation.

Chemical oxidation of the complex is complicated by its instability in water, because many of the commonly used oxidants are soluble only in water. The reagents that are commonly used for the non-aqueous oxidations are iodosyl benzene, tert-butylhydroperoxide, and amine oxides such as $Me_3N(O)$. Iodosyl benzene is a strong oxidant, and it is commonly used in metalloporphyrin chemistry. $TBA[(P_3O_9)Ru(C_6H_6)]$ was refluxed with PhIO in CH_2Cl_2 for 24 hours. No noticeable reaction occurred, and ^{31}P NMR showed only the presence of free ligand. The reaction was tried again in acetonitrile, and the PhIO did slowly disappear over two days. The solution appeared slightly darker orange, but no new peaks appeared in the NMR spectrum. It is possible that the PhIO merely decomposed over time without oxidizing the ruthenium complex. Similar results were obtained with ^{t}-butylhydroperoxide and $Me_3N(O)$.

Shortly after the $[(P_3O_9)Ru(C_6H_6)]^-$ was synthesized, a draft of a paper from Klemperer's group was received.[31] It reported the synthesis and characterization of several $(P_3O_9)^{3-}$ ruthenium complexes, including $(TBA)[(P_3O_9)Ru(C_6H_6)]$ and $(TBA)_4[(P_3O_9)_2Ru_2(CO)_4]$. Thus Klemperer's group was working along similar lines. The tricyclophosphate ruthenium benzene complex was independently prepared by the same reaction of $\{(C_6H_6)RuCl_2\}_x$ and $(TBA)_3(P_3O_9)\cdot 3H_2O$ in DMSO. The complex was characterized, though an x-ray structure was not obtained. The tricyclophosphate ruthenium carbonyl dimer was synthesized in ~40% yield from the reaction of $Ru_2Cl_4(CO)_6$ and excess $(TBA)_3(P_3O_9)\cdot 3H_2O$ in acetonitrile. The ruthenium metal centers of the dimer are reduced from Ru^{II} to Ru^{I} in the reaction. The authors found that the best yields were obtained when at least two equivalents of the tricyclophosphate salt were used. Based on this, they cite the stoichiometry of the reaction as shown in eq. 5. The proposed mechanism for this redox reaction involves nucleophilic

$$[Ru(CO)_3Cl_2]_2 + 4(P_3O_9)^{3-} + H_2O \longrightarrow [(P_3O_9)_2Ru_2(CO)_4]^{4-} + 2H(P_3O_9)^{2-} + 4Cl^- + CO + CO_2 \quad (5)$$

attack by water on a carbonyl, resulting in the formation of a metal-hydride and CO_2. The hydride is deprotonated by a base, reducing the metal.[32] Such redox reactions were probably occurring in the reaction of $(PPN)_3(P_3O_9)\cdot H_2O$ with $Ru_2Cl_4(CO)_6$ that was discussed earlier. That reaction was complicated by the presence of silver ion, however, and the NMR and IR spectra were different from those reported for the $[(P_3O_9)_2Ru_2(CO)_4]^{4-}$ anion. It is somewhat surprising that the metal should be reduced in the reaction, since coordination of the tricyclophosphate ligand would be expected to stabilize higher oxidation states. It is possible however, that the reduction occurs before coordination of the ligand.

Along with the synthetic chemistry that is presented, the draft makes an important observation: the presence of π-acid ligands is necessary for $(P_3O_9)^{3-}$ substitution of halides. The authors attribute this to the *trans*-labilizing effect of the π-acid ligands increasing the rate of substitution by the weak nucleophile, $(P_3O_9)^{3-}$. However, complexes such as $[Ru(H_2O)_6]^{2+}$ clearly

react with tricyclophosphate, but do not form stable products, suggesting that π-acid ligands may be important for stability of the products as well as for substitutional lability. Thus far, all $(P_3O_9)^{3-}$ complexes that have been characterized by Klemperer's group have π-acid ligands such as carbonyls, olefins, or arenes. Unfortunately, most of the complexes used as starting materials in this project lacked π-acid ligands, which may explain why they did not react or form isolable complexes.

At this point, it seemed that most of the likely possibilities for the low-valent route had been tried, so the high-valent route was explored. The two starting materials chosen for the high-oxidation state route were RuO_4 and $Ru_2Cl_6(PhCN)_4O$, since both of these materials were used successfully to make Klaui-ruthenium oxo dimers.[9] A solution of RuO_4 in carbon tetrachloride was stirred with an aqueous solution of $Na_3(P_3O_9)\cdot 6H_2O$ in a biphasic reaction. After 18 hours, no detectable reaction had occurred. The reaction between the Klaui ligand and RuO_4 is carried out in 1% H_2SO_4; the acid is important to the reaction, but the tricyclophosphate reaction was carried out at neutral pH because the hydrolysis of $(P_3O_9)^{3-}$ is catalyzed by acids and bases. Instead of using acid to activate the ruthenium tetraoxide, methanol was added to the biphase, to reduce the RuO_4 so that the ligand could coordinate. However, addition of MeOH to the biphase resulted only in an insoluble black precipitate, presumably RuO_2. Thus, efforts to reduce the tetraoxide *in situ* to a more labile species were unsuccessful.

The other high-valent species, $Ru_2Cl_6(PhCN)_4O$, did not react with $(PPN)_3(P_3O_9)\cdot H_2O$ in CH_2Cl_2. Attempts to generate cationic species via halide abstraction were uniformly unsuccessful.

Similarly, the ruthenium nitrido species $[(N)RuCl_4]^-$ failed to react with tricyclophosphate under a variety of conditions. The halides in the high valent species were not very labile to a weak nucleophile such as tricyclophosphate and, beyond the first chloride, were not susceptible to abstraction by silver ion.

As a final attempt to prepare high valent $(P_3O_9)^{3-}$ complexes, oxidations of the known tricyclophosphate complex $[(P_3O_9)Re(CO)_3]^{2-}$ were attempted. Rhenium forms very stable complexes in its highest oxidation

state, and so might readily form oxo complexes that could at least be isolated and characterized. Oxidation with a number of reagents (Me_3NO, H_2O_2, Br_2, Cl_2) failed to produce any tractable products. Me_3NO is commonly employed to oxidatively remove CO, but it has been noted that carbonyls with a fair degree of backbonding ($\nu(CO) < 2000\ cm^{-1}$) are generally inert to this nucleophilic reagent.[33] The carbonyl stretching modes for the $[(P_3O_9)Re(CO)_3]^{2-}$ ion are at 2018 and 1885 cm^{-1}; however these values represent the modes of three carbonyls, so comparison to the estimate for a single carbonyl stretching frequency is difficult.

Several attempts were also made to substitute tricyclophosphate onto the perrhenate ion, ReO_4^-, but these were not successful.

3. Conclusions

The new tricyclophosphate compounds $Ag_3(P_3O_9)\cdot H_2O$ and $[(P_3O_9)Ru(C_6H_6)]^-$ have been prepared and characterized. The silver salt is a useful synthon in the preparation of the organic-soluble TBA and PPN salts of the ligand. Attempts to chemically oxidize $[(P_3O_9)Ru(C_6H_6)]^-$ failed. The ruthenium complex did not display any reversible electrochemistry, suggesting that either electron transfer is very slow for the complex, or that the oxidation occurs at potentials outside the window examined.

Other efforts to prepare ruthenium tricyclophosphate complexes were unsuccessful. In general, it was found that reaction of tricyclophosphate with low-valent ruthenium starting materials led to uncharacterizable mixtures, and that the ligand failed to react with high-valent starting materials. During the course of this research, it came to our attention that the Klemperer group was also investigating tricyclophosphate ruthenium complexes. They prepared several low-valent complexes, including the arene complex described in this work, but did not report any successful oxidations of these complexes. In both this work and that done by the Klemperer group, the tricyclophosphate complexes that were isolated generally contained π-acid ligands. This π-acid character is important in stabilizing the anionic complexes.

As a final effort to prepare some high-valent tricyclophosphate complexes, rhenium complexes were investigated. Similar results were obtained as for the ruthenium complexes.

Tricyclophosphate was found to be a very hard ligand. It was found that the ligand immediately dissociated from the complex $[(P_3O_9)Ru(C_6H_6)]^-$ when it was dissolved in water. This problem complicated the oxidation reactions, since they had to be carried out in organic solvents. These results, along with similar ones found by the Klemperer group, suggest that tricyclophosphate is not an effective ligand for transition metal oxidation chemistry.

4. Experimental

$RuCl_3 \cdot 3H_2O$ and $K_2[RuCl_5OH_2]$ were purchased from Aesar and used as received. C_6H_8, AgOTf, HCO_2H, NaH_2PO_4, $(C_4H_9)_4NBr$, $(Ph_3P)_2NCl$ and $PhI(OAc)_2$ were purchased from Aldrich and used as received. Triphenyl phosphine (Aldrich) was recrystallized from MeOH prior to use. Acetonitrile, CH_2Cl_2 and MeOH were distilled under nitrogen from CaH_2. Diethyl ether was used from freshly opened cans. 1,2 Dichloroethane was used without further purification. The starting materials $Ru_2Cl_4(CO)_6$,[34] $RuCl_3(CH_3CN)_3$, $RuCl_3(PhCN)_3$, $Ru_2Cl_6(PhCN)_4O$,[35] RuO_4[9], $[Ru(H_2O)_6]OTs_2$,[36] $[Ru(NH_3)_6]Cl_2$,[37] $RuCl_3(PPh)_3$,[38] $[Ru(N)Cl_5]^-$,[39] and $\{(C_6H_6)RuCl_2\}_x$,[40] were prepared from literature procedures. PhIO was prepared from KOH and $PhI(OAc)_2$ by the literature procedure.[41] $Na_3(P_3O_9) \cdot 6H_2O$, was prepared from the literature procedures[18] or purchased from Johnson-Matthey. $(TBA)_3(P_3O_9) \cdot 3H_2O$, and $(PPN)_3(P_3O_9) \cdot H_2O$[16] were prepared from literature procedures or as detailed below.

^1H NMR spectra were recorded on either a Brucker 500 or on a G.E. 300 MHz NMR. Chemical shifts were referenced to residual protons in the solvent. ^{31}P NMR was recorded at 36.5 MHz on a JEOL FX-90Q equipped with an external ^7Li lock. The samples were referenced to 85% H_3PO_4 by the sample replacement method. UV-VIS spectra were recorded on a Hewlett-Packard HP8452 diode array spectrophotometer. IR spectra were recorded on a Perkin-Elmer 1600 series FT-IR spectrophotometer as either KBr pellets or in solution. The solution cells were Perkin-Elmer with CaF_2 windows (0.1mm

path length). Elemental analyses were performed by Fenton Harvey at Caltech, and also by Galbraith Laboratories, Knoxville TN.

(TBA)[(P_3O_9)Ru(C_6H_6)]

500mg $\{(C_6H_6)RuCl_2\}_x$ (1.0 mmol) was stirred in 40mL acetonitrile with 1.027g AgOTf (2 equiv.). The solution turned bright orange, and a white precipitate formed. The solution was gravity filtered, and 2.02g $TBA_3(P_3O_9)$ (1 equiv.) in 15mL acetonitrile was added. The solution was heated to 60°C for twenty minutes. 200mL Et_2O was added, and orange microcrystals precipitated. The crystals were collected by vacuum filtration, and washed with a small amount of ether. Recrystallization from CH_2Cl_2/Et_2O yielded 590mg 90% yield. Analysis for $C_{22}H_{42}NP_3O_9Ru$: Calculated C, 40.1; H, 6.4; N, 2.1; found C, 39.86; H, 6.25; N, 2.03

IR (KBr, 1400-600 cm^{-1}): 739s, 762s, 942vs, 976vs, 1102s, 1118m, 1266sh, 1289s, 1300s; ^{31}P NMR (CD_3CN 0.015M) -7.81ppm(s); ^1H NMR 5.71ppm(s, C_6H_6); uv-vis(CH_3CN, .0012M) 412nm(ε=395), 326nm(ε=815), 264(ε=355), 220(ε=1900)

PPN[(P_3O_9)Ru(C_6H_6)] was synthesized by the same route as the tetrabutyl ammonium analogue. The compound was recrystallized first from CH_2Cl_2/Et_2O and then x-ray quality crystals were grown by slow evaporation of a 1,2 dichloroethane solution. However, the x-ray structure revealed the presence of one water molecule per anion, giving the formula $(Ph_3P)_2N[(P_3O_9)Ru(C_6H_6)\cdot H_2O$.

$Ag_3(P_3O_9)\cdot H_2O$

10 g $Na_3(P_3O_9)\cdot 6H_2O$ was dissolved in 100mL of distilled water, and 12.12g $AgNO_3$ dissolved in 20mL water was added. A white precipitate formed immediately. The solution was stirred for one hour, then the precipitate was collected by vacuum filtration, washed twice with 10mL H_2O, once with acetone, then dried in vacuo. yield 12.2g 83% The elemental analysis corresponded to $Ag_3(P_3O_9)\cdot H_2O$ with ~7% contamination of $Na_3(P_3O_9)$

5. References

1. van Asselt, A; Trimmer, M.S.; Henling, L; Bercaw, J.E. *J. Am. Chem. Soc.* **1988,** *110,* 8254.
2. Howard, W. A.l; Parkin, G. *J. Am. Chem. Soc.* **1994,** *116,* 606.
3. Holm, R.H. *Chem. Rev.* **1987,** *87,* 1401.
4. (a) Jacobsen, E. N.; Marko, I.; France, M. B.; Svendsen, J. S.; Sharpless, K. B. *J. Am. Chem. Soc.* **1989,** *111,* 737. (b) Ogino, Y.; Chen, H.; Kwong, H.-L.; Sharpless, K. B. *Tetrahedron Lett.* **1991,** *32,* 3965.
5. Kochi, J.K.; Sheldon, R.A. *Metal Catalyzed Oxidations of Organic Compounds*: Academic: New York, 1981.
6. For a discussion of Hard-soft acid-base theory see Pearson, R. G. *Hard and Soft Acids and Bases;* Dowden, Hutchinson, and Ross: Stroudsberg, PA., 1973.
7. (a) Llobet, A.; Hodgson, D. J.; Meyer, T. J. *Inorg Chem.* **1990,** *29,* 3760. (b) Dovletoglou, A.; Adeyemi, S. A.; Lynn, M. H.; Hodgson, D. J.; Meyer, T. J. *J. Am. Chem. Soc* . **1990,** *112,* 8989. (c) Che, C.-M.; Yam, V. W.-W. *J. Am. Chem. Soc* . **1987,** *109,* 1262. (d) Che, C.-M.; Yam, V. W.-W.; Mak, T. C. *J. Am. Chem. Soc* . **1990,** *112,* 2284.
8. Ortiz de Montellano, P. R. *Cytochrome P-450: Structure, Mechanism and Biochemistry;* Plenum: New York, 1986.
9. (a) Groves, J. T.; Quinn, R. *J. Am. Chem. Soc* . **1985,** *107,* 5790. (b) Groves, J. T.; Quinn, R. *Inorg Chem.* **1984,** *23,* 3844. (c) Traylor, T. G.; Miksztal, A. R. *J. Am. Chem. Soc* . **1989,** *111,* 7443. (d) Traylor, T. G.; Xu, F. *J. Am. Chem. Soc* . **1988,** *110,* 1953.
10. (a) Lindsey, J.S.; Schreiman, I.C.; Kearney, P.C.; Marguerettaz, A.M. *J. Org Chem,* **1987,** *52,* 824. (b) Birnbaum, E. R.; Grinstaff, M. W.; Labinger, J. A.; Bercaw, J. E.; Gray, H. B. G. *J. Mol. Cat. (A)* **1995,** *104,* 119. (c) Grinstaff, M. W.; Hill, M. D.; Birnbaum, E. R.; Labinger, J. A.; Bercaw, J. E.; Gray, H. B. G. *Inorg Chem.* **1995,** *34,* 4896..
11. (a) Lyons, J. E.; Ellis, P. E., Jr. *Coord. Chem. Rev.* **1990,** *105,* 181
12. Castellino, A.J.; Bruice, T.C. *J. Am. Chem. Soc* . **1988,** *110,* 158.
13. Parkin, G.; Bercaw, J.E. *J. Am. Chem. Soc.* **1989,** *111,* 391.
14. Klaui, W.; Eberspach, W.; Schwarz, R. *J. Organomet. Chem.,* **1985,** 3 47.

15. Klaui, W. *Angew. Chem. Int. Ed. Engl.* **1990**, *29*, 627.
16. Power, J. M.; Evertz, K.; Henling, L.; Marsh, R.; Schaefer, W. P.; Labinger, J. A.; Bercaw, J. E. *Inorg Chem.* **1990**, *29*, 5085.
17. Kelson, E. P.; Henling, L. M.; Schaefer, W. P.; Labinger, J. A.; Bercaw, J. E. *Inorg Chem.* **1993**, *32*, 2863.
18. Blake, R. E. B. Ph.D. Thesis, Caltech, 1995.
19. Kelson, E P. Ph.D. Thesis, Caltech, 1994.
20. Blake, R. personal communication.
21. Liang, L.; Stevens, E. D.; Nolan, S. P. *Organometallics* **1992**, *11*, 3459.
22. Malgren; Lamm. *Z. Anorg. Alleg. Chem.* **1940**, 103.
23. Day, V.W.; Klemperer, W.G. *J. Organomet. Chem.*, **1981**, *205*, C31.
24. Besecker, C.; Klemperer, W.G. *Inorg. Chem.*, **1990**, *29*, 2345.
25. Besecker, C.; Day, V.W.; Klemperer, W.G. *Organometallics* **1985**, *4*, 564.
26. Day, V.W.; Klemperer, W.G. *J. Am. Chem. Soc.*. **1990**, *112*, 2031.
27. Wang, R.-C., University of Illinois, at Urbana-Champaign, 1987.
28. Bell, R. N. *Inorg. Synth.*, Audrieth, L.F. ed., **1950**, *3*, 103.
29. Evertz, K unpublished result.
30. Lyon, D. personal communication
31. This work, along with additional work, appeared the following year in two publications: (a) Day, V. W.; Eberspacher, T. A.; Klemperer, W. G.; Planalp, R. P.; Schiller, P. W.; Yagasaki, A.; Zhong, B. *Inorg Chem.*, **1993**, *32*, 1629. (b) Klemperer, W. G.; Zhong, B. *Inorg Chem.*, **1993**, *32*, 5821.
32. Catellani, M; Halpern, J. *Inorg Chem.*, **1980**, *19*, 566.
33. Koelle, U. *J. Organomet. Chem.* **1977**, *133*, 53. also, see Albers, M. O.; Coville, N. J. *Coord. Chem. Rev.* **1984**, *53*, 227 for a review on CO substitutions.
34. Colton, R.; Farthing, P. *Aust. J. Chem.*, **1971**, *24*, 903.
35. Dehand, J.; Rose, J. *J. Chem. Res.(S)* **1979**, 155.
36. Bernhard, P; Buer, M; Ludi, A. *Polyhedron* *9*, **1990**, 1095.
37. Ferguson, J. E.; Love, J. E. *Inorg Synth.* Cotton, F. A. ed. **1972**, *13*, 208.
38. Chatt, J.; Hayter, R.G. *J. Chem. Soc.*, **1961**, 896.
39. Griffith, W. P.; Pawson. *J. Chem. Soc., Dalton Trans.* **1973**, 1315.

40. Bennett, M. A.; Smith, A. K. *J. Chem. Soc., Dalton Trans.* **1974**, 233.
41. Saltzman, H.; Sharefkin, J. G.; *Org. Synth.* , Muslick, B. C. ed. **1963**, *43*, 60.

Chapter 2

Homogeneous Ziegler-Natta Catalysis

Abstract

A brief introduction to homogeneous Ziegler-Natta olefin polymerization is presented. The development of metallocene-based catalysts has been spurred by the superior properties of the homogeneously polymerized materials as well as by the potential of the homogeneous catalysts to produce new materials. Synthetic and mechanistic studies have established that the active species in the group IV polymerizations are the cationic metallocene alkyls. The well-defined nature of the active species in the homogeneous polymerizations has resulted in an unprecedented degree of control over the properties of the resulting material. Isoelectronic neutral group III metallocene catalysts have facilitated mechanistic studies on the fundamental steps involved in the polymerization of olefins. Neutral group IV metallocene analogues have been prepared by substitution of a divalent ligand for one of the Cp ligands of the metallocene. The neutral analogues display similar chemistry to the cationic metallocenes, though their activity is reduced. One cause of this reduced activity is the coordination of B-H bonds in the ligand to the electrophilic metal center. The aminoborole ligand is proposed as an improved Cp analogue, since it has no B-H bonds.

It has long been known that mixtures of group IV halides and alkyl aluminums are highly active for the polymerization of α-olefins,[1] and these systems, termed Ziegler-Natta catalysts, are used commercially to generate billions of pounds of polyolefins every year. These catalysts, however, are poorly defined mixtures, and their heterogeneous nature renders characterization of the active catalytic species difficult. Early transition metal metallocenes are one of the most widely studied classes of organometallic compounds.[2] In 1980, Sinn and Kaminsky[3] discovered that the addition of methylaluminoxane (MAO) to group IV metallocenes, such as Cp_2MCl_2 (M = Ti, Zr, Hf), resulted in new species that were highly active homogeneous olefin polymerization catalysts. As a consequence of this discovery, research in metallocene chemistry has gained new momentum (eq. 1).[4] The new homogeneous metallocene polymerization catalysts have several advantages over heterogeneous catalysts: they produce polymers with narrow molecular weight distributions; in many cases they are more active than the heterogeneous catalysts; they are much more efficient in co-polymerizations; and most interesting for organometallic chemists, homogeneous catalysts provide an opportunity for rational catalyst design.

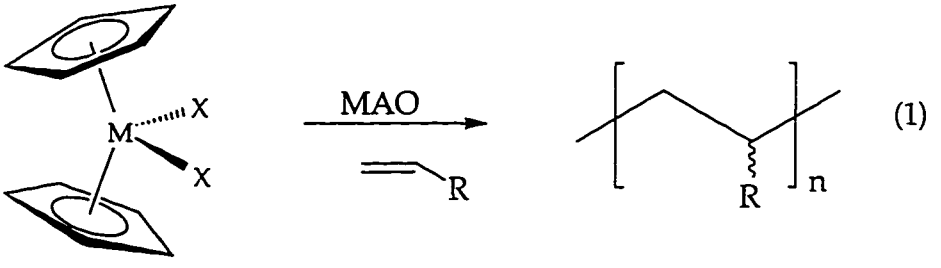

M=Ti,Zr,Hf
X= Cl,Me

A great deal of effort has been directed towards understanding both the steric and electronic factors which are involved in stereospecific olefin polymerization. Rigid ligand environments based on linked cyclopentadienyls (Cps), or *ansa*-metallocenes, have been used to probe the steric requirements for stereoregular olefin insertion. Both chiral and achiral metallocenes have been prepared and used as catalysts. The microstructures of the resulting polymers include atactic, syndiotactic,[5] isotactic,[6] hemiisotactic,[5,7] and stereoblock[8] (Figure 1). The microstructure of the polymers have profound effects on their physical properties; atactic

polypropylene, for instance is a gummy solid while isotactic polypropylene is a hard, crystalline material. Isotactic polypropylene is currently the most commercially important stereoregular polyolefin, though there is considerable interest in the potential of new materials such as syndiotactic or stereoblock polypropylene. The accessibility of such a wide variety of polymer microstructures from these metallocene catalysts is one of the major forces driving the design of new catalysts.

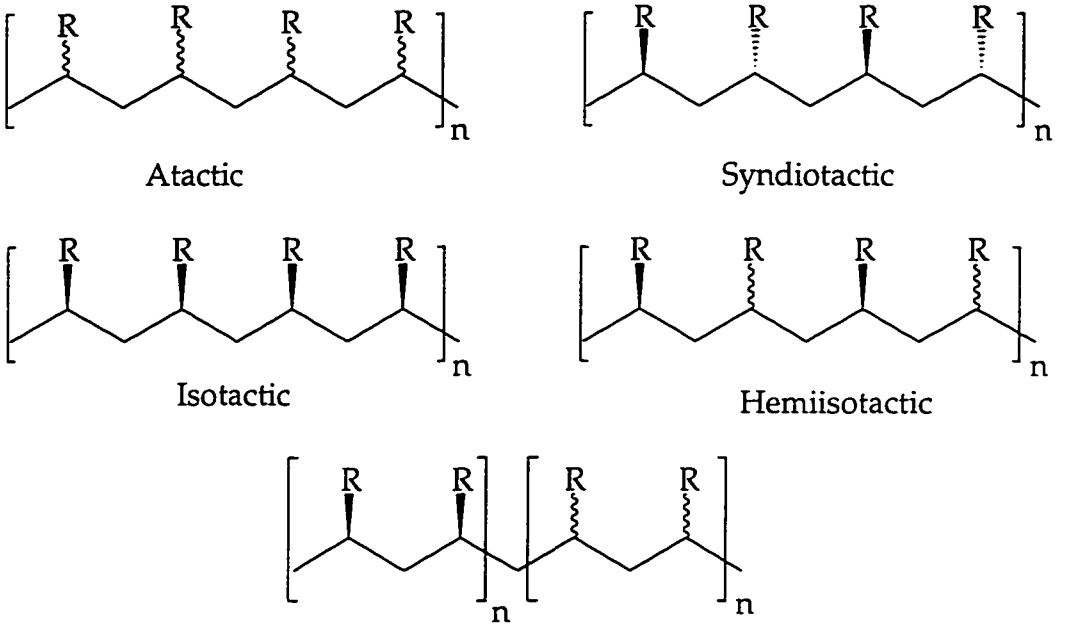

Figure 1: Polyolefin Microstructures

The electronic requirements for olefin polymerization have also been investigated. It is now generally accepted that the active catalytic species in Ziegler-Natta polymerization are d^0, 14 electron complexes of the type $[Cp_2MR]$ (M = Sc,Y, Ln, Ti^+, Zr^+, Hf^+) (Figure 2). The realization of this requirement has been due to two factors. The first was the observation that the neutral group three and lanthanide metallocene alkyls, d^0 14e species, are catalysts for olefin polymerization.[9] This result strongly implicated the isoelectronic group IV metallocenium cations as catalysts. Further evidence

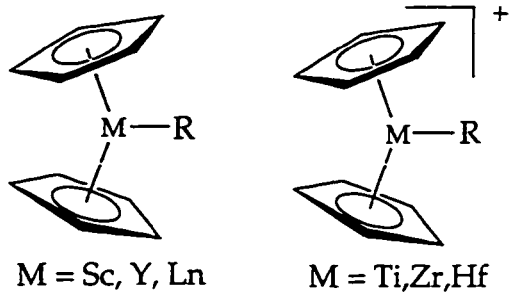

d^0, 14 electron species

Figure 2: Active Species in Homogeneous Ziegler-Natta Catalysis

appeared more slowly. The poorly understood nature of the oligomeric MAO and the necessity of using a large excess made it difficult to determine its role in activation and thus the identity of the active catalytic species. It was not until the development of new co-catalysts, capable of the stoichiometric activation of metallocene dialkyls, that cationic metallocene alkyls were isolated and established as the catalytic species in Ziegler-Natta polymerization.[10] Based on this work and the work of others,[11] it is now accepted that the role of MAO as an activator is to both alkylate metal halides to form metal alkyls, and to abstract halide to generate the active cationic species.

The new stoichiometric activators are all formally based on the ability to remove an alkyl anion, R^-, from the coordination sphere of the metallocene.[12] This can occur in a single step, as in the heterolytic cleavage of a metal alkyl bond by protonolysis or abstraction by a powerful Lewis acid, or in a sequence of steps, as in the one-electron oxidation of a metal alkyl bond, with subsequent loss of alkyl radical (Figure 3). The cations generated in this way are extremely Lewis acidic, and commonly form unreactive tight ion pairs or react irreversibly with the counter ions.[13] This problem has led to the development of polyfluorinated aryl-borate counterions, which are very weakly coordinating and relatively inert to the irreversible reactions that plague other counterions. Even using these so called non-coordinating anions, however, the catalyst reactivity is often related to the extent of ion separation, and the catalysts are unstable at room temperature in the absence of olefins. Thus, the catalysts must be generated *in situ*, further complicating

kinetic studies. As a consequence, some of the early mechanistic work on olefin polymerization by metallocene catalysts was conducted using

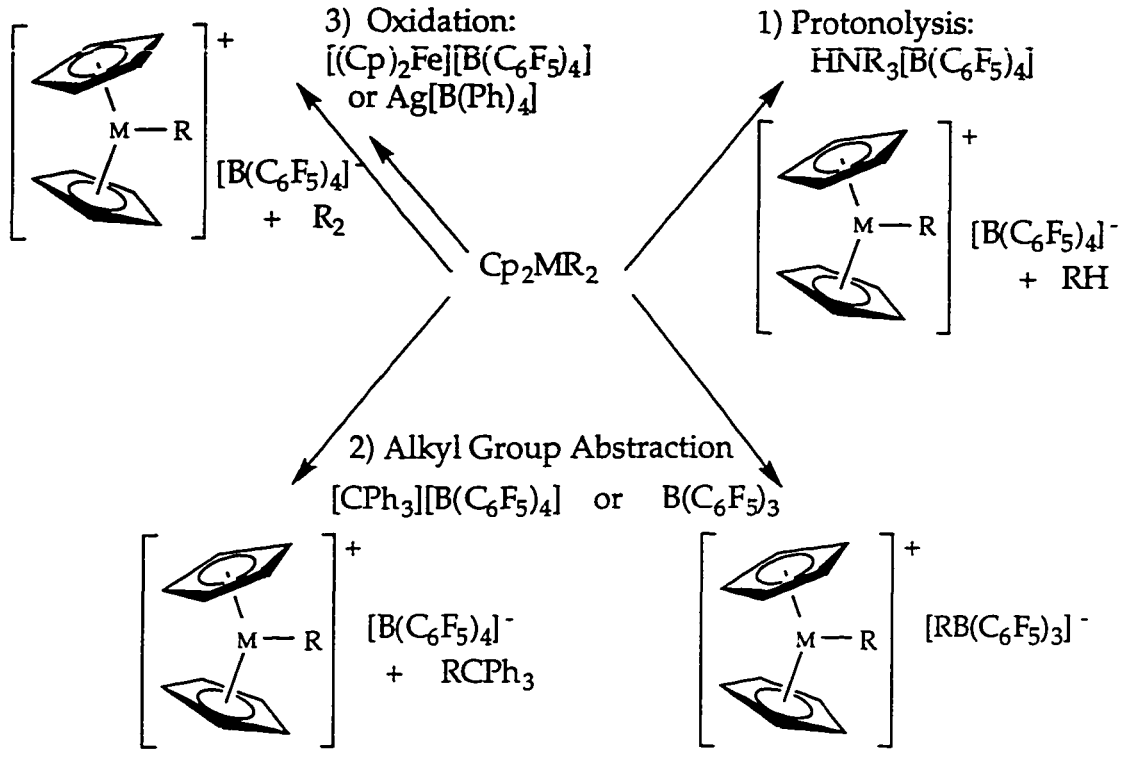

Figure 3: Metallocene Activation Methods

the neutral group III and lanthanide complexes where counterion effects were not an issue. These complexes are more stable than the cationic catalysts and also do not have the complications of counterion pairing. The neutral complexes are generally much less active for olefin polymerization, but this difference usually facilitates the mechanistic studies rather than the reverse.

Watson and coworkers were the first to use neutral d^0, 14e metallocenes as models for the active species in Ziegler-Natta polymerizations.[5a] They prepared the lutetium metallocene, Cp^*_2LuMe, which inserted olefins to form alkyls that underwent reactions such as β-hydride elimination, β-methyl elimination, and σ-bond metathesis. This system thus demonstrated all the reactions, for both chain propagation and chain termination steps, involved in olefin polymerization. One difference between the lutetium system and the cationic ones is the reactivity towards α-olefins; both systems are quite active for ethylene polymerization, but the

neutral lutetium pentamethylcyclopentadienyl metallocenes only oligomerizes higher olefins such as propylene.

Bercaw and coworkers have also studied the chain propagation and chain termination steps in Ziegler-Natta polymerizations , using permethylscandocene derivatives.[5c] The complexes rapidly polymerize ethylene at room temperature, but do not oligomerize α-olefins. Instead they form alkanes and alkenyl complexes via σ-bond metathesis reactions after the first insertion (eq. 2). This observation was rationalized on the basis of bad steric interactions between the ligands and the incoming olefin in the transition state for olefin insertion, resulting in the less crowded σ-bond metathesis transition state being favored.[14]

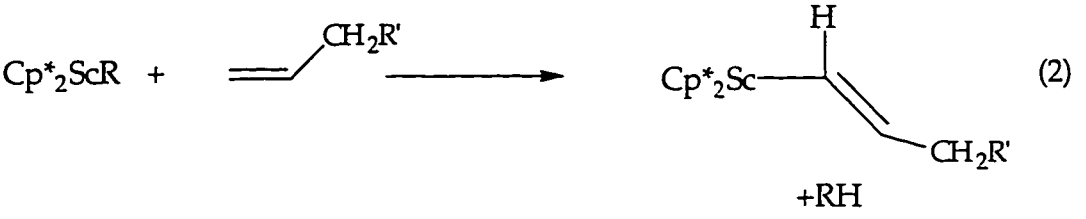

(2)

Modifications to the pentamethylcyclopentadienyl ligands to reduce their effective steric bulk have resulted in complexes that show increased reactivity towards α-olefins. The first such modification was to link the two Cp* groups via a dimethylsilylene linker. This linker has the effect of making the angle between the planes of the two Cp ligands more acute, thus opening the "wedge" of the metallocene. The resulting complex shows increased activity for olefin insertion compared to the unlinked species. The OpSc(H)PMe_3 and $[DpSc(\mu\text{-}H)]_2$ complexes are catalysts for olefin dimerization and α,ω-diene cyclization (Figure 4).[15] The reduction in the steric protection of the metal has the unfortunate complication, however, of allowing the metallocenes to dimerize (i.e. $[DpSc(\mu\text{-}H)]_2$). This is especially true when the ligands bonded in the wedge of the metallocene are good bridging ligands, such as hydrides or halides. The dimers are much less reactive than the monomers and in many cases, it is believed that the slowest step in the catalytic cycle is the dissociation of the dimers to the active monomers. Further reduction of the steric bulk of the ligand does in fact result in complexes which are active for the polymerization of α-olefins. The Cp*SiNRSc complex, shown in Figure 4, is

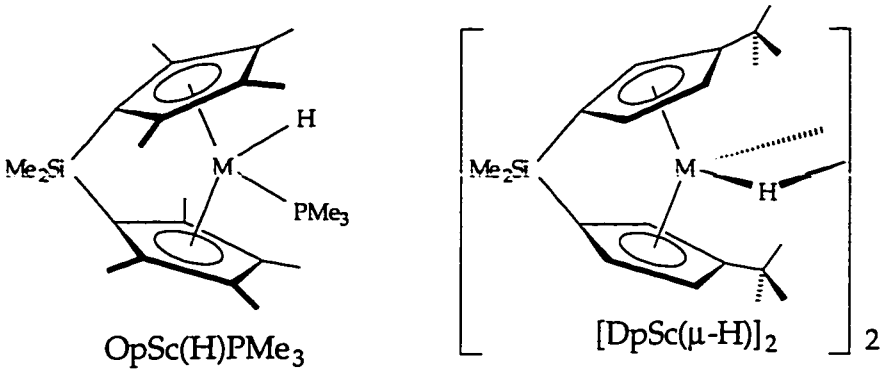

Olefin Dimerization/Cyclization Catalysts

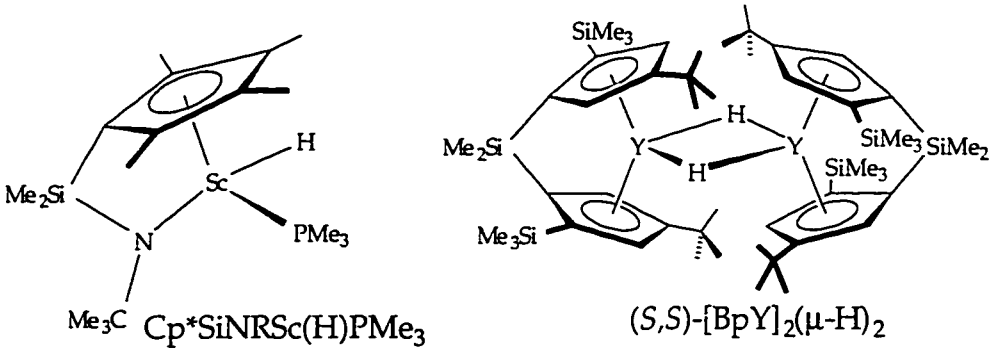

Olefin Polymerization Catalysts

Figure 4: Neutral Catalysts With Linked Cp's

both sterically and electronically less saturated than those previously discussed, since the formal replacement of a Cp ligand by an amide results in a net loss of two bonding electrons at the metal center. This complex polymerizes ethylene and α-olefins at room temperature. The C_2-symmetric Bp complex is a stereoregular olefin polymerization catalyst, producing highly isotactic polymers. These complexes demonstrate how rational design has led to successive improvements in catalysts, and underscore the potential of this approach in developing new polymerization catalysts.

The success of many groups in developing neutral homogeneous group III and lanthanide polymerization catalysts has led to efforts to prepare neutral group IV complexes capable of olefin polymerization. Neutral group IV polymerization catalysts might perhaps combine the advantages of both group III and cationic group IV catalysts, and so are an area of potential importance. Such complexes can be prepared by substitution of one of the Cp

ligands of a group IV metallocene with a divalent cyclopentadienyl analogue. The best known divalent analogues to cyclopentadienyl are the family of *nido*-carbaborane ligands. Hawthorne first pointed out that the dicarbollide dianion, $C_2B_9H_{11}^{2-}$, is isolobal to Cp^- and the which both have 6π electrons in delocalized orbitals that can coordinate to metals on a pentagonal face.[16] Since the first preparation of ferrocene analogues by Hawthorne and his coworkers over thirty years ago, many carbaborane complexes of transition metal,[17] lanthanide and actinide,[13b] and main group elements[18] have been.

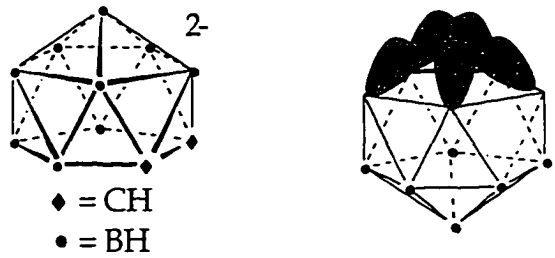

Figure 5: The Dicarbollide Anion and Its Orbitals For Metal Bonding

prepared. Despite their overall similarity, there are some key differences between carbaboranes and Cp ligands. The orbitals of the dicarbollide ligand are directed towards the center of the pentagonal face of the ligand, rather than perpendicular to it, as for the π-orbitals of Cp (Figure 5).[19] This "focusing" of the orbitals, along with the increased charge of the ligand compared to Cp, contribute to dicarbollide's improved ability to stabilize higher oxidation states relative to cyclopentadienyl. For instance, $(C_2B_9H_{11})_2Ni$, a rare example of an organometallic Ni^{IV} complex, is quite stable. The size of the dicarbollide ligand has been estimated as comparable to that of the pentamethylcyclopentadiene, which perhaps also helps to account for its ability to stabilize metals in atypical oxidation states.[20] A number of early transition metal carbaborane complexes have been prepared, though in most cases their reactivity was not studied in detail.

Jordan and coworkers were the first to undertake a systematic investigation of group IV dicarbollide complexes as metallocene analogs.[21] Treatment of Cp^*MMe_3 (M= Zr, Hf) with the diprotonated form of the ligand, $C_2B_9H_{13}$, results in the formation of sparingly soluble species whose structure was not originally known, but which were formulated as

$\{Cp^*(C_2B_9H_{11})MMe\}_x$ (M= Zr, Hf) (eq. 3). These species exhibit electrophilic reactivity characteristic of d^0, 14e metallocenes (Figure 6). For instance, the

$$Cp^*MMe_3 + C_2B_9H_{13} \xrightarrow{-2CH_4} \{Cp^*(C_2B_9H_{11})MMe\}_x \quad (3)$$

methyl derivatives polymerize ethylene, oligomerize propylene, insert 2-butyne, coordinate ligands, and upon thermolysis, lose an equivalent of methane to form μ-methylidene complexes. The structure of the Zr complex resulting from the insertion of 2-butyne shows that one of the C-H bonds of the methyl group on the α-carbon is coordinating to the metal. Such donation, termed a β-agostic interaction, is frequently observed for highly electrophilic complexes.[22] The titanium derivative was found to be unstable at room temperature, forming a fulvene derivative, (η^6-$C_5Me_4CH_2$)(η^5-$C_2B_9H_{11}$)Ti, via a σ-bond metathesis between the titanium methyl group and one of the methyls of the Cp*.[23] However, in studies of $Cp^*(C_2B_9H_{11})TiMe$ prepared *in situ*, this complex also showed electrophilic reactivity, such as ethylene dimerization, acetonitrile insertion, and PMe_3 coordination. The lower reactivity of the titanium derivative towards olefins compared to the Zr and Hf analogues was rationalized by the increase in effective steric crowding for the smaller 3d metal, as compared to the 4d and 5d elements.

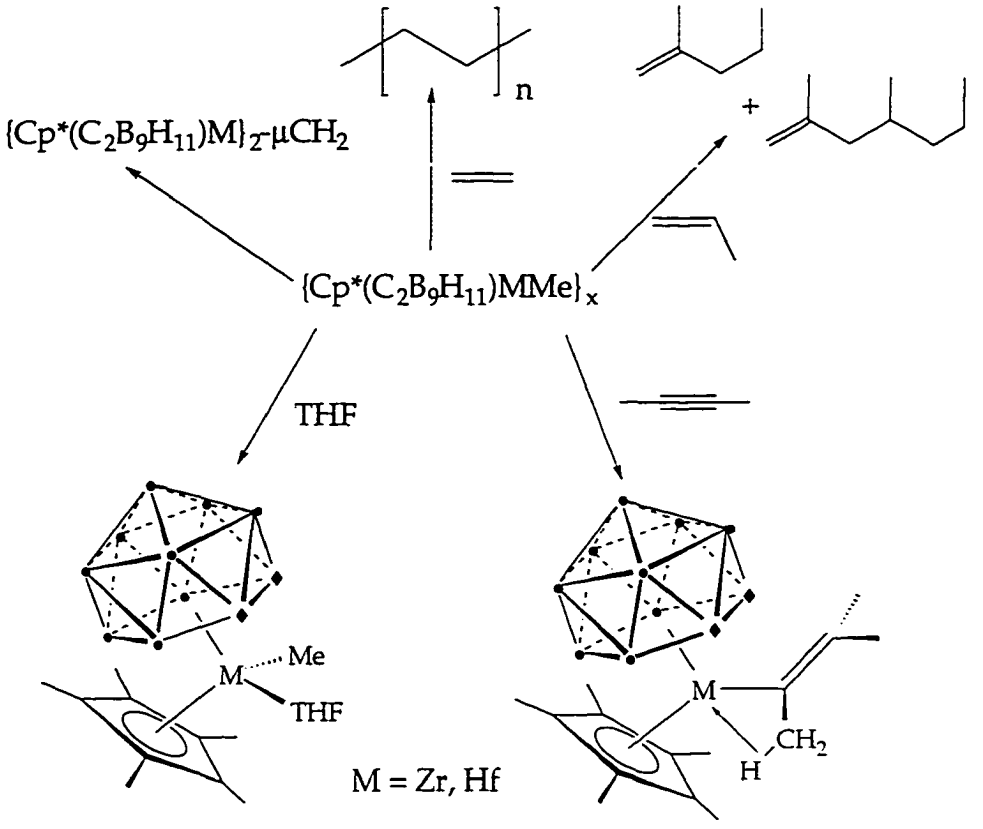

Figure 6: Reactivity of Group IV Dicarbollide Complexes

Recently, the structure of the sparing soluble complex previously formulated as $\{Cp^*(C_2B_9H_{11})HfMe\}_x$ was determined[24]. Surprisingly, the structure revealed the complex to be an unsymmetrical dimer containing one η^5-$(C_2B_9H_{11})$ ligand and one bridging dicarbollide (Figure 7). The structure was described as containing $Cp^*(\eta^5\text{-}C_2B_9H_{11})Hf^+$ and $Cp^*HfMe_2^+$ fragments bridged by a $C_2B_9H_{11}^{2-}$ group. The $Cp^*(\eta^5\text{-}C_2B_9H_{11})Hf^+$ fragment binds to the bridging dicarbollide via two B-H bonds on the open face of the dicarbollide. The $Cp^*HfMe_2^+$ fragment binds to the bridging dicarbollide via three B-H bonds, one of which is on the open face of the dicarbollide and the other two of which are in plane below. The authors point out that this structure raises questions about the exact nature of the active species for the ethylene polymerization exhibited by these complexes (Figure 6).

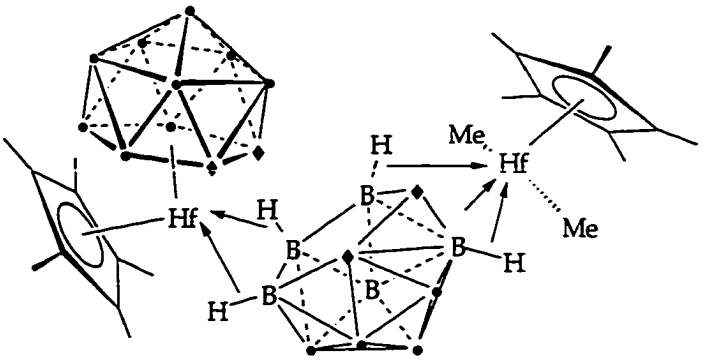

Figure 7: Structure of $\{Cp^*(C_2B_9H_{11})HfMe\}_x$

Jordan has also prepared and structurally characterized several tantalum dicarbollide complexes as potential metallocene analogs. $Cp(C_2B_9H_{11})TaMe_2$[25] and $(C_2B_9H_{11})_2TaMe_2Li$[26] have both been structurally characterized, and while they show some characteristics of electrophilic metallocenes (i.e. formation of an "ate" anionic complex by coordination of a second equivalent of MeLi for the bis(dicarbollide) complex), their reactivity towards olefins has not been reported.

Bercaw and coworkers have prepared dicarbollide derivatives of scandium and characterized alkyl and hydride derivatives.[27] Treatment of $[Cp^*Sc_2]x$ with $Na_2(C_2B_9H_{11})$ and addition of THF result in the formation of $Cp^*(C_2B_9H_{11})Sc(THF)_3$. This species can be alkylated with $LiCH(TMS)_2$, resulting in the formation of the anion $Li[Cp^*(C_2B_9H_{11})Sc(CH(TMS)_2)]$. This species does not react with ethylene, though it does react slowly with dihydrogen to form a dimeric hydride (eq. 4). The crystal structure shows clearly that the two scandium centers are bridged by B-H bonds of the

$$Li[Cp^*(C_2B_9H_{11})Sc(CH(TMS)_2)] \xrightarrow{H_2,\ 2\ weeks} \left[\ \right]^{2-} \quad (4)$$

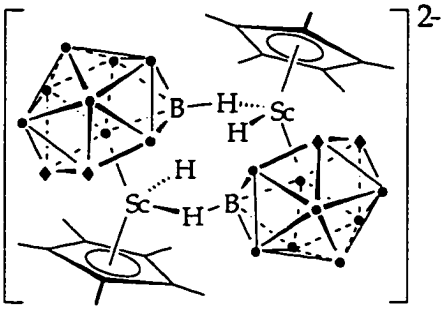

dicarbollide ligand. Such bridging interactions have been found for a number of dicarbollide complexes.[20,28] In the case of the scandium complex, the bridging interaction is strong enough to overcome the Coulombic repulsion

between the two anionic fragments, and even donor ligands (THF, PMe_3) or olefins do not break up the dimer.

The smaller carbaboranes $C_2R_2B_4H_4^{2-}$ (R = Et, TMS) have also been employed as ligands in early transition metal chemistry. Hosmane has prepared a number of lanthanide and group IV carbaborane complexes.[13,14,29] These complexes are structurally very similar to bent metallocenes, though as yet the alkyl derivatives and their reactivity have not been reported. Several of the complexes of the smaller carbaboranes also reveal agostic B-H interactions, both with lithium counterions, and with electrophilic transition metal centers.

Grimes and Finn and their coworkers have prepared a tantallocene analogue with hydrocarbyl ligands, the benzyne complex $Cp(C_2Et_2B_4H_4)Ta(\eta^2\text{-}C_6H_4)(PMe_3)$.[30] Remarkably, the complex is air and moisture stable, in contrast to other transition metal benzyne derivatives. The complex does not undergo coupling reactions with unsaturated substrates such as acetylenes or aldehydes. The low reactivity of this complex was attributed to the stabilizing power of the carbaborane ligand.

The results from these investigations supported the notion that substitution of a Cp with a divalent analogue could indeed lead to complexes whose reactivity mimicked that of the metallocenium cations. One disadvantage of the Cp analogues that were employed in these studies is that they all contained electron rich B-H bonds which readily coordinated the electrophilic metal centers. This coordination reduced the unsaturation at the metal center and thus the reactivity of the complexes. Use of dianionic ligands without such coordinating bonds might thus increase the reactivity of the resulting complexes. Herberich and his coworkers have synthesized several derivatives of boroles, which are formally divalent Cp analogues containing no B-H bonds (Figure 8).[31]

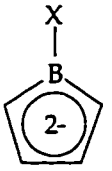

Figure 8: The Borole Ligand
($X = CH_3$, Ph, OR, NR_2)

Herberich has prepared many borole complexes of electron-rich, late transition metals.[32] One complication of borole chemistry is the competition between deprotonation of the ligand and nucleophilic attack at boron. Thus, attempts to deprotonate the borolene C_4H_6BR (R = alkyl, Ph) result in formation of borate species or intractable mixtures of the borates along with the deprotonated species (Figure 9).[33] As a consequence, the synthesis of alkyl and phenyl borole complexes involve a dehydrogenation reaction of the diprotonated form of the ligand rather than a discrete borollide dianion. This

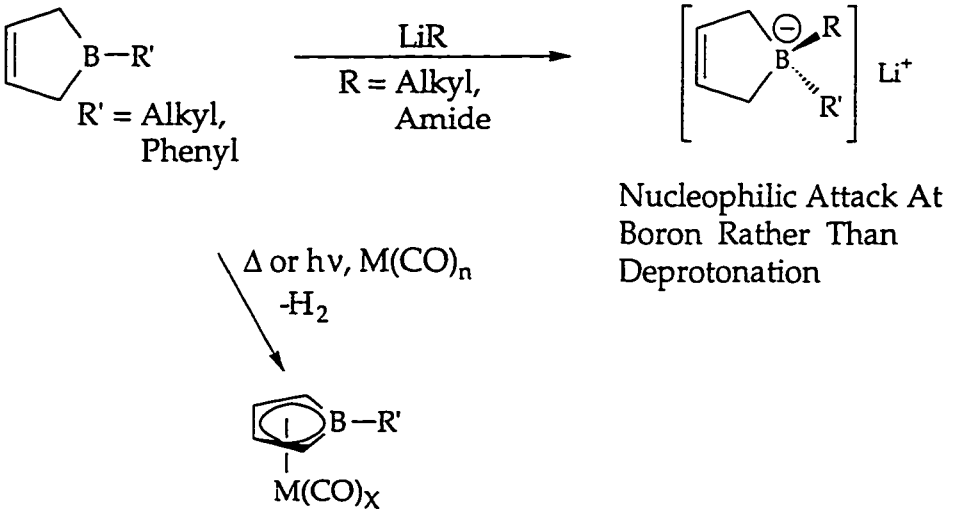

Figure 9: Synthesis of Alkyl Borole Derivatives

limitation presents a problem for applying the ligand to early transition metal chemistry. The common starting materials for these elements are already in their highest formal oxidation state and so are unable to participate in the oxidative/dehydrogenation reactions required to form the boroles from the borolenes. Fortunately, Herberich has found that amino groups provide sufficient steric and electronic protection of the boron to suppress the competitive quaternization reaction. Thus, treatment of an aminoborolene

with two equivalents of a bulky deprotonating agent results in the isolation of the borollide salt, $Li_2[C_4H_4BNR_2]$ (eq. 5).[34]

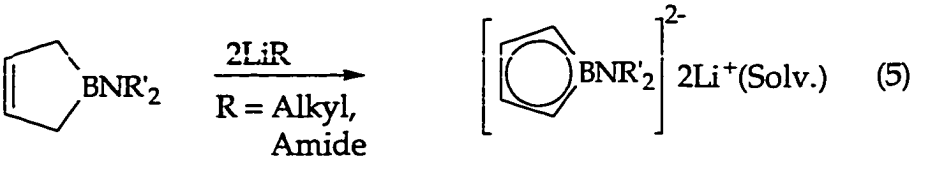

(5)

The boron-nitrogen interaction has profound consequences for the bonding within the borole, however. By competing with the π-electrons of the borole for the vacant orbital on boron, the nitrogen inhibits delocalization in the heterocycle. The B-N interaction thus reduces the aromaticity of the borole and raises the energy of its π-orbitals. Herberich has examined the bonding in aminoborole complexes of later transition metals and concluded that the best valence bond representation of the bonding is the neutral diene-like resonance form **B** rather than the borollide resonance form **A** (Figure 10).[35] Early transition metals are much more electropositive than later metals, so the diene-like form should contribute proportionately less in the bonding in these complexes. However, the amino group may also affect the reactivity of the early transition metal complexes in a more direct way. The proximity of the Lewis basic amino group to the electrophilic metal center may permit the two sites to react in a cooperative fashion. Such cooperativity might lead to activity for the heterolytic cleavage of bonds, for instance.

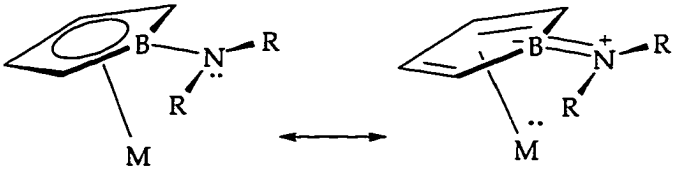

A - η^5 (M^{II}) Divalent Borollide Resonance Form

B - η^4 (M^0) Neutral Diene Resonance Form

Figure 10: Bonding in Aminoborole Complexes

In summary, early transition metal complexes of the borole ligand such as the ones shown in Figure 11 are isoelectronic to metallocenes and thus are of interest as neutral analogues of metallocenium catalysts. The complexes

also provide a method to compare the effects of charge and metal independantly of one another. Thus cationic hafnium complexes can be compared to neutral hafnium ones, and neutral group III and IV complexes compared to each other.

The borole ligand was chosen to avoid the complications other Cp analogues suffer from. The borole ligands lack coordinating B-H bonds, and so their complexes may be more reactive than those of the dicarbollide ligand. Additionally, the π-orbitals of the borole more nearly approximate the π-orbitals of Cp than those of carbaborane ligands do, which may also contribute to increased activity. The following two chapters describe the synthesis and characterization of group IV aminoborolle complexes and the study of their metallocene-like reactivity. Chapter 3 focuses on the synthesis of alkyl derivatives and the investigation of their reactivity with olefins and other unsaturated species. Chapter 4 focuses on studies of the amphiphilic character of the aminoborole complexes, in which the amino group of the borole acts in cooperation with the Lewis acidic metal center to heterolyze H-X bonds.

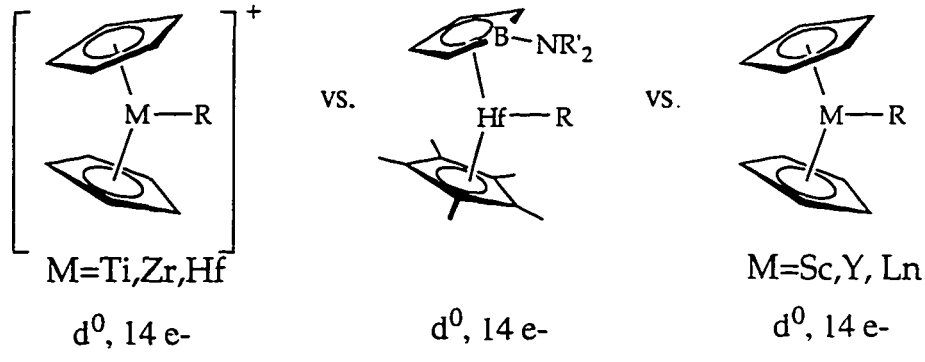

Figure 11: Aminoborole Complex Isoelectronic to Metallocene Olefin Polymerization Catalysts

References and Notes

1. Ziegler, K; Holzkamp, E; Breil, H; Martin, H. *Angew. Chem.* **1955**, *67*, 541.
2. (a) *Comprehensive Organometallic Chemistry II* Wilkinson, G.; Stone, F.G.A.; Abel, E.W., Eds.; Pergamon Press: Oxford, U.K.; **1995**; Vol. 4, chapters 2, 4-12. (b) *Comprehensive Organometallic Chemistry*, Wilkinson, G.; Stone, F.G.A.; Abel, E.W., Eds.; Pergamon Press: Oxford, U.K., **1982**; Vol. 3.
3. Sinn, H.; Kaminsky, W. *Adv. Organomet. Chem.* **1980**, *18*, 99.
4. (a) Brintzinger, H.H.; Fischer, D.; Mulhaupt, R.; Rieger, B.; Waymouth, R.M. *Angew. Chem. Intl. Ed. Eng.* **1995**, *34*, 1143. (b) Horton, A.D. *Trends Polym. Sci.* **1994**, *2*, 158.
5. Ewen, J. A.; Jones, R. L.; Razavi, A.; Ferrara, J. D. *J. Am. Chem. Soc.* **1988**, *110*, 6255.
6. Brintzinger's C2 symmetric catalyst was the first example: Kaminsky, W.; Kulper, K, Brintzinger, H. H.; Wild, F. R. W. P. *Angew. Chem. Intl. Ed. Eng.* **1985**, *24*, 507. However, a number of chiral catalysts, many of them C_2 symmetric, have been shown to produce isotatic PP, see ref. 4a for details
7. The exact assignment of the microstructure of this polymer is in dispute.
8. Coates, G. W.; Waymouth, R. M. *Science* **1995**, *267*, 217.
9. (a) Watson, P.L. *J. Am. Chem. Soc.* **1982**, *104*, 337. (b) Jeske, G.; Lauke, H; Mauermann, H.; Sweptson, P.N.; Schumann, H.; Marks, T.J. *J. Am. Chem. Soc.* **1985**, *107*, 8091. (c) Burger, B.J.; Thompson, M.E.; Cotter, W.D.; Bercaw, J.E. *J. Am. Chem. Soc.* **1990**, *112*, 1566. (d) den Haan, K. H.; Wielstra, Y; Teuben, J. H. *Organometallics* **1987**, *6*, 2053. (e) Evans, W. J.; Dominguez, R.; Hanusa, T. P. *Organometallics* **1986**, *5*, 263.
10. Jordan, R.F. *Adv. Organomet. Chem.*, **1991**, *32*, 325.
11. (a) Long, W. P.; Breslow, D. S. *Liebigs. Ann. Chem.* **1975**, 463. (b) Harlan, C. J.; Bott, S. G.; Barron, A. R. *J. Am. Chem. Soc.* **1995**, *117*, 6465.

12. Guram, A.; Jordan, R.F. In *Comprehensive Organometallic Chemistry II* Wilkinson, G.; Stone, F.G.A.; Abel, E.W., Eds.; Pergamon Press: Oxford, U.K.; **1995**; Vol. 4, 589.
13. (a) Strauss, S.H. Chem. Rev., 1993, 93, 927. (b) Bochmann, M. *Angew. Chem. Intl. Ed. Eng.* **1992**, *31*, 1181.
14. Thompson, M. E.; Baxter, S. M.; Bulls, A. R.; Burger, B. J.; Nolan, M. C.; Santarsiero, B. D.; Schaefer, W. P.; Bercaw, J. E. *J. Am. Chem. Soc.* **1987**, *109*, 203.
15. (a) Piers, W. E.; Shapiro, P. J.; Bunel, E. E.; Bercaw, J. E. *J. Am. Chem. Soc.* **1987**, *109*, 203. (b) Bunel, E. E. Ph. D. Thesis, Caltech, 1989.
16. Hawthorne, M. F.; Young, D. C.; Wegner, P. A. *J. Am. Chem. Soc.* **1965**, *87*, 1818.
17. For leading references, see (a) *Comprehensive Organometallic Chemistry II* Wilkinson, G.; Stone, F.G.A.; Abel, E.W., Eds.; Pergamon Press: Oxford, U.K.; **1995**; Vol. 1, chapter 9. (b) Saxena, A. K.; Hosmane, N. S. *Chem. Rev.* **1993**, *93*, 1081.
18. For leading references, see (a) *Comprehensive Organometallic Chemistry II* Wilkinson, G.; Stone, F.G.A.; Abel, E.W., Eds.; Pergamon Press: Oxford, U.K.; **1995**; Vol. 1, chapter 7.
19. Mingos, D. M. P. *J. Chem. Soc., Dalton Trans.* **1977**, 602. Dewar, M. J. S.; McKee, M. L. *Inorg, Chem.* **1980**, *19*, 2662.
20. Hanusa, T. P. *Polyhedron* **1982**, *1*, 663.
21. Crowther, D. J.; Baenziger, N. C.; Jordan, R. F. *J. Am. Chem. Soc.* **1991**, *113*, 1455.
22. Brookhart, M; Green, M. L. H.; Wong, L. -L. *Prog. Inorg. Chem.* **1988**, *36*, 1.
23. Kreuder, C.; Jordan, R. F.; Zhang, H. *Organometallics* **1995**, *14*, 2993.
24. Crowther, D. J.; Swenson, D. C.; Jordan, R. F. *J. Am. Chem. Soc.* **1995**, *117*, 10403.
25. Uhrhammer, R.; Crowther, D. J.; Olson, J. D.; Swenson, D. C.; Jordan, R. F. *Organometallics* **1992**, *11*, 3098.
26. Uhrhammer, R.; Su, X. -Y.; Swenson, D. C.; Jordan, R. F. *Inorg, Chem.* **1994**, *33*, 4398.
27. Bazan, G. C.; Schaefer, W. P.; Bercaw, J. E. *Organometallics* **1993**, *12*, 2126.

28. (a) Behnken, P. E.; Marder, T. B.; Baker, R. T.; Knobler, C. B.; Thompson, M. R.; Hawthorne, M. F. *J. Am. Chem. Soc.* **1985**, *107*, 32. (b) Hlatky, G. G.; Turner, H. W.; Eckman, R. R. *J. Am. Chem. Soc.* **1989**, *111*, 2728. (c) Yang, X.; King, W. A.; Sabat, M.; Marks, T. J. *Organometallics* **1993**, *12*, 4254.

29. Hosmane, N. S.; Wang, Y.; Zhang, H.; Maguire, J. A.; Waldhor, E.; Kaim, W.; Binder, H.; Kremer, R. K. *Organometallics* **1994**, *13*, 4156.

30. Houseknecht, K. L.; Stockman, K. E.; Sabat, M.; Finn, M. G.; Grimes, R. N. *J. Am. Chem. Soc.* **1995**, *117*, 1163.

31. (a) *Comprehensive Organometallic Chemistry II* Wilkinson, G.; Stone, F.G.A.; Abel, E.W., Eds.; Pergamon Press: Oxford, U.K.; **1995**; Vol. 1, chapter 5, pp. 202-204. (b)

32. (a) Herberich, G. E.; Boveleth,W.; Hessner, B.; Koffer. D. P. J.; Negele, M.; Saive, R. *J. Organomet. Chem.* **1986**, *308*, 153. (b) Herberich, G. E.; Buschges, U.; Hessner, B.; Luthe, H. *J. Organomet. Chem.* **1986**, *312*, 13. (c) Herberich, G. E.; Hessner, B.; Saive, R. *J. Organomet. Chem.* **1987**, *319*, 9. (d) Herberich, G. E.; Boveleth,W.; Hessner, B.; Hostalek, M; Koffer. D. P. J.; Negele, M.; *J. Organomet. Chem.* **1987**, *319*, 311. (e) Herberich, G. E.; Hessner, B.; Negele, M.; Howard, J. A. K. *J. Organomet. Chem.* **1987**, *336*, 29. (f) Herberich, G. E.; Negele, M. *J. Organomet. Chem.* **1988**, *350*, 81. (g) Herberich, G. E.; Hessner, B.; Koffer. D. P. J.; *J. Organomet. Chem.* **1989**, *362*, 243. (h) Herberich, G. E.; Hausman, I; Hessner, B.; JNegele, M.;. *Organomet. Chem.* **1989**, *362*, 259.

33. Substituted borole dianions have been prepared by reduction of the corresponding dienes: $K_2[C_4BPh_5]$ Eisch, J. J.; Galle, J. E.; Kozima, S. *J. Am. Chem. Soc.* **1986**, *107*, 253. $K_2[C_4BEt_3Me_2]$: Wrackmeyer, B. *Organometallics* **1984**, *3*, 1. Their coordination chemistry has not been explored except for one report on complexes of the pentaphenylborole: Herberich, G. E.; Buller, B.; Hessner, B.; Oschman W. *J. Organomet. Chem.* **1980**, *195*, 253.

34. (a) Herberich, G. E.; Ohst, H. *Z. Naturforsch.* **1983**, *B38*, 1388. (b) Herberich, G. E.; Hostalek, M.; Laven, R.; Boese, R. *Angew. Chem. I ntl. Ed. Eng.* **1990**, *31*, 1181.

35. Herberich, G. E.; Hessner, B.; Ohst, H.; Raap, I. A. *J. Organomet. Chem.* **1988**, *348*, 305. Authors prepared *cis*-$Cr(CO)_2(C_4H_4BN(CHMe_2)_2)_2$ and $Mn(CO)(C_4H_4BN(CHMe_2)_2)_2$ and structurally characterized the complexes. Comparison of the aminoborole structures with phenylborole complexes of the same metals show that the boron-metal bonds in the aminoborole complexes are considerably longer. Similarly, based on the boron nitrogen and boron carbon bond distances, there is considerable B-N double bond character and little B-C double bond character in the complexes. Based on the structural evidence, the authors conclude the aminoborole ligand is η^4-bound. The similarity between the EPR spectra of $Mn(CO)(C_4H_4BN(CHMe_2)_2)_2$ and its butadiene analogue support the conclusion that the metal centers in the complexes are formally zero valent.

Chapter 3

Synthesis and Reactivity of Pentamethylcyclopentadienyl Aminoborole Complexes of Group IV

Abstract

The preparations of chloro, iodo, and allyl derivatives of pentamethylcyclopentadienyl aminoborole hafnium and zirconium complexes are described. The chloro derivative, $Cp^*[C_4H_4BN(CHMe_2)_2]HfCl{\cdot}LiCl$, is prepared by treatment of Cp^*HfCl_3 with $Li_2(THF)\{C_4H_4BN(CHMe_2)_2\}$. The structures of the chloro derivatives $Cp^*[C_4H_4BN(CHMe_2)_2]HfCl{\cdot}LiCl(Et_2O)_2$ and $\{Cp^*[C_4H_4BN(CHMe_2)_2]HfCl{\cdot}LiCl\}_2$ were determined by single crystal X-ray analysis. Cp^*HfI_3 is prepared from Cp^*HfCl_3 and BI_3. The iodo derivative, $Cp^*[C_4H_4BN(CHMe_2)_2]HfI{\cdot}LiI(THF)$, was prepared by treatment of Cp^*HfI_3 with $Li_2(THF)\{C_4H_4BN(CHMe_2)_2\}$. Treatment of $Cp^*[C_4H_4BN(CHMe_2)_2]HfCl{\cdot}LiCl$ with allyl magnesium bromide yields $Cp^*[C_4H_4BN(CHMe_2)_2]Hf(\eta^3\text{-}C_3H_5)$, whose structure was determined by X-ray analysis. The allyl species was active for the polymerization of ethylene, but not for the polymerization of α-olefins. Addition of ligands to the allyl derivative results in the formation of $Cp^*[C_4H_4BN(CHMe_2)_2]Hf(C_3H_5)(L)$ (L = PMe_3, pyridine, CO). The structure of $Cp^*[C_4H_4BN(CHMe_2)_2]Hf(\eta^3\text{-}C_3H_5)(CO)$ was determined by X-ray analysis. Treatment of $Cp^*[C_4H_4BN(CHMe_2)_2]Hf(\eta^3\text{-}C_3H_5)(CO)$ with PMe_3 results in the formation of the dieneolate complex $Cp^*[C_4H_4BN(CHMe_2)_2]Hf(OCHCHCHCH_2)(PMe_3)$. $Cp[C_4H_4BN(CHMe_2)_2]ZrCl{\cdot}LiCl(Et_2O)x$ is prepared by treatment of $CpZrCl_3$ with $Li_2(THF)\{C_4H_4BN(CHMe_2)_2\}$. Addition of $LiC_6H_4CH_2NMe_2$ to $Cp[C_4H_4BN(CHMe_2)_2]ZrCl{\cdot}LiCl(Et_2O)_x$ results in the formation of $Cp[C_4H_4BN(CHMe_2)_2]Zr(C_6H_4CH_2NMe_2)$. The Cp zirconium complex did not react with olefins. $[C_4H_4BN(CHMe_2)_2]_2Hf(PMe_3)_2$ was prepared by treatment of $HfCl_4$ with two equivalents of $Li_2(THF)\{C_4H_4BN(CHMe_2)_2\}$ and excess PMe_3. The electronic spectra of several aminoborole complexes were investigated and the low energy transitions assigned as borole-metal charge transfer transitions.

1. Introduction

The initial goal of the project was to prepare stable, soluble complexes containing both the desired ancillary ligands, pentamethylcyclopentadienyl and aminoborole. Alkylation of this species would then afford the target complex, $Cp^*(C_4H_4BN(R)_2)MR'$. For this project, the diisopropylaminoborole was chosen as the borole ligand, and hafnium chosen as the group IV metal.

The choice of the diisopropylamino substituent over dimethylamino or diethylamino substituents was dictated by the expected higher solubility and stability for this derivative compared to the smaller dimethyl and diethyl derivatives. Herberich has prepared complexes of each of the three aminoboroles, and found that the diisopropylamino substituent resists substitution more effectively than either of the other smaller substituents.[1] Since our principal interest in the ligand was as an ancillary one, the more resilient diisopropylamino derivative was the appropriate choice. It was also expected that the bulky isopropyl groups would best prevent the nitrogen from coordinating to large electrophiles such as the group IV metals. Additionally, the larger alkyl substituents should help to ensure the solubility of the aminoborole complexes in hydrocarbon solvents, a concern since electrophilic complexes often react with or bind irreversibly the more polar organic solvents.

Hafnium was chosen over the other group IV metals due to the superior stability of its highest oxidation state. Initially, we made several attempts to prepare titanium aminoborole complexes. However, all our attempts were unsuccessful. The results indicated that Ti^{IV} was reduced during the metallation reactions with the aminoborole salt. Efforts to prepare Ti^{III} aminoborole species also failed. Reasoning that the problems preparing Ti complexes were due to redox/disproportionation reactions, and that these were a result of the comparative stability of the lower oxidation states of Ti, we switched to hafnium. Hafnium, by virtue of the substantial difference in stabilities of its highest and lower oxidation states, is much less prone to reduction than is titanium. The zirconium analogues of many of the complexes described in this chapter have also been prepared and their characterization is described elsewhere.[2]

2a. Preparation of Chloro, Iodo, and Allyl Derivatives of Pentamethylcyclopentadienyl Aminoborole Hafnium Complexes

Treatment of Cp^*HfCl_3 with one equivalent of $Li_2(THF)\{C_4H_4BN(CHMe_2)_2\}$ in toluene, followed by work-up in petroleum ether, results in the isolation of $Cp^*[C_4H_4BN(CHMe_2)_2]HfCl{\cdot}LiCl$ (**1**) as an amorphous orange powder (eq. 1). As isolated, the product is sparingly soluble in hydrocarbon solvents, but its solubility is greatly improved by addition of just a few equivalents of ether or other heteroatom containing solvent. In THF-d_8 solution, $Cp^*[C_4H_4BN(CHMe_2)_2]HfCl{\cdot}LiCl$ is deep red in color and displays the expected C_s symmetry (^1H and ^{13}C NMR), consistent with a structure in which the two chlorides are bound symmetrically. The equivalence of all the methyl groups of the isopropyl substituents indicates that rotation about the B-N bond is fast on the NMR time scale.

$$Cp^*HfCl_3 + Li_2(THF)\{C_4H_4BN(CH(Me)_2)_2\} \xrightarrow[2.\ \text{Pet. Ether}]{1.\ \text{Toluene -LiCl}} \quad (1)$$

$Cp^*[C_4H_4BN(CH(Me)_2)_2]HfCl{\cdot}LiCl$
1 (orange powder)

Recrystallization of a sample of **1** by vapor diffusion of toluene into a diethyl ether solution results in the isolation of plate-shaped purple crystals of the bis(ether) adduct, **1-(Et$_2$O)$_2$**. A crystal was selected and an X-ray structure obtained. An ORTEP representation of the structure is shown in Figure 1, and selected bond distances and angles are listed in Table 1.

Comparison of the structure to those of other aminoborole complexes suggests that in the hafnium complex the aminoborole is η^5-bound. The B-N bond distance of 1.435(9) Å is slightly longer than that found for $[C_4H_4BN(CHMe_2)_2]_2Cr(CO)_2$ (1.423(4) Å) and $[C_4H_4BN(CHMe_2)_2]_2Mn(CO)$ (1.407(2) Å).[3] However, this distance and the planar bond angle around N do still indicate a strong boron-nitrogen interaction. The boron-carbon bond distances are slightly shorter for the hafnium derivative, implying greater delocalization in this derivative. The average B-C distance is 1.549(4) Å for $[C_4H_4BN(CHMe_2)_2]_2Cr(CO)_2$, 1.558(3) for $[C_4H_4BN(CHMe_2)_2]_2Mn(CO)$, and 1.526(10) Å for **1-(Et$_2$O)$_2$**. Unfortunately, as there are no alkyl- or aryl-borole complexes of hafnium to compare with, it is difficult to measure the effect of

the boron-nitrogen interaction on the metal-boron bond, as Herberich was able to do in the case of the chromium complex. A comparison of the ratio between the M-B bond (M = Hf, Cr, Mn) as found by X-ray crystallography and the sum of the covalent radii of M and B suggests stronger metal-boron bonding for **1-$(Et_2O)_2$**, however.[4] The Hf-B distance of 2.693 Å is 16% longer than the sum of the covalent radii (2.322 Å), while in $[C_4H_4BN(CHMe_2)_2]_2Mn(CO)$, the Mn-B distance is 26% greater than the covalent radii, and in $[C_4H_4BN(CHMe_2)_2]_2Cr(CO)_2$, the Cr-B bond is 22% longer than the sum of the covalent radii.

The other features of the structure are unexceptional. The bond lengths for the hafnium-chloride bonds are consistent with what is observed for other metallocene chloride lithium chloride adducts.[5] The difference between the two hafnium chloride bonds, 0.035 Å, is somewhat larger than usual, though by no means exceptional.[6]

Table 1. Selected Distances (Å)* and Angles (°)* for $Cp^*\{\eta^5\text{-}C_4H_4BN(CHMe_2)_2\}HfCl_2Li(Et_2O)_2$.

Hf -Cp*	2.219	Hf -C1	2.360(7)
Hf -Cl1	2.496(2)	Hf -C2	2.358(8)
Hf -Cl2	2.531(2)	Hf -C3	2.418(8)
Cl1 -Li	2.417(13)	Hf -C4	2.498(7)
Cl2-Li	2.410(13)	Hf -B	2.693(8)
Li-O1	1.921(14)	Cl1 -Hf -Cl2	87.7
Li-O2	1.962(14)	Cp* -Hf -$Centroid_{Bo}$	133.0
C1 -C2	1.390(11)	C5 -N -B	123.4
C2 -C3	1.382(12)	C8 -N -B	120.7
C3 -C4	1.442(11)	C8 -N -C5	115.6
B -N	1.435(9)		

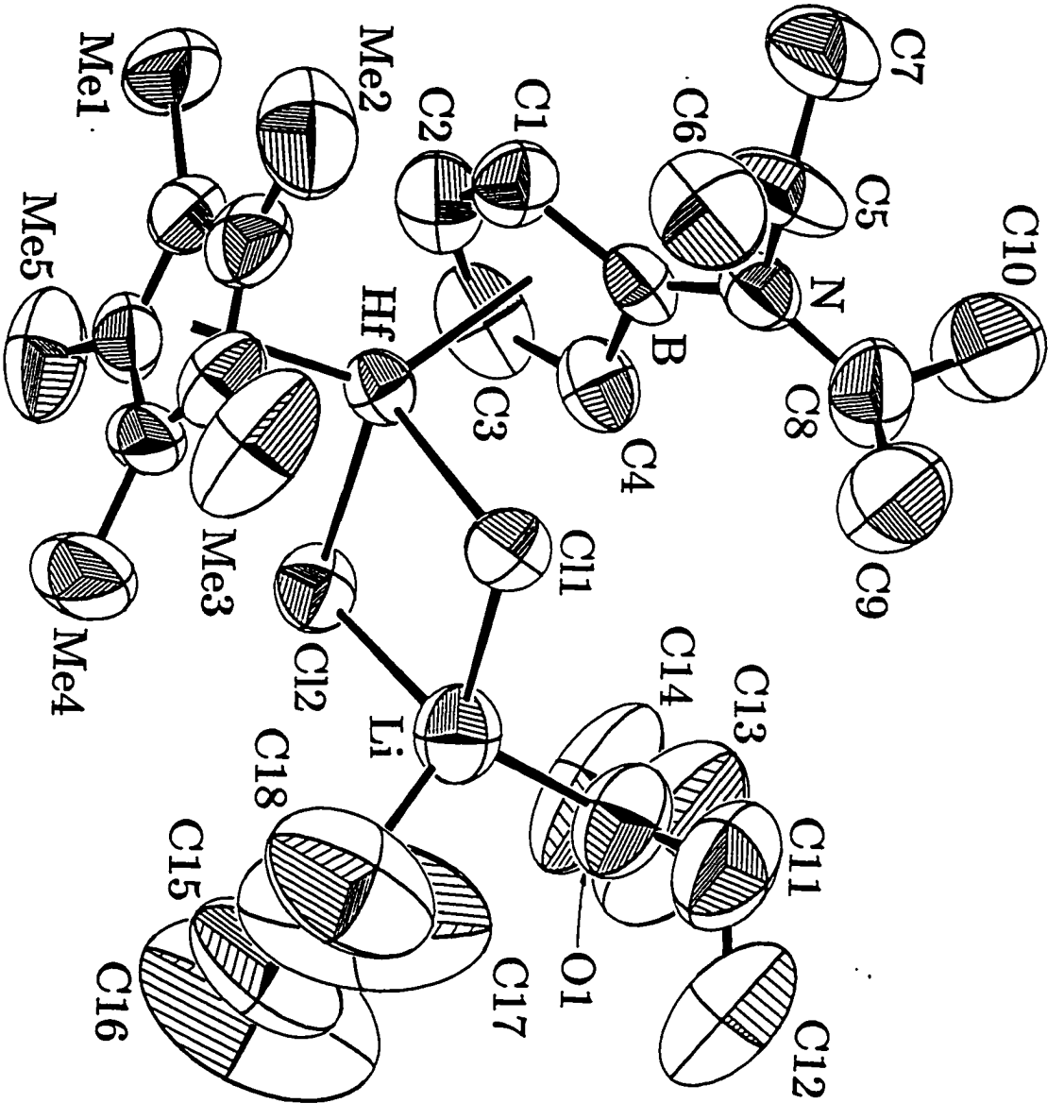

Figure 1: ORTEP Diagram of $Cp^*\{\eta^5\text{-}C_4H_4BN(CHMe_2)_2\}HfCl\cdot LiCl(Et_2O)_2$

Though the structure of **1-(Et_2O)$_2$** clarified the bonding of the crystalline solvated adduct, the exact nature of the solvent free species Cp*{η^5-$C_4H_4BN(CHMe_2)_2$}HfCl·LiCl was still unclear. The compound was an amorphous powder, and there was evidence for the presence of non-stoichiometric amounts of lithium chloride.[7] We were interested in the structure of the solvent free species for a number of reasons. First, the complex displayed considerable solvatochromic behavior, which was difficult to account for. Also, we were interested in how, in the absence of solvent, the coordination sphere of the lithium ion was filled. So when it was discovered that **1** could be recrystallized by heating at 80°C in a ~3:1 mixture of benzene:hexafluorobenzene for two weeks, we decided to have an X-ray structure determination made. A single orange-red crystal was selected and data was collected at low temperature (160 K).[8] An ORTEP drawing of the structure is shown in Figure 2, and selected bond distances and angles are listed in Table 2. Rigorous comparison of the bond lengths in the dimeric structure and in **1-(Et_2O)$_2$** is difficult because the two structures were determined at different temperatures (160 vs. 295 K). For this reason, discussion of the structure in Figure 2 will be limited to the differences in the overall structural features. The structure is dimeric, and the two halves of the dimer are related

Table 2. Selected Distances (Å)* and Angles (°)* for [Cp*{η^5-$C_4H_4BN(CHMe_2)_2$}$HfCl_2Li$]$_2$.

Hf -Cp*	2.207	Hf -C1	2.421(5)
Hf -Cl1	2.510(1)	Hf -C2	2.372(5)
Hf -Cl2	2.492(1)	Hf -C3	2.417(5)
Cl1 -Li	2.378(8)	Hf -C4	2.501(5)
Cl2-Li^i	2.450(8)	Hf -B	2.654(5)
Cl1-Li^i	2.693(8)	Cl1 -Hf -Cl2	88.0
Li-N	2.068(8)	Cp* -Hf -Centroid$_{Bo}$	132.0
C1 -C2	1.434(7)	C5 -N -B	114.2
C2 -C3	1.411(7)	C8 -N -B	113.0
C3 -C4	1.437(7)	C8 -N -C5	112.9
B -N	1.509(6)		

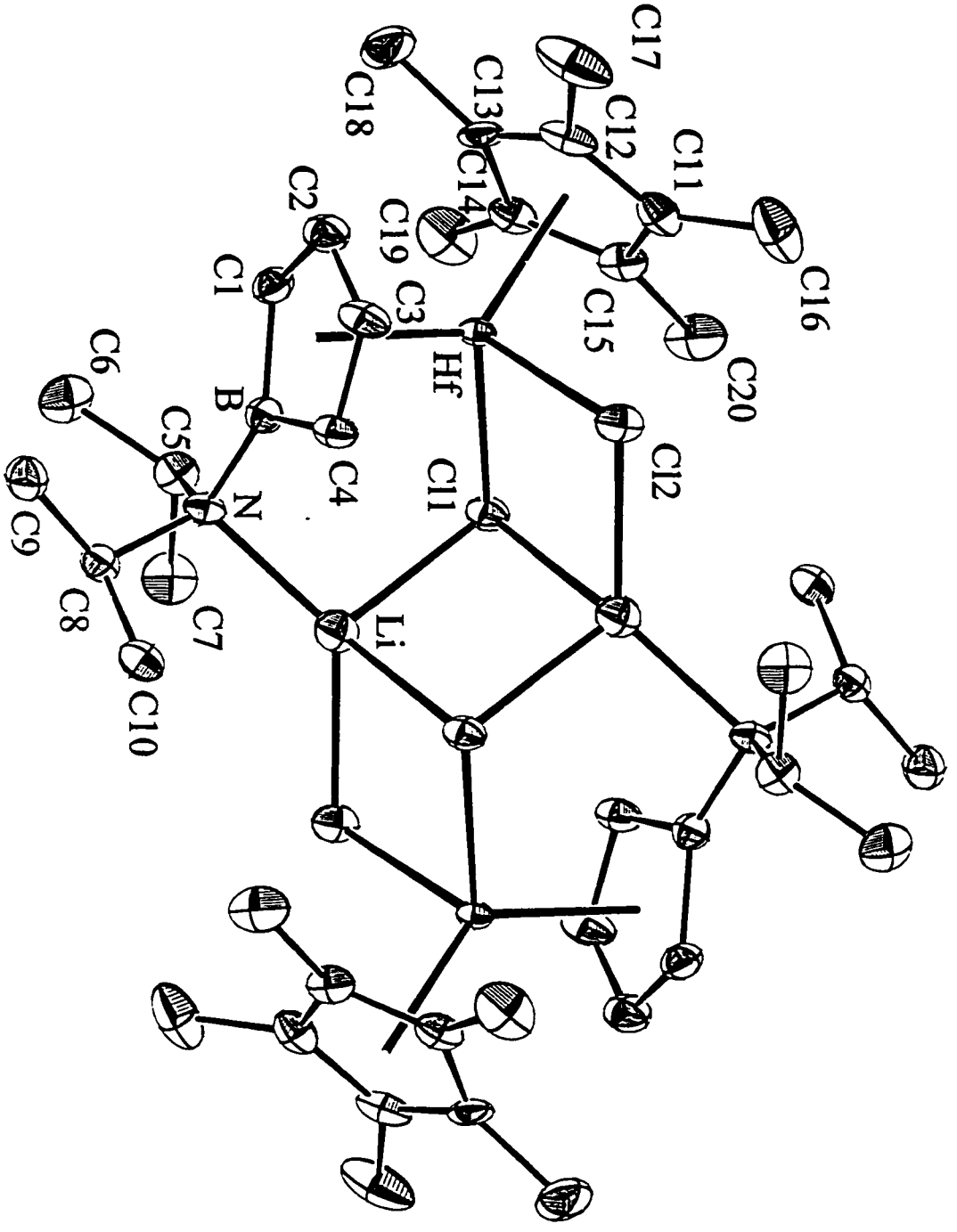

Figure 2: ORTEP Diagram of $[Cp^*\{\eta^5\text{-}C_4H_4BN(CHMe_2)_2\}HfCl_2Li]_2$

crystallographically by a center of symmetry. The bond lengths for the Cp* and chloride ligands are quite similar to those found in the structure of **1-$(Et_2O)_2$**. The principal difference between the two structures arises as a consequence of the coordination of the lithium ion by the amino group in the second structure. As shown in Figure 2, the nitrogen of each aminoborole ligand coordinates to the lithium ion which bridges the chlorides of the other half of the dimer. The N-Li distance of 2.068(8) Å is typical and representative of distances for Li bound to tertiary amines.[9] As a result of the lithium nitrogen interaction, the boron-nitrogen bond is lengthened considerably, to 1.509(6) Å. Thus, the coordination of the aminoborole ligand in this complex can be unambiguously described as pentahapto. The rather small difference in the Hf-B bond distances is consistent with a significant Hf-B interaction in both **1-$(Et_2O)_2$** and the dimer. Also, the striking difference in the color of the two derivatives suggest that the B-N interaction has an important effect on the energy of the transition in the visible region. This hypothesis is supported by the solvatochromism of the complex, since the coordination of lithium in solution will necessarily depend on the solvent.

Herberich has also noted that aminoboroles can coordinate lithium ion via the nitrogen of the amino group.[10] In the structure of $Li_2(C_4H_4BNEt_2)$·TMEDA (Figure 3), which is also a centrosymmetric dimer, two lithium ions are sandwiched between the two aminoboroles. The remaining Li(TMEDA) moieties are bound to the outer faces of the boroles. Each of the sandwiched lithium ions is η^5-coordinated to one aminoborole and η^1-coordinated to the amino group of the other. The lithium-N_{amino} bond distance is 2.028(3) Å, and the B-N bond distance is 1.515(3) Å, similar to the distances found in the structure of the hafnium dimer.

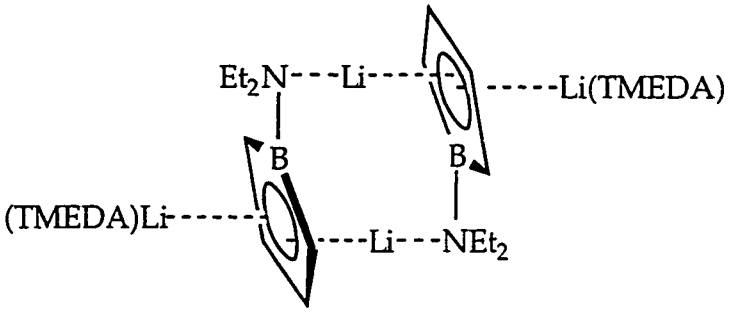

Figure 3: Structure of $Li_2(TMEDA)\{C_4H_4BNEt_2\}$

Due to its crystallinity, the dietherate complex **1-$(Et_2O)_2$** should, in principle, be the best starting material for preparing new aminoborole derivatives. However, it was found that the crystals partially desolvated over time, resulting in material containing non-stoichiometric amounts of ether. As this precluded an accurate and consistent value for the molecular weight, the unsolvated form of **1** was used in preference to **1-$(Et_2O)_2$** in further reactions of the complex.

Treatment of Cp*{η^5-$C_4H_4BN(CHMe_2)_2$}HfCl·LiCl with one equivalent of an alkyl lithium or Grignard reagent results, not in exclusive formation of the expected alkyl, Cp*{η^5-$C_4H_4BN(CHMe_2)_2$}HfR, but rather in the formation of mixtures of dialkyl "-ate" complexes, unreacted started material, and possibly the desired monoalkyl. This problem of over alkylation to form anionic species is frequently observed in the chemistry of the highly electrophilic group III, and lanthanide metallocenes.[11] Although use of the sterically bulky alkyl, $CH(SiMe_3)_2$, normally allows isolation of a neutral metallocene alkyl free of coordinated solvent and lithium halide, attempts to obtain Cp*{η^5-$C_4H_4BN(CHMe_2)_2$}HfCH$(SiMe_3)_2$ were uniformly unsuccessful. These mixtures were intractable, and resisted all efforts at purification. In general, the reactions with the largest alkyl groups were observed to be the cleanest by ^{1}H NMR. In favorable cases, alkylations with LiCH$(SiMe_3)_2$ at low temperature, there did appear to be one major product in ~75% yield. However, the very high solubility of the resulting alkyl species prevented their purification or recrystallization. Use of benzyl Grignard or benzyl potassium resulted in less soluble species that should have been easier to purify. However, repeated precipitations of the these products from mixed aromatic/aliphatic solvents did not result in improvements of the purity of the product as measured by ^{1}H NMR and elemental analysis. The oily nature of all the solids obtained, as well as the poor agreement of the elemental analyses with the expected values, suggested that all the products obtained were relatively impure. It is likely that the amino group's demonstrated ability to coordinate lithium ion contributed to the difficulties in purifying the alkyl derivatives. It has been recognized that salt coordination by electrophilic metal complexes is much more common when the alkali metal is ligated by donor atoms.[12]

Often, it is possible to avoid salt coordination by employing alkylating agents based on metals other than lithium. The relatively high solubility of LiCl favors salt coordination, thus switching to alkylating agents based on other alkali metals, magnesium, or even main group metals suppresses salt formation due to the lower solubility of these metal halides. Complex **1**, however, already contains an equivalent of lithium chloride, so there is always lithium ion in the reaction mixture during the alkylations. For this reason, it is not surprising that use of potassium, magnesium, and zinc alkyls did not effect the clean conversion of **1** to the desired alkyl.

Reasoning that the larger size of iodide and weaker hafnium-halogen bond energy might disfavor the coordination of excess iodide, we set out to prepare the iodo aminoborollide derivatives of hafnium. Treatment of Cp^*HfCl_3 with one equivalent of BI_3 in toluene yields the off-white solid, Cp^*HfI_3 (**2**) (eq. 2). The triiodide complex **2**, obtained in 85% yield, is considerably more soluble in aromatic solvents than is Cp^*HfCl_3.

$$Cp^*HfCl_3 + BI_3 \longrightarrow \underset{\mathbf{2}}{Cp^*HfI_3} + BCl_3 \qquad (2)$$

The reaction between Cp^*HfI_3 and $Li_2\{C_4H_4BN(CHMe_2)_2\}(THF)$ affords a blue microcrystalline powder, which analyzes approximately as $Cp^*\{\eta^5\text{-}C_4H_4BN(CHMe_2)_2\}HfI\cdot LiI(THF)$ (**3**) (eq. 3).

$$Cp^*HfI_3 + Li_2(THF)\{C_4H_4BN(CH(Me_2)_2)\} \longrightarrow \underset{\mathbf{3}}{Cp^*Hf\{C_4H_4BN(CH(Me_2)_2)\}I\cdot LiI(THF)} \qquad (3)$$

The presence of a molecular mirror plane of symmetry, evident from the ^1H, is further evidence for the presence of an equivalent of coordinated LiI. In contrast to the what is found for **1**, the peak for the methyl groups of the isopropyls of **3** appears as a broad hump at room temperature, suggesting that B-N bond rotation is comparable to the NMR time scale. Upon heating to the sample 70°C, the peak sharpens into the expected doublet. The origin of the increase in the barrier to B-N bond rotation in the iodo derivative is unclear. It may be that the two large iodides in the wedge of the pseudo-

metallocene inhibit B-N rotation due to steric interactions with the isopropyl groups. Alternatively, intra or intermolecular coordination of the lithium ion by the amino group may hinder rotation of this group. The retention of only one equivalent of coordinated solvent by the iodide derivative is also different from what is found for the chloride derivative. The origin of this difference is unclear, though the larger size of iodide may again be responsible.

Unfortunately, $Cp^*\{\eta^5\text{-}C_4H_4BN(CHMe_2)_2\}HfI\cdot LiI(THF)$ was found to react with alkylating agents identically to the chloride derivative.

Failure of our attempts to prepare simple monoalkyl derivatives led to a new strategy to employ an alkyl group that could chelate, and thus prevent coordination of solvent, halide, and additional alkylate. The allyl ligand has a well precedented ability to chelate to d^0 early transition metals,[13] and has even been shown to form stable complexes of the type $[Cp^*_2M(\eta^3\text{-}C_3H_5)]^+$ (M = Ti, Zr),[14] isoelectronic to the desired complexes $Cp^*\{\eta^5\text{-}C_4H_4BN(CHMe_2)_2\}Hf(\eta^3\text{-}C_3H_5)$.

Treatment of $Cp^*\{\eta^5\text{-}C_4H_4BN(CHMe_2)_2\}HfCl\cdot LiCl$ with allyl magnesium bromide in diethyl ether does indeed yield the desired allyl complexes, $Cp^*\{\eta^5\text{-}C_4H_4BN(CHMe_2)_2\}Hf(\eta^3\text{-}C_3H_5)$ (**4**), free of coordinated solvent and halide (eq. 4).

$$Cp^*\{\eta^5\text{-}C_4H_4BN(CHMe_2)_2\}HfCl\cdot LiCl + (C_3H_5)MgBr \xrightarrow[-LiCl\ -MgBrCl]{Et_2O} \mathbf{4} \quad (4)$$

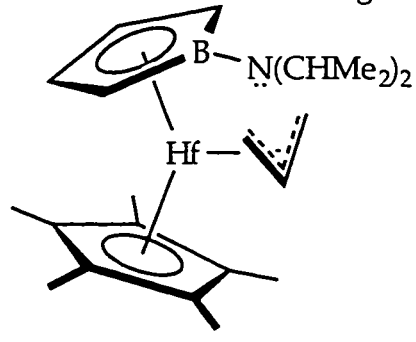

4

The deep blue allyl complex, **4**, is best purified by recrystallization from hot heptane. The complex displays a molecular plane of symmetry (^1H and ^{13}C NMR); the allyl hydrogens appear as an AM_2X_2 spin system at room temperature (300 MHz), consistent with η^3-coordination. This AM_2X_2 spin system is maintained even at 80°C, indicating that the allyl is strongly η^3 coordinated. Addition of donors ligands dramatically lowers the barrier for η^3-η^1 interconversion. At room temperature, in the presence of one equivalent of a donor ligand (*e. g.* THF, PMe_3, pyridine), the allyl hydrogens appear as an AX_4 spin system, consistent with rapid η^3-η^1 interconversion on the NMR time scale.

In order to confirm the η^3-coordination of the allyl, a single crystal of **4** was selected, and an X-ray structure obtained. An ORTEP drawing of the molecule is shown in Figure 4. Selected bond distances and angles are listed in Table 3. Overall, the bond distances and angles for the Cp* and aminoborollide ligands are very similar to those found in the structure of $Cp^*\{\eta^5\text{-}C_4H_4BN(CHMe_2)_2\}HfCl\cdot LiCl(Et_2O)_2$. The B-N bond distance of 1.414(10) Å indicates considerable double bond character. As expected, the allyl ligand is bound symmetrically: the carbon-carbon bond distances are essentially identical and the hafnium-carbon distances are all very similar.

Table 3. Selected Distances (Å)* and Angles (°)* for $Cp^*\{\eta^5\text{-}C_4H_4BN(CHMe_2)_2\}Hf(\eta^3\text{-}C_3H_5)$.

Hf -Cp*	2.185	Hf -C1	2.428(8)
Hf -C11	2.460(10)	Hf -C2	2.365(8)
Hf -C12	2.423(10)	Hf -C3	2.374(8)
Hf -C13	2.451(10)	Hf -C4	2.421(8)
B -C1	1.559(12)	Hf -B	2.691(9)
B -C4	1.572(12)	C11 -C12 -C13	124.1
B -N	1.414(10)	Cp* -Hf -$Centroid_{Bo}$	134.9
C1 -C2	1.411(11)	C5 -N -B	124.3
C2 -C3	1.392(12)	C8 -N -B	118.4
C3 -C4	1.424(11)	C8 -N -C5	114.9
C11 -C12	1.364(14)		
C12.-C13	1.369(14)		

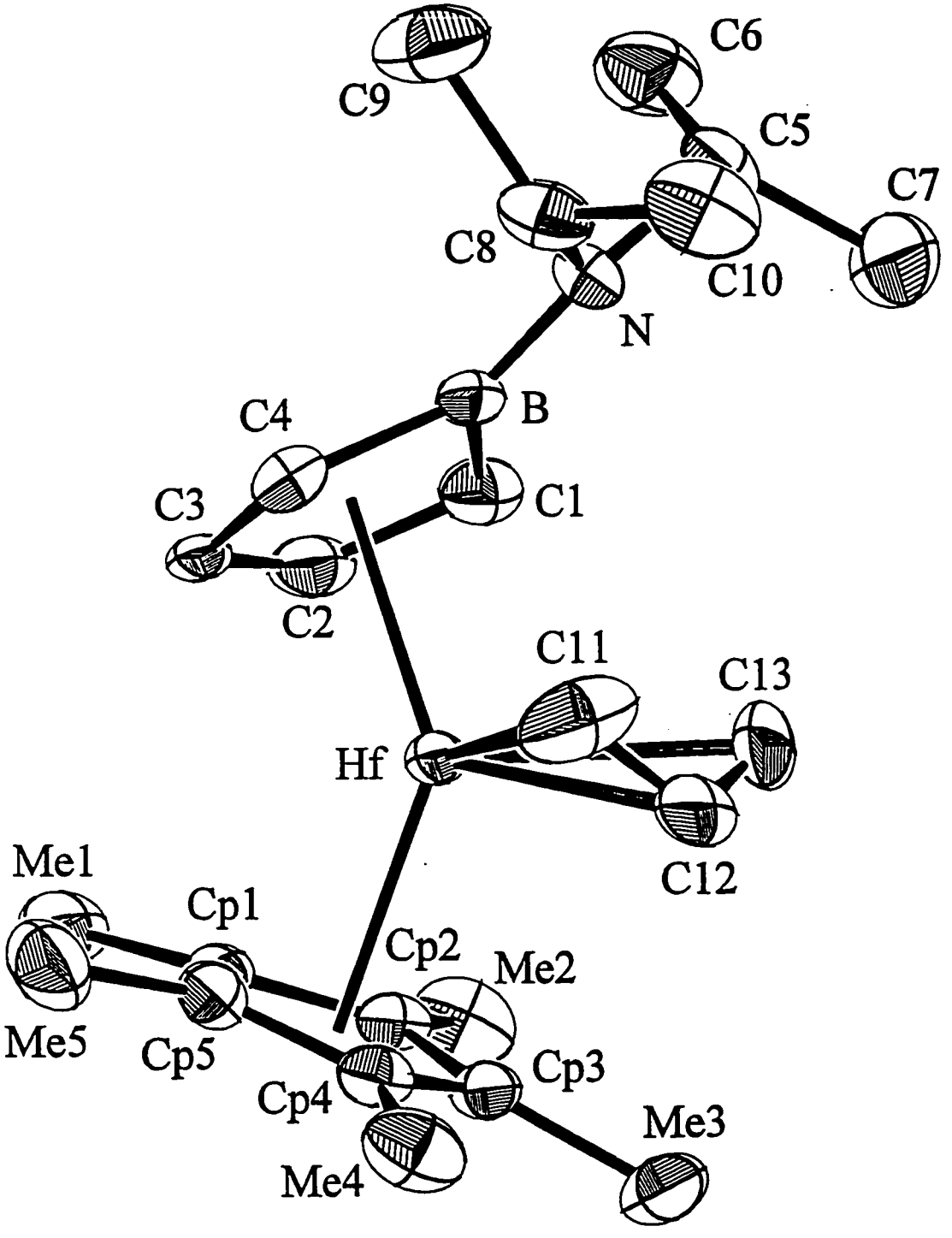

Figure 4: ORTEP Diagram of $Cp^*\{C_4H_4BN(CHMe_2)_2\}Hf(\eta^3\text{-}C_3H_5)$

2b. Reactions of the Allyl Derivative

The addition of PMe_3 to $Cp^*\{C_4H_4BN(CHMe_2)_2\}Hf(\eta^3\text{-}C_3H_5)$ results in a large blue shift in the visible transition of the allyl complexes from blue to yellow. This dramatic color change permitted study of this equilibrium by titrating **4** with PMe_3 and monitoring the disappearance of the band in the visible region with UV-vis spectroscopy. At 23°C, K_{eq} for the addition of PMe_3 to the hafnium allyl, **4**, was found to be 2200 M^{-1} (Figure 5).

As discussed previously, in the presence of PMe_3 the allyl hydrogens appear as an AX_4 spin system, which indicates only that there is rapid η^3-η^1 interconversion of the allyl and does not distinguish between (η^1-C_3H_5) and (η^3-C_3H_5) structures. IR spectroscopy has been found to be a useful method for distinguishing between η^3- and η^1-coordinated allyls.[15] The presence of a medium-to-weak intensity stretch at 1523 cm^{-1} in the IR spectrum of $Cp^*\{\eta^5\text{-}C_4H_4BN(CHMe_2)_2\}Hf(C_3H_5)(PMe_3)$ is consistent with η^3-coordination. So the PMe_3 adduct is formulated as $Cp^*\{\eta^5\text{-}C_4H_4BN(CHMe_2)_2\}Hf(\eta^3\text{-}C_3H_5)(PMe_3)$ (**5**).

Addition of pyridine to allyl **4** results in a less dramatic color change, from blue to purple. The NMR spectrum of the pyridine adduct is similar to that of $Cp^*\{\eta^5\text{-}C_4H_4BN(CHMe_2)_2\}Hf(\eta^3\text{-}C_3H_5)(PMe_3)$; however, IR evidence suggests that the allyl ligand is η^1-bound in this case.[16] Since pyridine almost certainly coordinates to hafnium in the wedge of the pseudometallocene, (η^3-C_3H_5) coordination may well be precluded. Thus the available evidence suggests the 16 electron formulation for $Cp^*\{\eta^5\text{-}C_4H_4BN(CHMe_2)_2\}Hf(\eta^1\text{-}C_3H_5)(py)$ (**6**) (Figure 6).

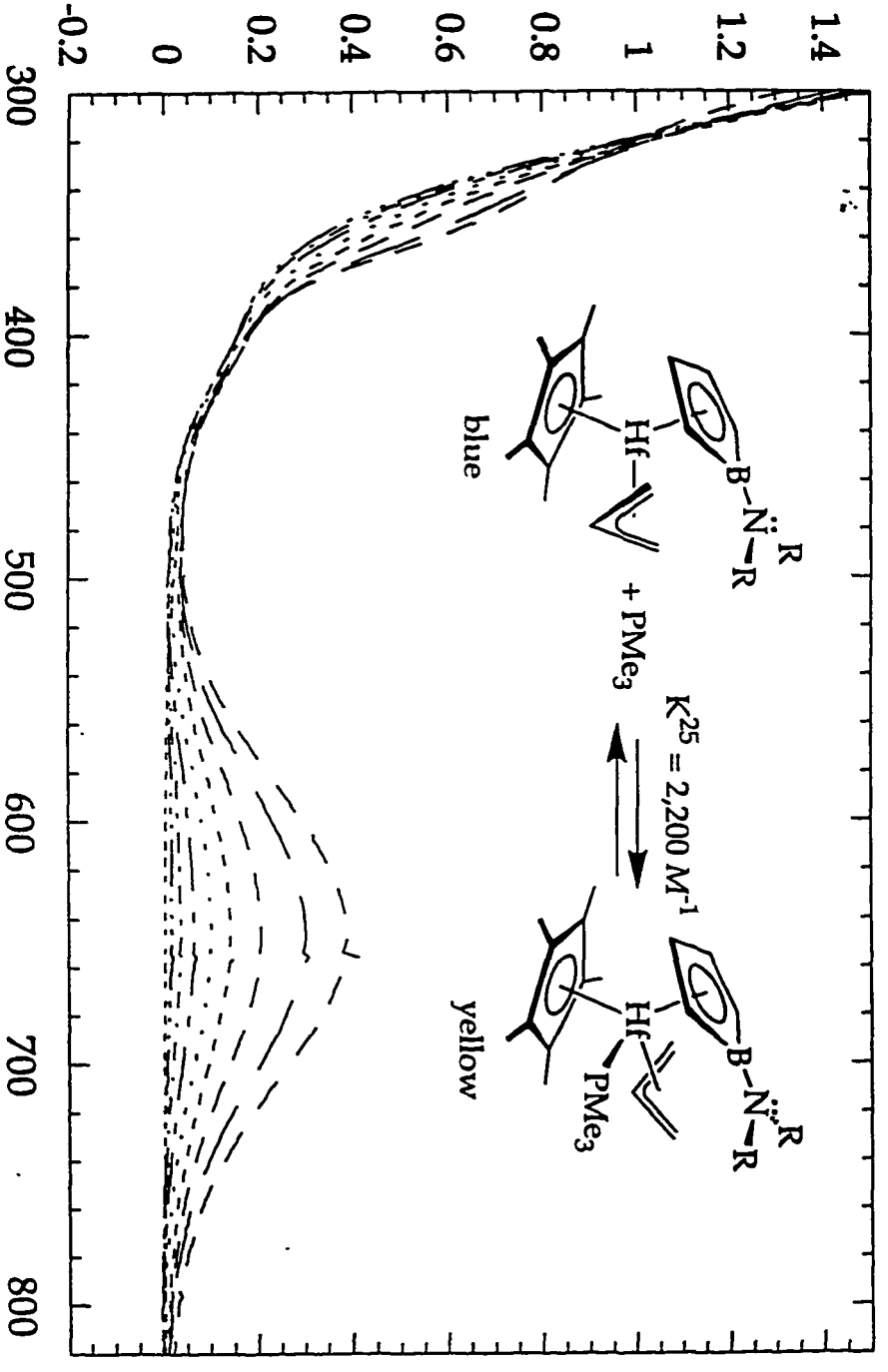

Figure 5: Addition of PMe_3 to $Cp^*\{\eta^5\text{-}C_4H_4BN(CHMe_2)_2\}Hf(\eta^3\text{-}C_3H_5)$ Monitored By UV-vis

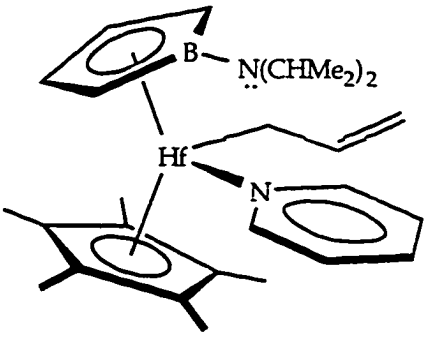

6

Figure 6: Proposed Structure of
$Cp^*\{C_4H_4BN(CHMe_2)_2\}Hf(C_3H_5)(py)$

The reports by Stryker[17] and others on the formation of stable d^0 group IV allyl-carbonyl complexes encouraged us to try the addition of CO to allyl complex **4**. Addition of 1 atm of CO to **4** resulted in an immediate color change from blue to orange-red. The ^1H NMR spectrum for this new compound (**7**) is complex, with two resonances in the Cp* region in ~2:1 ratio. The IR spectrum shows an intense stretch at 1997 cm^{-1}, consistent with the presence of a hafnium bound carbonyl, and the ^{13}C NMR shows two resonances (δ 236.3, 236.0) in the metal bound-CO region. In the absence of light and potential ligands (PMe_3, excess CO), samples of **7** are stable in solution for up to several weeks, and it may be stored at -20°C in a glove box refrigerator for months without noticeable decomposition. In the presence of excess CO or ligands such as PMe_3, decomposition occurs. Given the difficulties in interpreting the very complex NMR spectra for **7**, and the encouraging evidence from the IR and ^{13}C NMR spectra that the new complex is quite stable, we sought to obtain structural evidence that the complex was a *bona fide* d^0 carbonyl. Recrystallization of a toluene solution of **7** by slow cooling from 23°C to -80°C resulted in the isolation of 20% yield of small red-orange crystals. An X-ray diffraction study confirmed the structure as $Cp^*\{\eta^5\text{-}C_4H_4BN(CHMe_2)_2\}Hf(\eta^3\text{-}C_3H_5)(CO)$. A drawing with 30% thermal ellipsoids is shown in Figure 7, and selected bond distances and angles are shown in Table 4. Generally, the bond distances are very similar to what is found for the parent allyl derivative, **4**. The principal differences between the two structures, aside from the presence of the carbonyl, are the increase in the Hf-B distance to 2.819(11) Å, and the orientation of the allyl. In

Table 4. Selected Distances (Å)* and Angles (°)* for $Cp^*\{\eta^5\text{-}C_4H_4BN(CHMe_2)_2\}Hf(\eta^3\text{-}C_3H_5)(CO)$.

Hf -C54	2.143(12)	C54 -O54	1.172(12)
Hf -C52	2.512(10)	Hf -C51	2.509(10)
Hf -C53	2.492(10)	B -N	1.435(13)
Hf-B	2.819(11)	C53-C54	2.66
C51 -C52	1.37(2)	C52 -C53	1.379(14)
C51 -C52 C53	125.2	C41 -N -C31	117.5
B -N -C31	118.1	B -N -C41	123.2
Hf -C54 -O54	176.4		

contrast to its orientation in $Cp^*\{\eta^5\text{-}C_4H_4BN(CHMe_2)_2\}Hf(\eta^3\text{-}C_5H_3)$, the allyl ligand in **7** is rotated so that the central carbon is directed towards the aminoborollide ligand in the carbonyl adduct. This difference led us to wonder whether the two species observed by NMR are not merely due to the presence of two rotational isomers of the allyl ligand, *i. e.* slow rotation of the η^3-allyl on the NMR time scale (eq. 5).

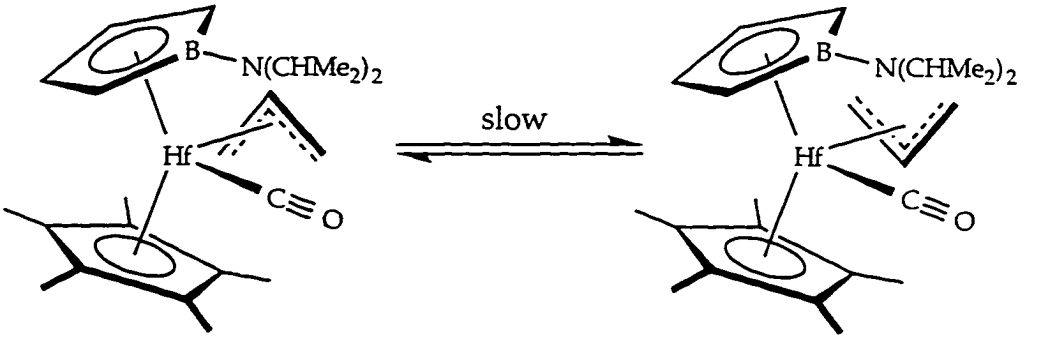

(5)

Additional evidence for this hypothesis comes from Stryker and coworkers, who reported that allyl ligand of the CO complex, $[Cp^*_2Zr(\eta^3\text{-}C_3H_5)(CO)]^+$, isoelectronic to **7**, is static on the NMR time scale, with all five allyl protons inequivalent. Finally, we note that samples of recrystallized $Cp^*\{\eta^5\text{-}C_4H_4BN(CHMe_2)_2\}Hf(\eta^3\text{-}C_5H_3)(CO)$ have identical NMR spectra to samples generated in situ from **4** and CO, supporting the notion that the two observed species are due to some interconversion slow on the NMR time scale. It is unclear why only one carbonyl stretch for the two rotamers is observed in its infrared spectrum. It is possible that the stretches are simply too close in energy to be resolved by our instrument (4 cm^{-1}

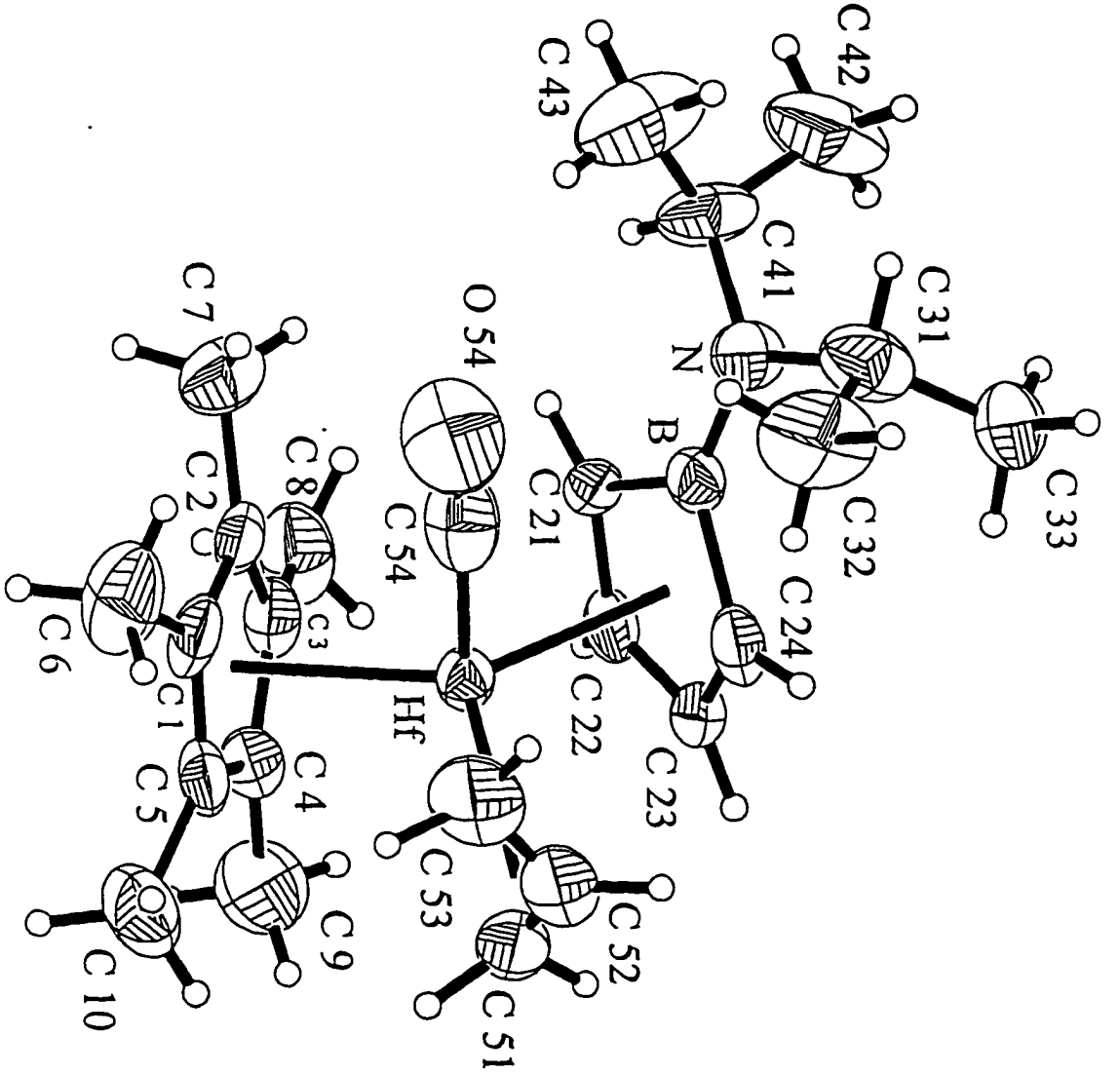

Figure 7: ORTEP Diagram of $Cp^*\{\eta^5\text{-}C_4H_4BN(CHMe_2)_2\}Hf(\eta^3\text{-}C_3H_5)(CO)$

resolution). The very similar ^{13}C resonances for the two carbonyls (0.3 ppm different) suggest that the IR stretching frequencies are also likely to be very similar.[18]

The relatively low energy of the carbonyl stretching frequency for **7** suggests that the metal center is surprisingly able to engage in backbonding with the carbonyl. Backbonding, the donation of electron density from filled metal orbitals to the π^* orbitals of the CO ($d \rightarrow \pi^*$) (Figure 8), is formally not possible for d^0 metals. The discovery that, despite the expected weakness of

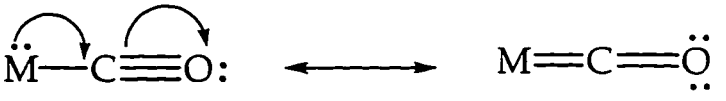

Figure 8: Backbonding in Metal Carbonyls

the metal-carbonyl bond in d^0 complexes , such "non-classical" carbonyl complexes could be isolated has spurred interest in their preparation and characterization.[19] Table 5 lists the metrical and vibrational data for a number of non-classical carbonyls of zirconium[20,21,22,23,24] and hafnium,[25,26] and includes data for several d^2 carbonyls[27,28] for comparison.[29]

Upon inspection of the data in Table 5, it is obvious that, based on the carbonyl stretching frequencies, most of the so-called non-classical carbonyls of group IV complexes show evidence for backbonding. There have been two explanations proposed to account for the substantial decrease in the stretching frequencies of many d^0 carbonyls:[30] donation from metal-ligand bonding orbitals to the in-plane CO π^* orbital ($\sigma \rightarrow \pi^*$), and contributions to the bonding by other, non-d^0 resonance forms. The first explanation, the hyperconjugative-type donation to CO from metal-ligand orbitals was originally proposed to account for the reduction in CO stretching frequency in the complexes $Cp^*_2MH_2(CO)$ (M = Zr, Hf).[31] It has also been proposed for other complexes, notably for the silanimine complex $Cp_2Zr(\eta^2\text{-}Me_2Si{=}NBu^t)(CO)$, which has a surprisingly low ν(CO) of 1797 cm^{-1}.[23] In several cases, contributions from d^2 resonance structures have been invoked to explain backbonding found in formally d^0 complexes. Thus Bercaw and coworkers attributed the backbonding observed in the complex $Cp^*_2Zr(CO)(\eta^2\text{-}OCHCH_2{}^iPr)$ to contribution from the d^2 aldehyde-adduct

resonance form.[32] Similarly, Parkin has discussed the bonding in the $Cp^*_2Zr(\eta^2\text{-}Te_2)(CO)$ complex in terms of a major contribution from a d^0 and a minor contribution from a d^2 resonance form to explain the low carbonyl stretching frequency and the slightly shorter than expected Te-Te bond. However, it should be pointed out that the two explanations are by no means mutually exclusive. For instance, the low ν(CO) in Berry's silanimine carbonyl complex could reasonably be attributed to some contribution from a d^2 resonance structure. Likewise, the backbonding in Parkin's $\eta^2\text{-}Te_2$ complex could be partially due to a hyperconjugative interaction, especially as the authors note that the distance between the carbonyl carbon and the closer Te atom is within the sum of their van der Waals radii. In both cases, the authors reach conclusions based on the sum of the structural and spectroscopic data, and there is necessarily an element of subjectivity in deciding on how to best describe the bonding.

The bond distances and the carbonyl stretching frequency for $Cp^*\{\eta^5\text{-}C_4H_4BN(CHMe_2)_2\}Hf(\eta^3\text{-}C_5H_3)(CO)$ certainly indicate a significant degree of backbonding to the carbonyl in this complex. Examination of the results in Table 5 indicates that potentially both sources of backbonding are present in complex **7**. The carbonyl stretching frequency of $Cp^*_2Hf(C_3H_5)(CO)^+$ indicates that the metal-allyl bonding orbital can donate hyperconjugatively to CO. In fact, Stryker attributes the static coordination of the allyl to this donation. However, backbonding in **7** could equally well be attributed to increased electron density at the metal center as a consequence of an increased contribution from the Hf^{II} resonance form. The increase in the Hf-B distance is certainly consistent with such an increase in the d^2 (i.e. the η^4-aminoborole) resonance form. This distance (2.819(11) Å) is the longest by ca. 0.1 Å of eight hafnium aminoborole structures that have been determined.[33]

Structural evidence for hyperconjugation is more ambiguous. The distance between the carbonyl carbon and the nearest allyl carbon is 2.66 Å, while the sum of the estimated van der Waals radii for the sp and sp^2 carbons is 2.9 Å. In the zirconium silanimine complex, the carbonyl carbon and silicon are 2.347(7) Å apart (sum of the van der Waals radii ~ 3.4 Å). For the ditelluride, $d(C_{co}\text{-}Te)$ is 2.93 Å (sum of the van der Waals radii ~ 3.6 Å). Based

Table 5. d^0 Carbonyl Compounds:
Metrical and IR Data For Selected Group IV CO Complexes

Complex	d(M-CO), Å	d(C-O), Å	ν(CO), cm^{-1}	Reference
CO (gas phase)		1.128	2143	29
$[Cp^*_2Zr(allyl)CO]^+$			2079	17
$Cp^*_2HfH_2(CO)$			2036	28
$Cp^*_2ZrH_2(CO)$			2044	28
$[Cp_2Zr(CHMe\{EP\}CO]^+$			2095	21
Cp*(ABo)Hf(allyl)(CO)	2.143(12)	1.172(12)	1997	This work
$[Cp_2Hf(C_3H_4R_1^-)(CO)]^+$	2.246(7)	1.109(8)		27
$[Cp^*_2Zr(\eta^2\text{-}C(O)CH_3)CO]^+$	2.25(1)	1.13(1)	2105	22
$[Cp_2Zr(\eta^2\text{-}C(O)CH_3)CO]^+$			2176	22
$Cp_2(\eta^2\text{-}Me_2Si{=}NBu^t)(CO)$	2.145(5)	1.162(7)	1797	23
$Cp^*_2Zr(\eta^2\text{-}OCHCHMe_2)(CO)$			1940	32
$Cp^*_2Zr(\eta^2\text{-}Te_2)(CO)$	2.241(7)	1.123(9)	2006	24
$Cp^*_2Zr(\eta^2\text{-}S_2)(CO)$	2.261(6)	1.126(8)	2057	25
$Cp^*_2Zr(\eta^2\text{-}Se_2)(CO)$	2.253(13)	1.128(16)	2037	25
$Cp_2Hf(CO)_2$	2.16(2)	1.14(2)	1969, 1878	30
$Cp^*_2Hf(CO)_2$	2.14(2)	1.16(1)	1940, 1844	30

Abbreviations: (ABo) = $\{C_4H_4BN(CHMe_2)_2\}$. R_1- = $CH_2B(Ph_F)_3$. {EP} = {6-ethylpyrid-2-yl}.

on this comparison and the uncertainty in the bond lengths and van der Waals radii, it does not appear that the two carbons are significantly closer than the sum of their van der Waals radii.[34] Thus the structural evidence favors additional d^2 character rather than hyperconjugation. Additional evidence for the importance of the resonance effect comes from a comparison of the magnitude of the two effects. Based on the greater degree of backbonding observed for the η^2-aldehyde and η^2-ditelluride complexes compared to the dihydride complexes, the evidence suggests that the resonance effect is larger than the hyperconjugative effect unless a more polarizable atom such as silicon is present. Therefore because of the structural evidence, and because resonance effects appear to be larger than hyperconjugative ones, it is likely that the major part of the observed backbonding in **7** is due to increased contribution from the diene-like, neutral resonance form of the aminoborole.

The reactivity of the $Cp^*\{\eta^5\text{-}C_4H_4BN(CHMe_2)_2\}Hf(\eta^3\text{-}C_5H_3)(CO)$ complex has also been investigated. As discussed previously, the complex is quite stable in the absence of additional ligands, but reacts further in the presence of phosphines, CO, etc. When it was observed by ^1H NMR that the reaction with phosphines led to a single product, this reaction was examined in more detail. Upon treatment of $Cp^*\{\eta^5\text{-}C_4H_4BN(CHMe_2)_2\}Hf(\eta^3\text{-}C_5H_3)(CO)$ with excess PMe_3, the red-orange solution changes color to deep red over the course of six hours. The new product displays C_1 symmetry by ^1H and ^{13}C NMR, with all four hydrogens of the borole heterocycle inequivalent and has one equivalent of coordinated PMe_3. The five hydrogens of the original allyl ligand appear as five inequivalent, overlapping peaks. Due to the overlap of the peaks, it was not possible to measure all the coupling constants in this five spin system. However, the peak at lowest and highest field are well-enough separated that their coupling constants could be measured. The most downfield peak (δ = 7.18 ppm) is a doublet, with $^3J_{HH}$ = 5.5 Hz, and the most upfield peak (δ = 4.87 ppm) is also a doublet, with $^3J_{HH}$ = 10.5 Hz. Comparison of the infrared spectrum of the product with that of the starting complex reveals the disappearance of the carbonyl stretch at 1997 cm^{-1}, and the appearance of two relatively low energy bands at 1624 and 1580 cm^{-1}. In the ^{13}C-labelled derivative, prepared from $Cp^*\{\eta^5\text{-}C_4H_4BN(CHMe_2)_2\}Hf(\eta^3\text{-}C_5H_3)(^{13}CO)$, the bands shift to 1618 and 1560

cm^{-1}. More informative is the ^1H NMR of the ^{13}C-labelled product: the peak at 7.18 ppm is coupled to the labelled carbon, with $^1J_{CH}$ = 174 Hz, consistent with sp^2 hybridization at this carbon. This result indicates that one of the allyl hydrogens is now bonded to the labelled carbon. The observed isotope shift of both the stretching frequencies indicates that the two stretches are coupled with one another, as for a conjugated diene. Thus the most reasonable structure for the product is a dieneolate complex **8**, as shown in eq. 6. The assignment of the *cis* stereochemistry about the first double bond of the dieneolate is based on the low ($^3J_{HH}$ = 5.5 Hz) coupling constant between the two hydrogens of this double bond.[35]

The mechanism for this transformation involves initial insertion of the carbonyl into the allyl ligand, followed by a formal 1,2 hydrogen shift in the acyl intermediate to generate the product. Migratory insertion of CO

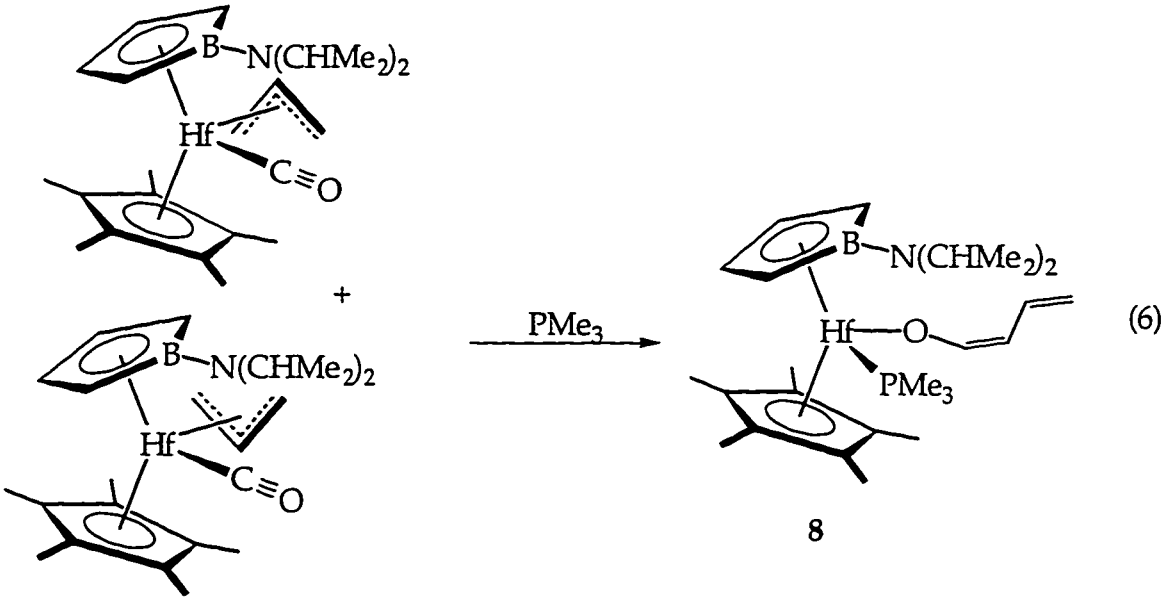

(6)

8

into allyl ligands is known. In these reactions, the insertion is believed to occur from an η^1-allyl intermediate.[36] Formal 1,2 hydrogen shifts also have precedence in the CO insertion chemistry of electrophilic metallocenes.[37] The unusual reactivity of early transition metal acyls is attributed to the oxophilicity of the these metals, resulting in η^2-coordination of the acyls and carbenoid character at the acyl carbon (Figure 9).

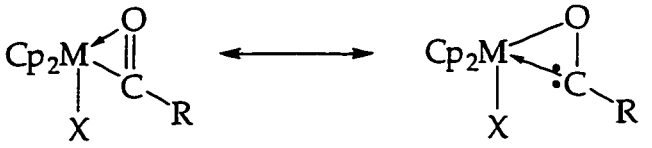

Figure 9: Carbenoid Character of Oxophilic Metal Acyls

The reactivity of allyl derivatives with hydrogen and olefins has also been investigated. Addition of dihydrogen (1 atm, -80°C) to $Cp^*\{\eta^5\text{-}C_4H_4BN(CHMe_2)_2\}Hf(\eta^3\text{-}C_3H_5)(PMe_3)$ results in formation of the PMe_3 coordinated hydride, $Cp^*\{\eta^5\text{-}C_4H_4BN(CHMe_2)_2\}Hf(H)(PMe_3)$ (**9**), which is stable for about twelve hours at room temperature under 1 atm of H_2 (eq 7).

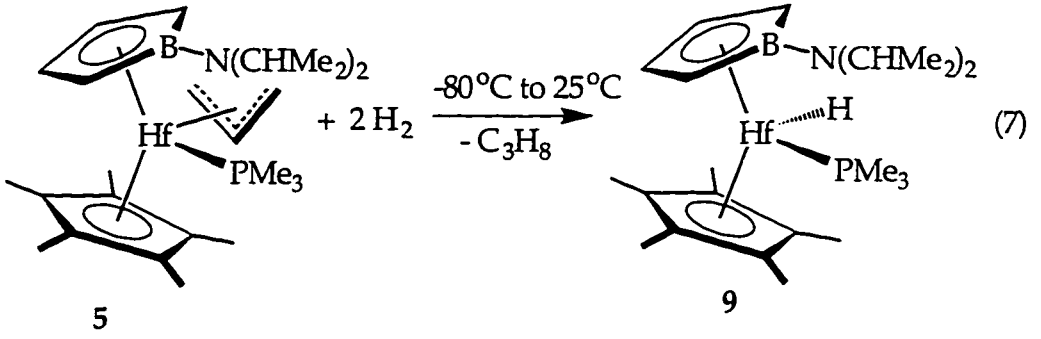

(7)

The ^1H NMR spectrum of the PMe_3 hydride is consistent with the expected C_1 symmetry. The Hf-H resonance appears at high field (δ = 14.4 ppm), as has been observed for other hafnium hydrides,[38] and the hydrogens of the aminoborole ring appear as four broad singlets between 5.4 and 4.0 ppm. Addition of dihydrogen to the allyl **4** results in propane and decomposition to a variety of unidentified products.

Addition of ethylene to a solution of **4** results in the rapid formation of polyethylene (eq. 8). However, complex **4** is not active for the polymerization of α-olefins. The olefin polymerization activity of the group IV aminoborole complex is thus very similar to what is found for the group IV dicarbollide

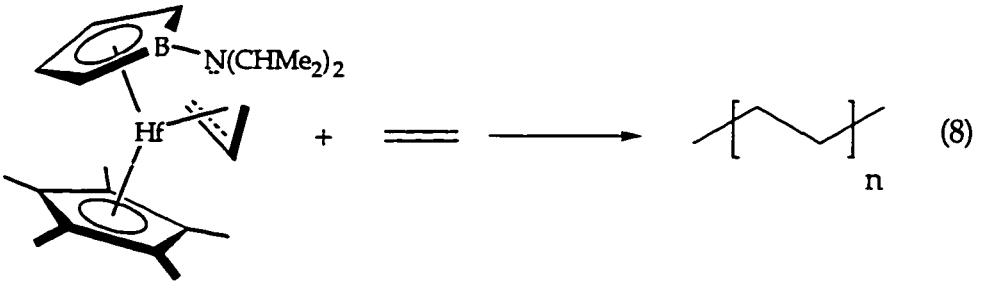

4

complexes and for the group III metallocenes. In his studies of the related dicarbollide complexes, Jordan has observed that the polymerization activity of the neutral dicarbollide complexes is much less than that of the metallocenium ions. In their reactions with α-olefins, metallocenium cations produce high molecular weight polymers while the dicarbollide analogs produce only oligomers. It was suggested that at least part of the difference in reactivity is due to bond strength differences between cationic and neutral complexes. They cited theoretical[39] and experimental[40] evidence that in cationic complexes, M-R bonds are strengthened relative to M-H bonds due to the greater electron releasing properties of the alkyl. He proposed that this ground-state destabilization of the hydride accounted for the greater polymer productivity of the cations relative to the neutral analogue, since this destabilization should increase the barrier[41] to β-hydride elimination (the major chain termination step in olefin polymerization). The arguments advanced by Jordan could certainly also be applied to the aminoborole complexes, and may account, at least in part, for the lower activity of these complexes.

As discussed in the introductory chapter, one way to increase the olefin insertion activity of catalysts is to reduce the steric crowding around the metal center. Substitution of Cp for Cp* should decrease both the steric and electronic saturation at the metal center, since Cp is a smaller, more weakly donating ligand than Cp*. For these reasons, Cp aminoborole complexes were investigated. Treatment of commercially available $CpZrCl_3$ with one equivalent of the aminoborole in ether resulted in the formation of a species whose composition analyzed approximately as $Cp\{C_4H_4BN(CHMe_2)_2\}ZrCl{\cdot}LiCl(Et_2O)_x$. This species is similar to **1-$(Et_2O)_2$** in that partial desolvation occurs over time, resulting in a material containing a

non-stoichiometric amount of solvent. In contrast to what is observed for Cp* derivatives, reaction of $CpZrCl_3$ with the aminoborole salt in toluene did not result in the solvent free species, but rather in an intractable mixture. The poor solubility of $CpZrCl_3$ in toluene may be responsible for the difference between the cyclopentadienyl and permethylcyclopentadienyl derivatives. Addition of allyl magnesium bromide to olive-green $Cp\{C_4H_4BN(CHMe_2)_2\}ZrCl{\cdot}LiCl(Et_2O)_2$ was likewise unsuccessful in generating the allyl derivative, resulting instead in mixtures of products. Thus for the less crowded Cp derivative, allyl does not appear to chelate strongly enough to exclude excess halide or solvent. Use of the more strongly chelating 1-lithio-2-dimethylaminomethylbenzene[42] does result in clean formation of dark green $Cp[C_4H_4BN(CHMe_2)_2]Zr(C_6H_4CH_2NMe_2)$ (**10**) (eq. 9).

$$Cp\{C_4H_4BN(CHMe_2)_2\}ZrCl{\cdot}LiCl(Et_2O)_2 + LiC_6H_4CH_2NMe_2 \longrightarrow \mathbf{10} \qquad (9)$$

In solution, complex **10** displays the expected C_1 symmetry (^1H and ^{13}C NMR). In the ^1H NMR, the peaks for the isopropyl methyls appear as a single broad peak at room temperature, suggesting that rotation about the B-N bond is more hindered in this complex. The increased barrier to rotation about the B-N bond compared to what is found in complex **4** is probably due to the larger size of the N,N-dimethylbenzylamine group relative to the allyl ligand. The broad peak sharpens into the expected two doublets at 60°C.

Complex **10** does not react with either ethylene or higher olefins. It reacts with dihydrogen over twelve hours, resulting in decomposition to N,N-dimethylbenzylamine and uncharacterized organometallic products. This complex is thus actually less reactive than the allyl derivative. The lower reactivity of **10** is probably due to the increased strength of the hafnium-phenyl and hafnium nitrogen bonds relative to the hafnium allyl bond.

Finally, the bis(aminoborole) hafnium complex has been prepared and isolated as the bis(trimethylphosphine) adduct, $\{C_4H_4BN(CHMe_2)_2\}_2Hf(PMe_3)_2$ (**11**), by addition of two equivalents of $Li_2(THF)\{C_4H_4BN(CHMe_2)_2\}$ to $HfCl_4$, followed by addition of excess phosphine (eq. 10). In solution, deep blue **11** displays the expected molecular

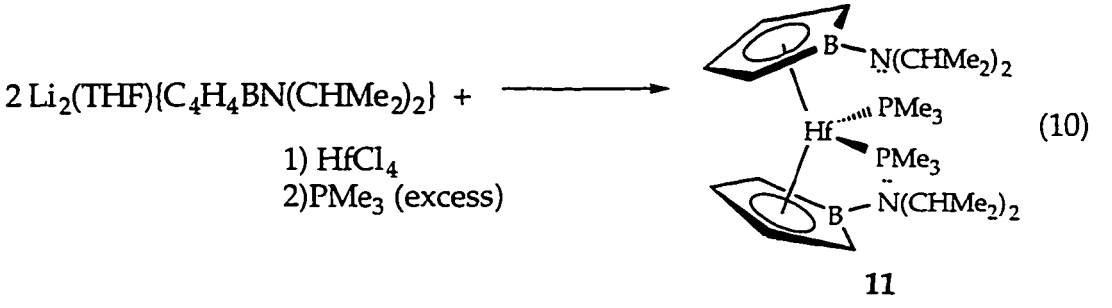

(10)

11

mirror plane of symmetry. Complex **11** is a rare case in which the zirconium analogue of a hafnium aminoborole complex appears to unstable; attempts to prepare the zirconium analogue have all failed.[43] The difference in the stability of **11** and the zirconium derivative is likely due to the greater stability of Hf^{IV} compared with Zr^{IV}.

2c. Electronic Spectroscopy of Pentamethylcyclopentadienyl Aminoborole Complexes

The beautiful colors for $Cp^*\{\eta^5\text{-}C_4H_4BN(CHMe_2)_2\}M(\eta^3\text{-}C_3H_5)$ (M = Zr,Hf), like $Cp^*\{\eta^5\text{-}C_4H_4BN(CHMe_2)_2\}MCl\cdot LiCl$ (M = Zr, Hf), stand in contrast to most zirconocene and hafnocene derivatives, which are commonly pale yellow to colorless. In order to establish the nature of the low energy transitions responsible for their colors, the electronic spectra of **4** and its zirconium analogue were examined (Figure 10). The deep green color of $Cp^*\{\eta^5\text{-}C_4H_4BN(CHMe_2)_2\}Zr(\eta^3\text{-}C_3H_5)$ is due to a broad transition centered around λ = 749 nm (pentane), with an extinction coefficient of 2000 $M^{-1}cm^{-1}$. The blue color of the hafnium analog, **4**, arises from a broad transition with λ_{max} = 656 nm (pentane) and ε = 2500 $M^{-1}cm^{-1}$ (Figure 10).

Considerable evidence indicates that the aminoborole-hafnium interaction is responsible for the low energy transition. First, as previously mentioned, the parent metallocenes do not display this low energy transition. Also, perturbation of the amino group by coordination to cations such as lithium or proton (see chapter 4) dramatically blue shifts the energy of the transition. Since the observed colors are a consequence of the metal-aminoborole bonding, understanding the bonding in these complexes can help to determine the nature of the transitions. Several resonance structures contribute to the description of the bonding of the aminoborole complexes (Figure 11): structure **A**, the borolldiyl form described as ($\eta^5\text{-}L_2Z$ = $\eta^5\text{-}LX_2$) in the Green classification,[44] in which the ligand is a divalent cyclopentadienyl analog; structure **B**, the diene-like ($\eta^4\text{-}L_2$) form, which Herberich has concluded is the best valence bond description for late metal aminoborole complexes; and structure **C**, the divalent ($\eta^4\text{-}LX_2$) form whose bonding resembles that of early transition metal diene complexes.[45] In resonance forms **A** and **C**, the metal is formally tetravalent, d^0, whereas in form **B**, the metal is divalent, d^2.

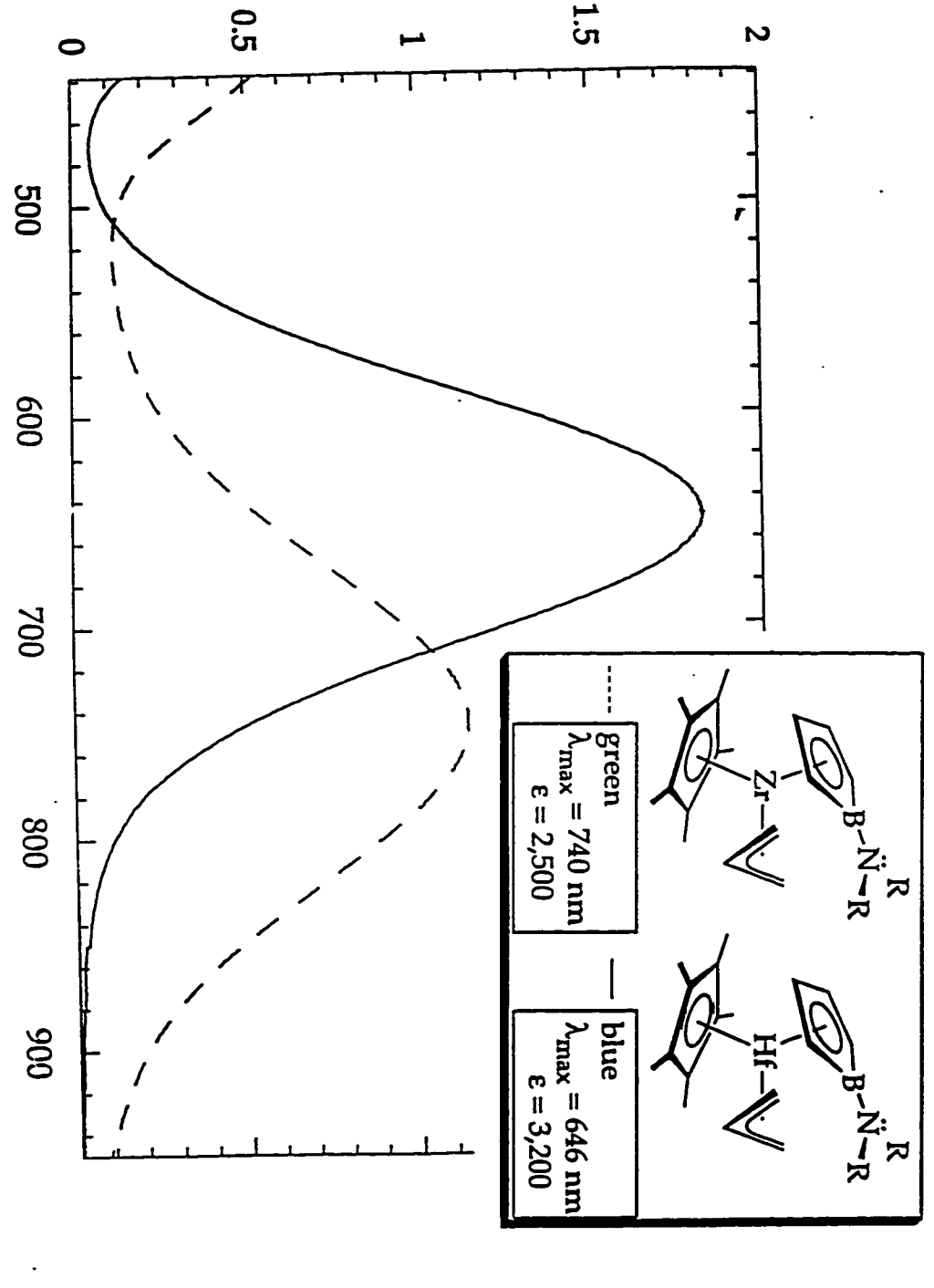

Figure 10: Electronic Spectra of $Cp^*\{\eta^5\text{-}C_4H_4BN(CHMe_2)_2\}M(\eta^3\text{-}C_3H_5)$ (M = Zr, Hf)

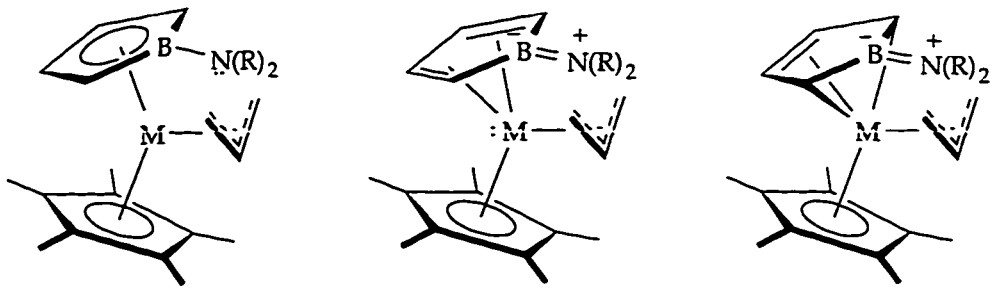

$(\eta^5\text{-}L_2Z = \eta^5\text{-}LX_2)M^{IV}$ $(\eta^4\text{-}L_2)M^{II}$ $(\eta^4\text{-}LX_2)M^{IV}$

A **B** **C**

Figure 11: Resonance Contibutors to Aminoborole Bonding

These limiting resonance pictures of the bonding suggest three possibilities for the electronic transitions in the visible region: (1) resonance structures **A** and **C** are the best descriptions of the ground state, implying a ligand to metal charge transition (LMCT), excited state ~ $\{Cp^*\{\eta^5\text{-}C_4H_4BN(CHMe_2)_2\}^{(+)}M^{III(-)}((\eta^3\text{-}C_3H_5)\}^*$; (2) resonance structure **B** is the best ground state description, implying a metal to ligand charge transition (MLCT), excited state ~ $\{Cp^*\{\eta^5\text{-}C_4H_4BN(CHMe_2)_2\}^{(-)}M^{III(+)}((\eta^3\text{-}C_3H_5)\}^*$; or (3) resonance structure **B** whereby the formal d^2 metal center undergoes a ligand field excitation.

The observed blue shift in the transition upon substitution of hafnium for zirconium is clearly inconsistent with option (2), a MLCT, since hafnium should be more easily oxidized resulting in a red shift. Therefore, the transition must be due to either a LMCT or a ligand field transition. The small solvatochromic shifts (λ_{max} = 646 nm (toluene, ε = 3200 M^{-1} cm^{-1}); λ_{max} = 644 nm (methylene chloride, ε = 3000 M^{-1} cm^{-1}) and molar extinction coefficients observed for **4** would generally argue in favor of a ligand field transition.[46] However, a closer inspection of the literature reveals many examples of charge transfer transitions with similar parameters.[47,48,49] The small solvatochromic shifts may be an indication of strong delocalization, resulting in modest dipole changes in the excited state and thus little sensitivity to solvent polarity. In this sense, the aminoborole complexes are quite similar to d^0 metallocenes. Titanocene dichloride, for instance, displays equally small solvatochromic shifts and even smaller extinction coefficients.

Further evidence for the LMCT assignment comes from previous work in the Bercaw group. It was shown that the energy of the visible transition for $Cp^*\{\eta^5\text{-}C_4H_4BN(CHMe_2)_2\}ZrCl\cdot LiCl$ is similar to the difference between the oxidation and reduction potentials of this complex, as expected for a charge transfer transition.[50] Also, it has been recognized that other divalent Cp analogues red shift the energy of the LMCT transitions, though not so dramatically.[51] So all the evidence is consistent with the assignment of the transition as having predominantly LMCT character. To the extent that the neutral diene-like resonance form of the aminoborole contributes to the bonding, some mixing will occur, leading to a slight increase in the metal orbital character of the HOMO and in the ligand orbital character of the LUMO. Thus the bonding in the aminoborole complexes is not static, but can change depending on the precise nature of the other ligands bound to the metal. The relative contributions of the two divalent resonance forms of the aminoborole is more difficult to assess, but given the short B-N distances found in the complexes, contribution from C should not be neglected.

Although no calculations on bent pseudo-metallocene fragments containing aminoborole and Cp ligands have been reported, calculations on the bent metallocene fragment and on the borole π-orbitals have been reported.[52] The frontier orbitals of the bent metallocene fragment[53] are shown in Figure 12, and the borole orbitals[54] are shown in Figure 13.

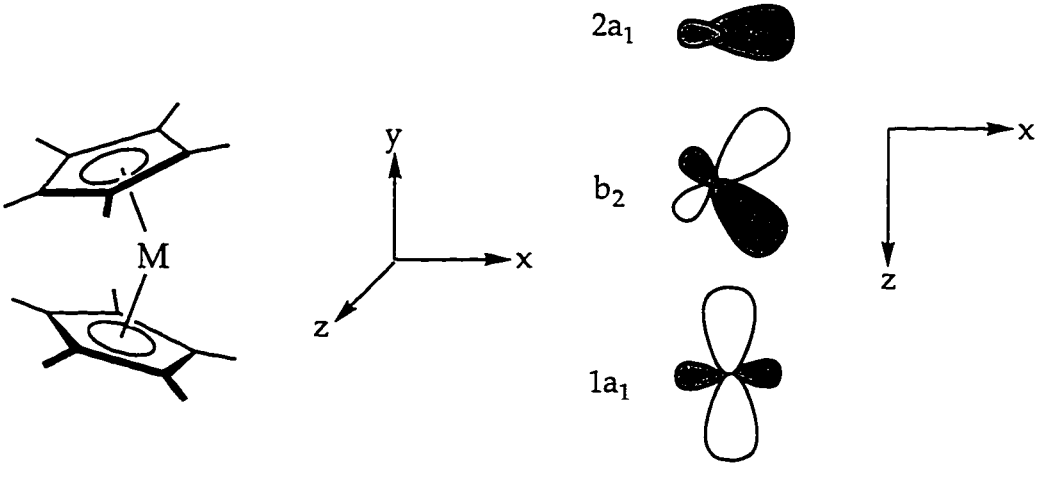

Figure 12: Frontier Molecular Orbitals of Bent Metallocene

The π-orbitals of the aminoborole are similar to Cp, though the degeneracy of the HOMO and LUMO of Cp is raised by the introduction of the boron atom.

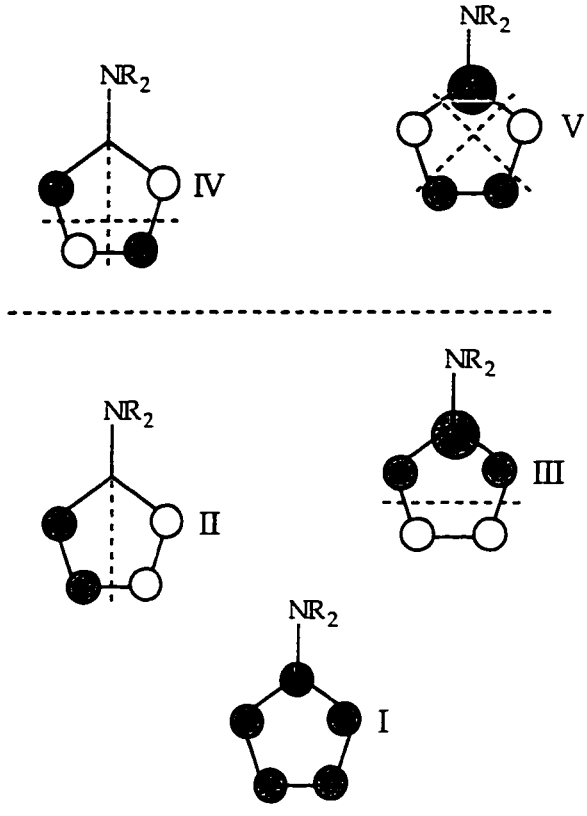

Figure 13: Ordering of π-Orbitals of Aminoborole

For each of the formerly degenerate pairs of orbitals, the orbital with boron at a non-nodal position is destabilized, due to the lower electronegativity of boron. It should be noted that the amino group would be expected to increase the separation between the orbitals. The amino lone pair should not affect the orbitals with a node passing through the boron atom very much, but should destabilize the orbitals with a nonzero contribution from the boron. Herberich and others have undertaken extended Hückel calculations on the regular sandwich complex $Cp(C_4H_4BH)Rh$, and found that the HOMO of this complex is derived principally from orbital III.[55] This conclusion is consistent with the observation that the outer face of the borole readily coordinates other metals to form triple-decker complexes.[56] Since the π-bonding orbitals are stabilized by varying amounts in the bent metallocenes, it is not possible to state with certainty which orbital will be the HOMO in the resulting complex. However, based on the large (2 eV) energy gap calculated for the two orbitals, and the expectation that the energy gap will be widened by the

effect of the amino group, the most likely case is that orbital III will be the major contributor to the HOMO. The evidence that the B-N interaction has an important effect on the energy of the low energy transition is certainly consistent with the assignment of orbital III as the HOMO.

It is more difficult to assign the LUMO for the aminoborole complexes. If the substitution of the borole for the Cp is not too great a perturbation, then the frontier orbitals should be similar to those pictured in Figure 12. Of course, substitution of aminoborole may have more serious consequences, and the orbitals may no longer resemble those in Figure 12. In the absence of any evidence it is not possible to make an assignment with confidence.

It is not necessary, however, to have a precise assignment of the LUMO or even for the HOMO in order to account qualitatively for all the observations concerning the low energy transition. The observed blue shift in the energy of the transition upon coordination of PMe_3 and CO is readily understood as a consequence of the complexes reaching coordinative saturation. The resulting $18e^-$ complexes have no vacant orbital of low-energy to participate in the LMCT. The relatively low energy of the LMCT for the pyridine coordinated allyl, $Cp^*\{\eta^5\text{-}C_4H_4BN(CHMe_2)_2\}Hf(py)(C_3H_5)$, is also consistent with the original assignment of **6** as the $16e^-$, η^1-allyl complex.

The observed transitions of the halide complexes can also be interpreted in terms of LMCT transitions. In ether, complex **1** displays the low energy transition expected for a $16e^-$ complex. In THF, the band is shifted to higher energy, suggesting that the coordination at the hafnium has changed in an important way. The most probable explanation is that, in THF, **1** forms solvent separated ion pairs $Cp^*\{\eta^5\text{-}C_4H_4BN(CHMe_2)_2\}HfCl_2^-$ and $Li^+(THF)_x$. The increased charge on the hafnium in the anion would be expected to shift the LMCT to higher energy, as is observed. The red shift of the visible transition in the iodo derivative is also consistent with LMCT. The LMCT transitions of iodo derivatives are found at lower energies than those for the corresponding chloro derivatives due to the increased polarizability of the heavier halide.[46] The red color of the formally $16e^-$ dieneolate derivative **8** is somewhat anomalous, as the other $16e^-$ complexes are commonly blue to purple in color. For instance, the structurally similar complex $Cp^*\{\eta^5\text{-}C_4H_4BN(CHMe_2)_2\}HfCl(PMe_3)$ is blue-purple in color, with

λ_{max} = 572 nm (ε = 830 $M^{-1}cm^{-1}$).[57] The difference between the two complexes must be a consequence of the superior π-donating ability of the alkoxide.[58]

3. Conclusions

Neutral aminoborole hafnium complexes have been prepared as metallocene analogues. The complexes display many of the reactions characteristic of electrophilic metallocenes, such as salt coordination, ethylene polymerization, CO reduction, and σ-bond metathesis. The aminoborole complexes were not active for the polymerization of higher olefins, however. This reduced activity was attributed to the decrease in electrophilic character compared to the cationic metallocenium catalysts. In contrast to d^0 metallocenes, the aminoborole complexes display electronic transitions in the visible region. These low energy transitions were assigned as LMCT, from a predominantly borole-based HOMO to a metal-based LUMO. All the observed spectroscopy was found to be qualitatively consistent with the LMCT assignment.

4. Experimental

All manipulations were performed using glove box and high-vacuum line techniques.[59] Solvents were dried over Na/benzophenone and stored over Na/benzophenone (THF, ether) or titanocene[60] (toluene, petroleum ether, heptane). NMR solvents: benzene-d_6 was dried over $LiAlH_4$ and then over sodium metal; THF-d_8 was purified by vacuum transfer from Na/benzophenone.

Argon was purified by passage over MnO on vermiculite and activated 4Å molecular sieves. Cp^*ZrCl_3[61] and Cp^*HfCl_3[38] were prepared from $LiCp^*$ and the metal tetrahalides (Aesar) following the literature procedures. $Li_2(THF)\{C_4H_4BN(CHMe_2)_2\}$ was prepared following Herberich's procedure. $Li(C_6H_4NMe_2)$ was prepared following the literature procedure. AllylMgBr (Aldrich), CO (Matheson), BI_3 (Aldrich), $CpZrCl_3$ (Strem) and PMe_3 (Aldrich) were all used as received. Pyridine (Aldrich) was purified by vacuum transfer from CaH_2.

NMR spectra were carried out on a Bruker AM-500 spectrometer at 500 MHz for proton and 125.8 MHz for carbon and a GE QE300 spectrometer at

300MHz for proton and 75.5 MHz for carbon. Infrared spectra were recorded on a Perkin-Elmer 1600 Series FTIR. UV-vis spectra were recorded on a Hewlett-Packard 8452A and a Cary 14 spectrophotometer modified by OLIN using a 1.0 mm path length, air-free cell. Elemental analyses were carried out by Mr. Fenton Harvey at Caltech.

$Cp^*[C_4H_4BN(CHMe_2)_2]HfCl{\cdot}LiCl$ (1).

A swivel frit assembly was charged with 1.0g (2.38 mmol) Cp^*HfCl_3 and 592 mg $Li[C_4H_4BN(CHMe_2)_2](THF)$ (1 eq.). On the vacuum line, 125 mL toluene was condensed in at -78°C, and the solution was allowed to gradually warm to ambient temperature overnight. The deep red solution was filtered and volatiles were evaporated. Petroleum ether (75 mL) was condensed in, and then evaporated, to assist in removing residual THF. Petroleum ether (75 mL) was condensed in again, and the resulting red-orange slurry was stirred for two hours to ensure precipitation of the product. The slurry was then filtered and the orange powder washed with a small amount of petroleum ether, yielding 830 mg (63%) of $Cp^*[C_4H_4BN(CHMe_2)_2]HfCl{\cdot}LiCl$ as an orange powder.

^1H NMR (300 MHz, THF-d_8): 5.05 (m, 2H, H3, H4); 3.44 (sept., $^3J_{HH}$ = 7 Hz, 2H, $NCH(CH_3)_2$); 3.29 (m, 2H, H2, H5); 1.87 (s, 15H, $C_5(CH_3)_5$); 1.06 (d, $^3J_{HH}$ = 7 Hz, 12H, $2NCH(CH_3)_2$). $^{13}C\{^1H\}$ NMR (75 MHz, THF-d_8): 119.2 (s, $C_5(CH_3)_5$); 116.1 (s, C3,C4); 87.3 (br, C2,C5); 47.0 (s, $NCH(CH_3)_2$); 23.8 (s, $NCH(CH_3)_2$); 12.0 (s, $C_5(CH_3)_5$). UV-vis: (Et_2O) 561 (650); (THF) 492 (550). Elemental analysis, calculated for $C_{20}H_{33}BCl_2HfNLi$: C 43.33; H 6.31; N 2.52. Found: C 43.11; H 5.98; N 2.20.

$Cp^*[C_4H_4BN(CHMe_2)_2]HfCl{\cdot}LiCl(Et_2O)_2$ (1-$(Et_2O)_2$).

In the glovebox, $Cp^*[C_4H_4BN(CHMe_2)_2]HfCl{\cdot}LiCl$ (50 mg) was dissolved in a minimum of Et_2O (~3 mL). This sample was transferred by pipette into a small glass vial with a snap-top lid. A needle was poked through the lid, and the vial set inside a large vial containing 7 mL of petroleum ether. The larger vial was closed, and parafilm wrapped around the lid. The two vials were then set in the glove box freezer for three weeks, during which time small

blue-purple plates crystallized. The solvent was decanted by pipette, and a crystal selected and sealed in a glass capillary.

{Cp*[$C_4H_4BN(CHMe_2)_2$]HfCl·LiCl}$_2$

A 300mg sample of amorphous Cp*[$C_4H_4BN(CHMe_2)_2$]HfCl·LiCl was loaded into a small wide-mouth bomb. Benzene (~10 mL) and perfluorobenzene (~3 - 4 mL) were condensed in. The mixture was heated at 80°C for 10 days, during which time the orange powder recrystallized into small, intergrown orange-red crystals. A small amount of colorless amorphous precipitate (presumably excess LiCl) also formed. About one small spatula worth of crystals were smeared on a coverslide covered with paratone oil. The coverslide with the crystals was brought out of the glovebox sealed in a jar. The crystallographer (LMH) selected a crystal in the air, mounted it on a goniometer, and collected data while the crystal was in a low temperature nitrogen stream.

Cp*HfI_3 (2).

A small swivel frit assembly was charged with 3.75g (8.9 mmol) Cp*$HfCl_3$ and 3.50g (1.0 eq) BI_3. Toluene (35 mL) was condensed in and the resulting mixture stirred for 4 hours at room temperature. No reaction was evident, so the solution was heated to 70°C. The solids dissolved. The reaction was kept at 70°C for 90 minutes, then cooled to RT. Volatiles were evaporated and petroleum ether (20 mL) condensed in. The off-white solid was isolated by filtration, and washed once, yielding 5.4g (87%) of Cp*HfI_3.

^{1}H NMR (benzene-d_6 , 300 MHz): 2.07 (s, $C_5(CH_3)_5$).

Cp*[$C_4H_4BN(CHMe_2)_2$]HfI·LiI(THF) (3).

A small frit was charged with 4.05g (5.82 mmol) Cp*HfI_3 and 1.45g Li_2[$C_4H_4BN(CHMe_2)_2$](THF) (1 eq.). Toluene (75 mL) was condensed in at

-78°C, and the solution allowed to warm up slowly overnight. The deep purple solution was allowed to settle for 1h. and then filtered. Volatiles evaporated. On a clean frit, the crude product was filtered in toluene (50 mL) and volatiles evaporated. Petroleum ether was condensed in, and the resulting slurry filtered. 2.75g (70%) of deep blue $Cp^*[C_4H_4BN(CHMe_2)_2]HfI{\cdot}LiI(THF)$ isolated as a powder.

^1H NMR (benzene-d_6 , 300 MHz; 70°C): 5.57 (m, 2H, H3, H4); 4.72 (m, 2H, H2, H5); 3.90 (sept., $^3J_{H-H}$ = 6.6 Hz, 2H, 2 C*H*$(CH_3)_2$); 3.75 (m, 4H, α-THF); 2.10 (s, 15H, $C_5(CH_3)_5$); 1.30 (d, $^3J_{H-H}$ = 6.6 Hz, 12H, 2 CH$(CH_3)_2$); 1.25 (m, 4H, β-THF). Elemental analysis, calculated for $C_{24}H_{41}BHfI_2LiNO$: C 35.62; H 5.07; N 1.73. Found: C 34.62; H 4.78; N 0.87.

$Cp^*\{\eta^5\text{-}C_4H_4BN(CHMe_2)_2\}Hf(\eta^3\text{-}C_5H_3)$ (4).

A swivel frit assembly was charged with 2.00 g (3.86 mmol) of $Cp^*\{\eta^5\text{-}C_4H_4BN(CHMe_2)_2\}HfCl{\cdot}LiCl$. Et_2O (75 mL) was condensed onto the solid at -78°C. At 0°C, 4 mL (solution 1.0 M in Et_2O, 1.05 eq.) of allyl magnesium bromide was syringed into the frit against an argon counterflow. After stirring for three hours, the resulting green solution was filtered and the volatiles evaporated at reduced pressure. Using a new frit, the solid was taken up in 50 mL of toluene and filtered. The insoluble solids were washed repeatedly, until the filtrate was pale blue in color. Volatiles evaporated under reduced pressure. The residue was slurried in 30 mL of petroleum ether and a deep blue solid isolated by filtration at -78°C. Crude yield 1.40g (70%). Recrystallization from hot heptane afforded 700mg (35%) of crystalline $Cp^*\{\eta^5\text{-}C_4H_4BN(CHMe_2)_2\}Hf(\eta^3\text{-}C_5H_3)$. In order to obtain satisfactory elemental analysis, it was necessary to recrystallize the sample a second time and to grind the sample with V_2O_5 to facilitate oxidation.

^1H NMR (benzene-d_6 , 500 MHz): 6.99 (m, 1H, H_c allyl); 5.34 (m, 2H, H3, H4); 4.02 (m, 2H, H2, H5); 3.66 (d, $^3J_{H-H}$ = 15.4 Hz, 2H, H_{anti} allyl); 3.58 (sept., $^3J_{H-H}$ = 6.8 Hz, 2H, 2 C*H*$(CH_3)_2$); 1.70 (d, $^3J_{H-H}$ = 9 Hz, H_{syn} allyl); 1.35 (s, 15H, $C_5(CH_3)_5$); 1.28 (d, $^3J_{H-H}$ = 6.8 Hz, 12H, 2 CH$(CH_3)_2$). ^{13}C NMR (benzene-d_6 , 125.8 MHz): 135.4 (d, $^1J_{C-H}$ = 147 Hz, C_m allyl); 112.3 (s,

$C_5(CH_3)_5$); 107.31 (d, $^1J_{C-H}$ = 158 Hz, C3, C4); 81.5 (br, C2, C5); 61.77 (t, $^1J_{C-H}$ = 157 Hz, C_t allyl); 48.51 (d, $^1J_{C-H}$ = 133 Hz, $CH(CH_3)_2$); 24.58 (q, $^1J_{C-H}$ = 125 Hz, $CH(CH_3)_2$); 10.81 (q, $^1J_{C-H}$ = 126 Hz, $C_5(CH_3)_5$). IR (Nujol): 1504(w); 1437(m); 1426(s); 1322(s). UV-vis (pentane): 656 (2,500); 330 (3,800); 236 (10,000). Elemental analysis, calculated for $C_{23}H_{38}BHfN$: C 53.37; H 7.34; N 2.70. Found: C 53.31; H 7.71; N 2.85.

$Cp^*\{\eta^5\text{-}C_4H_4BN(CHMe_2)_2\}Hf(\eta^3\text{-}C_5H_3)(PMe_3)$ (5).

A swivel frit assembly was charged with 150mg $Cp^*\{\eta^5\text{-}C_4H_4BN(CHMe_2)_2\}Hf(\eta^3\text{-}C_5H_3)$. Petroleum ether (10mL) was condensed in. Using a gas bulb, 1.1 eq. (.32 mmol) PMe_3 was condensed in at -78°C. The solution was warmed to RT, then the resulting yellow-green solution was filtered at -78°C, yielding 60mg (50%) of $Cp^*\{\eta^5\text{-}C_4H_4BN(CHMe_2)_2\}Hf(\eta^3\text{-}C_3H_5)(PMe_3)$ as a pale green solid.

^{1}H NMR (benzene-d_6 , 300 MHz): 5.58 (br, 1H, H_c allyl); 4.87 (br, 2H, H3, H4); 3.55 (sept., $^3J_{H-H}$ = 6.7 Hz, 2H, 2 $CH(CH_3)_2$); 2.7(br, 2H, H2, H5); 2.51 (d-br, 4H, H_t allyl); 1.65 (s, 15H, $C_5(CH_3)_5$); 1.4 (d-br, 12H, 2 $CH(CH_3)_2$); 0.95 (d, $^2J_{P-H}$ = 7 Hz, 9H, $P(CH_3)_3$). IR(Nujol): 1523(w); 1415(s); 1356(m); 1329(s).

$Cp^*\{\eta^5\text{-}C_4H_4BN(CHMe_2)_2\}Hf(\eta^1\text{-}C_3H_5)(py)$ (6).

A J. Young type NMR tube was charged with 35mg (0.068 mmol) $Cp^*\{\eta^5\text{-}C_4H_4BN(CHMe_2)_2\}Hf(\eta^3\text{-}C_3H_5)$ and 0.75 mL benzene-d_6 . A gas bulb was used to add 1.0 eq. of pyridine, resulting in a color change from blue to purple. The IR spectrum was obtained by evaporating the solvent and making a mull of the residue.

^{1}H NMR (benzene-d_6 , 300 MHz): 8.2 (br, 2H, $H_o$py); 7.00 (quint., $^3J_{HH}$ = 12 Hz, 1H, H_c allyl); 6.70 (m, 1H, H_p py); 6.52(m, 2H, H_m py); 5.56 (br, 2H, H3, H4); 4.24 (br, 2H, H2, H5); 3.41 (sept., $^3J_{H-H}$ = 6.7 Hz, 2H, 2 $CH(CH_3)_2$); 2.89 (d, $^3J_{H-H}$ = 12 Hz, 4H, H_t allyl); 1.57 (s, 15H, $C_5(CH_3)_5$); 1.1 (br, 12H, 2 $CH(CH_3)_2$). IR(Nujol): 1602(m); 1440(s); 1407(m); 1325(s)

$Cp^*\{\eta^5\text{-}C_4H_4BN(CHMe_2)_2\}Hf(\eta^3\text{-}C_3H_5)(CO)$ (7).

A swivel frit assembly was charged with 0.50g $Cp^*\{\eta^5\text{-}C_4H_4BN(CHMe_2)_2\}Hf(\eta^3\text{-}C_3H_5)$. Toluene (15 mL) was condensed into the frit. CO (1 atm) was admitted to the frit with the solution at room temperature. The solution was stirred vigorously for 3 minutes, during which time the color changed from deep blue to red-orange. The solution was cooled to -78°C, and the excess CO removed. The solution was warmed to RT, then slowly cooled to -78°C and allowed to remain at that temperature overnight. Filtration at the same temperature yielded 100mg (18%) $Cp^*\{\eta^5\text{-}C_4H_4BN(CHMe_2)_2\}Hf(\eta^3\text{-}C_3H_5)CO$ as an orange-red microcrystalline solid.

^1H NMR (benzene-d_6 , 500 MHz): 5.90 (br, 1H); 5.46 (br, 2H); 4.78 (br, 2H); 4.59 (br, 1H); 4.48 (m, 2H); 4.02 (m, 1H); 3.62 (br-overlapping, 3H); 3.36 (br-overlapping, 5H); 3.08 (d, $J_{H\text{-}H}$ = 8.8 Hz, 1H); 2.98 (d, $J_{H\text{-}H}$ = 8.9 Hz, 2H); 2.81 (m, 2H); 2.68 (br, 1H); 2.43 (d, $J_{H\text{-}H}$ = 15.6 Hz, 1H); 2.27 (m, 2H); 2.21 (m, 2H); 1.83 (br, 1H); 1.62 (m, 2H); 1.57 (s, 30H); 1.47 (s, 16H); 1.40 (br-mult., 6H); 1.3 (br-mult., 19H); 1.17 (br, 10H). $^{13}C\{^1H\}$ NMR (benzene-d_6 , 125.8MHz): 236.5; 236.1; 123.5; 121; 109.59; 108.6; 107.7; 96.7; 80 (br); 75.3(br); 71 (br); 63.3 (br); 62.3; 55.0; 54.5; 53.8; 49.2; 48.0; 46.2; 46.6; 23.9 (br); 23.5 (br); 23 (br); 11.4; 11.0. IR (Nujol): 1997 (s); 1432 (s); 1407 (m); 1328 (s); 1245(m); 1198(s). Elemental analysis, calculated for $C_{24}H_{38}BHfNO$: C 52.84; H 6.96; N 2.57. Found: C 50.34; H 6.51; N 2.39.

$Cp^*[C_4H_4BNH(CHMe_2)_2]Hf(OCHCHCHCH_2)(PMe_3)$ (8).

A J. Young type NMR tube was charged with 85 mg $Cp^*[C_4H_4BN(CHMe_2)_2]Hf(\eta^3\text{-}C_3H_5)(CO)$ and 1.5 mL of C_6D_6. Using a gas bulb, PMe_3 (2 eq.) was condensed into the tube. The reaction was stored overnight, during which time the color changed from orange to deep red, and then the solution was transferred into a small flask. The solution was frozen at 0°C, and the volatiles evaporated, resulting in a quantitative yield of $Cp^*[C_4H_4BNH(CHMe_2)_2]Hf(OCHCHCHCH_2)(PMe_3)$ as a red powder.

^{1}H NMR (300 MHz, benzene-d_6): 7.18 (d, $^3J_{HH}$ = 5.5 Hz, 1H, OC*H*CHCHCH$_{cis}$H$_{trans}$); 7.08 (m, 1H, OCHCHC*H*CH$_{cis}$H$_{trans}$); 5.55 (m, 1H, H3, H4); 5.08 (m, 2H, OCHC*H*CHC*H*$_{cis}$H$_{trans}$); 4.87 (d, $^3J_{HH}$ = 10.5 Hz, 1H, OCHCHCHCH$_{cis}$*H*$_{trans}$); 4.75 (m, 1H, H3, H4); 4.35 (m, 1H, H2, H5); 3.75 (m, 1H, H2, H5); 3.65 (pseudo sept., $^3J_{HH}$ = 6.6 Hz, 2H, NC*H*(CH$_3$)$_2$); 1.85 (s, 15H, C$_5$(C*H*$_3$)$_5$); 1.35 (d, $^3J_{HH}$ = 6.6 Hz, 6H, NCH(C*H*$_3$)$_2$); 1.25 (d, $^3J_{HH}$ = 6.6 Hz, 6H, NCH(C*H*$_3$)$_2$); 0.83 (d, $^2J_{PH}$ = 7 Hz, 9H, P(C*H*$_3$)$_3$). ^{13}C NMR (75 MHz, benzene-d_6): 156.5 (d, $^1J_{CH}$ = 174 Hz, OCHCHCHCH$_{cis}$H$_{trans}$); 132.1 (d, $^1J_{CH}$ = 144 Hz, OCHCHCHCH$_{cis}$H$_{trans}$); 117.12 (d, OCHCHCHCH$_{cis}$H$_{trans}$); 116.1 (s, C$_5$(CH$_3$)$_5$); 111.37 (d, C3, C4); 108.17 (pseudo t, OCHCHCHCH$_{cis}$H$_{trans}$); 105.6 (d, C3, C4); 92.5 (br. d, C2, C5); 86.0 (br. d, C2, C5); 47.45 (d, $^1J_{CH}$ = 132 Hz, NCH(CH$_3$)$_2$); 24.06 (q, NCH(C*H*$_3$)$_2$); 23.96 (q, NCH(C*H*$_3$)$_2$); 15.22 (d, $^1J_{PC}$ = 18 Hz, P(CH$_3$)$_3$); 11.84 (q, $^1J_{CH}$ = 126 Hz, C$_5$(CH$_3$)$_5$). IR (pentane); 1624 cm^{-1} ν(CC); 1580 cm^{-1} ν(CC). IR-^{13}CO derivative (pentane); 1618 cm^{-1} ν(CC); 1560 cm^{-1} ν(CC). Elemental analysis, calculated for C$_{27}$H$_{47}$BHfNOP: C 52.84; H 6.96; N 2.57. Found: C 50.34; H 6.51; N 2.39.

Cp*{η^5-C$_4$H$_4$BN(CHMe$_2$)$_2$}Hf(H)(PMe$_3$) (9).

A J. Young type NMR tube was charged with 25 mg Cp*{η^5-C$_4$H$_4$BN(CHMe$_2$)$_2$}Hf(η^3-C$_3$H$_5$)(PMe$_3$) and 0.75 mL benzene-d_6 . On the vacuum line, the tube was filled with 1 atm. of H$_2$. Upon mixing, the solution changed color briefly to red, then became deep blue.

^{1}H NMR (benzene-d_6 , 300 MHz): 14.4 (s, 1H, Hf-*H*); 5.76 (m, 1H); 5.40 (m, 1H); 5.06 (m, 1H); 4.06 (m, 1H); 3.56 (sept., $^3J_{H-H}$ = 6 Hz, 2H, C*H*(CH$_3$)$_2$); 2.00 (s, 15H, C$_5$(C*H*$_3$)$_5$); 1.39 (d, $^3J_{H-H}$ = 6.7 Hz, 12H, CH(C*H*$_3$)$_2$); 0.74 (d, $^2J_{P-H}$ = 4 Hz, 9H, P(C*H*$_3$)$_3$).

Polymerization of ethylene by 4

A small glass bomb was charged with **4** (12mg) and 10-15 mL of toluene. 1-2 g Ethylene was purified by condensing into a solution of 200 mg titanocene in 25mL toluene. The ethylene was transferred into the glass

bomb containing the catalyst solution at 77K and the solution allowed to thaw behind a blast shield. Polymerization (evident by formation of a white precipitate) began while the solution was still cold, resulting in the solution warming to slightly above room temperature. The solution became too viscous to stir due to the precipitated polymer. Yield ~1g polyethylene.

$Cp[C_4H_4BNH(CHMe_2)_2]Zr(C_6H_4CH_2NMe_2)$ (10).

A swivel frit assembly was charged with 1.0g (2.2 mmol) $Cp[C_4H_4BNH(CHMe_2)_2]ZrCl{\cdot}LiCl(Et_2O)x$ and 350 mg (1.1 eq.) $LiC_6H_4CH_2NMe_2$. Toluene (20 mL) was condensed in, and the mixture was stirred at room temperature overnight. The deep green solution was filtered by gravity and volatiles were evaporated. Using a new frit, the crude product was again dissolved in toluene and filtered. Volatiles were evaporated. The crude product was recrystallized from a mixture of 7 mL toluene and 15 mL petroleum ether at -78°C, yielding 700 mg (50%) of $Cp[C_4H_4BNH(CHMe_2)_2]Zr(C_6H_4CH_2NMe_2)$ as a dark green, microcrystalline solid.

^1H NMR (300 MHz, benzene-d_6): 7.1-7.2 (m, 3H, phenyl H's); 6.85 (d, $^3J_{HH}$ = 7Hz, 1H, phenyl H); 6.50 (m, 1H, H3, H4); 6.16 (s, 5H, C_5H_5); 5.97 (m, 1H, H3, H4); 4.13 (d, $^2J_{HH}$ = 15 Hz, 1H, Benzylic H); 3.65 (psd. sep., $^3J_{HH}$ = 7Hz, 2H, $NCH(CH_3)_2$); 3.21 (m, 1H, H2, H5); 3.08 (m, 1H, H2, H5); 2.70 (d, $^2J_{HH}$ = 15 Hz, 1H, benzylic H); 1.51 (s, 3H, N-CH_3); 1.40 (s, 3H, N-CH_3); 1.36 (br, 12H, $2NCH(CH_3)_2$). ^{13}C NMR (75 MHz, benzene-d_6): 190.26; 142.35; 138.48; 125.77; 124.44; 123.93; 123.52; 120.56; 112.70 (C_5H_5); 87.0 (br, C2, C5); 82.0 (br, C2, C5); 71.20 (Benzylic CH_2); 51.75 ($N(CH_3)$); 47.60 (br, $NCH(CH_3)_2$); 47.58 ($N(CH_3)$); 24.10 (br, $NCH(CH_3)_2$). The methyl groups of the isopropyls sharpen up into the expected two doublets at 60°C. UV-vis λ_{max} = 710 nm (ε = 770 M^{-1} cm^{-1}). Elemental analysis, calculated for $C_{24}H_{35}BN_2Zr$: C 63.59; H 7.72; N 6.18. Found: C 61.18; H 7.89; N 6.32.

$[C_4H_4BN(CHMe_2)_2]_2Hf(PMe_3)_2$ (11).

A swivel frit assembly was charged with 1.00 g (4.0 mmol) $Li_2(THF)\{C_4H_4BN(CHMe_2)_2\}$ and 930 mg (0.5 eq.) $HfCl_4(THF)_2$. THF (50 mL)

was condensed in at -78°C, and the solution warmed up slowly overnight. The red solution was evaporated to a dark solid. Toluene (50 mL) was condensed in, and the red-brown solid was filtered and washed three times. The solid was loaded into a different frit, and toluene (40 mL) and excess PMe_3 condensed in. The deep blue solution was filtered to remove LiCl, and volatiles evaporated. Petroleum ether (25 mL) was condensed in, and the dark blue solid isolated by cold filtration. The sample was recrystallized by dissolving 450 mg in 10 mL toluene and adding 15 mL to the top half of the frit. The two solutions mixed overnight; the resulting solution was cooled to 0°C, and the solid isolated by filtration as a blue powder (yield 40%).

^1H NMR (300 MHz, C_6D_6): 5.95 (m, 4H, H3, H4); 3.73 (sept., $^3J_{HH}$ = 6.6 Hz, 4H, $4NCH(CH_3)_2$); 3.58 (m, 4H, H2, H5); 1.58 (sept., $^3J_{HH}$ = 6.6 Hz, 24H, $4NCH(CH_3)_2$); 0.58 (d, $^2J_{PH}$ = 6 Hz, 18H, $2P(CH_3)_3$). $^{13}C\{^1H\}$ NMR (75.5 MHz, C_6D_6): 109.5 (s, C3, C4); 81.0 (br, C2, C5); 47.89 (s, $NCH(CH_3)_2$); 24.3 (br, $CH(CH_3)_2$); 20.68 (d, $^1J_{PC}$ = 18 Hz, $P(CH_3)_3$). UV-vis: 610 (1,300). Elemental analysis, calculated for $C_{26}H_{54}B_2HfN_2P_2$: C 47.60; H 8.22; N 4.27. Found: C 40.04; H 6.50; N 3.09.

5. References and Notes

1. Herberich, G. E.; Englert, U.; Hostalek, M.; Laven, R. *Chem. Ber.* **1991**, *124*, 17.
2. Quan, R. W. Ph.D. Thesis, Chapter 4, Caltech, **1994**. see also Pastor, A. P.; Kiely, A. F.; Henling, L. M.; Day, M. W.; Bercaw, J. E. *J. Organomet. Chem.* in press.
3. Herberich, G. E.; Hessner, B.; Ohst, H. *J. Organomet. Chem.* **1988**, *305*, 305.
4. Covalent radii are from *The Nature of the Chemical Bond*, 3rd Ed. Pauling, L.; Cornell University Press, Ithaca, **1960**, p. 253-257. It should be noted that the metal-lignd distances are expected to be longer than the sum of the covalent radii for a π-bound ligand, and their use for comparison is strictly as a means to account for the differences in size of the metal centers.
5. Yoder, J., Day, M. W.; Bercaw, J. E. unpublished results and Marsh, R. E.; Schaefer, W. P.; Coughlin, E. B.; Bercaw, J. E. *Acta Cryst.* **1992**, C48, 1773.
6. In the complexes in reference 5, the metal-chloride distances are only 0.01 Å and 0.014 Å different, for instance. However, Gamboratta and coworkers have prepared a bis benzimindinato-Ti-Cl·LiCl(TMEDA) complex in which the two Ti-Cl bonds are different by 0.035 Å. see Dick, D. G.; Duchateau, R.; Edema, J. H.; Gamboratta, S. *Inorg. Chem.* **1993**, *32*, 1959.
7. Soxhlet extraction of a sample of **1** in toluene resulted in approximately 0.5 eq of LiCl remaining in the extraction thimble. Nelson, C. M. unpublished results.
8. During structural characterization, it was noted by the crystallographer that the crystals of 1 are dichroic. Henling, L. M. unpublished results.
9. For a review of structures of organolithium compounds, see Setzer, W.; Schleyer, P. von R. *Adv. Organomet. Chem.* **1985**, *34*, 353.
10. Herberich, G. E.; Hostalek, M.; Laven, R. *Angew. Chem. Int. Ed. Engl.* **1990**, *29*, 317.
11. Edelmann, F. T. In *Comp. Organomet. Chem.* II Wilkinson, G.; Stone, F. G. A.; Abel, E.W. Eds.; Pergamon, Oxford, **1995**, Vol. 4, 11.

12. For leading references on salt coordination by organolanthanides, see Schavarien, C. J.; Mechelen, J. B. van. *Organometallics* **1991,** 10, 1704.

13 (a) Cardin, D. J.; Lappert, M. F.; Raston, C. L.; Riley, P. I. In *Comp. Organomet. Chem.* Wilkinson, G.; Stone, F. G. A.; Abel, E.W. Eds.; Pergamon, Oxford, **1982,** Vol. 3, 620 (b) Jordan, R. F.; LaPointe, R. E.; Bradley, P. K.; Baenziger, N. *Organometallics* **1989,** *8,* 2892. (c) Martin, H. A.; Lemaire, P. J.; Jellinek, F. *J. Organomet. Chem.* **1968,** *14,* 149.

14. (a) Horton, A. D. *Organometallics* **1992,** *11,* 3271 (b) Tjaden, E. B.; Casty, G. L.; Stryker, J. M. *J. Am. Chem. Soc.* **1993,** *115,* 9815.

15. (a) Tjaden, E. B.; Stryker, J. M. *J. Am. Chem. Soc.* **1993,** *115,* 2083 and references therein.

16. Complex **6** shows a medium intensity peak in the IR spectrum at 1602 cm^{-1}. It is not possible to definitively assign this as an η^1-allyl stretch, as pyridine also absorbs in this region; however, based on the intensity of the stretch, and the fact that it appears at slightly higher energies than those of free pyridine, we think that this assignment is the most reasonable one.

17. Antonelli, D. M.; Tjaden, E. B.; Stryker, J. M. *Organometallics* **1994,** *13,* 763.

18. Parkin has pointed out in his excellent discussion of d^0 zirconium carbonyls the empirical correlation between ν_{CO} stretching frequencies and ^{13}C shifts for zirconium carbonyls, see Howard, W. A.; Parkin, G.; Rheingold, A. L. *Polyhedron* **1995,** *14,* 25 and also footnotes 45-46 in that reference for similar correlations found in other systems.

19. see Ellis, J. E.; Beck, W. *Angew. Chem. Int. Ed. Engl.* **1990,** *29,* 317 for a perspective and leading references, as well as (a) Hurlburt, P. K.; Anderson, O. P.; Strauss, S. H. *J. Am. Chem. Soc.* **1991,** *113,* 6277, (b) Adelhelm, M.; Bacher, W; Hohn, E. G.; Jacob, E. *Chem. Ber.* **1991,** *124,* 159, (c) Willner, H.; Aubke, F. *Inorg. Chem.* **1990,** *29,* 2195..

20. Guram, A. S.; Swenson, D. C.; Jordan, R. F. *J. Am. Chem. Soc.* **1992,** *114,* 8991,

21. Guo, Z.; Swenson, D. C.; Guram, A. S.; Jordan, R. F. *Organometallics* **1994,** *13,* 766.

22. Procopio, L. J.; Carroll, P. J.; Berry, D. H. *Polyhedron* **1995,** *14,* 45.

23. Howard, W. A.; Parkin, G.; Rheingold, A. L. *Polyhedron* **1995,** *14,* 25.

24. Howard, W. A.; Trnka, T. M.; Parkin, G. *Organometallics* **1995**, *14*, 4037.

25. Temme, B.; Erker, G.; Karl, J.; Luftmann, H.; Frohlich, R.; Kotila, S. *Angew. Chem. Int. Ed. Engl.* **1995**, *34*, 1755.

26. (a) Manriquez, J. M.; McAlister, D. R.; Sanner, R. D.; Bercaw, J. E. *J. Am. Chem. Soc.* **1978**, *100*, 2716. (b) Manriquez, J. M.; McAlister, D. R.; Sanner, R. D.; Bercaw, J. E. *J. Am. Chem. Soc.* **1976**, *98*, 6733. (c) Roddick, D. M.; Fryzuk, M. D.; Seidler, P. F.; Hillhouse, G. L.; Bercaw, J. E. *Organometallics* **1985**, *4*, 97.

27. Sikora, D. J.; Rausch, M. D.; Rogers, R. D.; Atwood, J. L. *J. Am. Chem. Soc.* **1979**, *101*, 5079.

28. Sikora, D. J.; Rausch, M. D.; Rogers, R. D.; Atwood, J. L. *J. Am. Chem. Soc.* **1981**, *103*, 1265.

29. *Principles and Applications of Organotransition Metal Chemistry* Collman, J. P.; Hegedus, L. S.; Norton, J. R.; Finke, R. G.: Univesity Science, Mill Valley, **1987**, p. 114.

30. In the absence of backbonding, metal carbonyl stretching frequencies should be higher than that of free CO, due to the weakly C-O antibonding character of the carbon lone pair.

31. Marsella, J. A.; Curtis, C. J.; Bercaw, J. E.; Caulton, K. G.

32. Roddick, D.M.; Bercaw, J.E. *Chem. Ber.* **1989**, *122*, 1579. The relationship between the metalla-epoxide and the aldehyde adduct is analagous to the well know metallacyclopropane/olefin adduct description of coordinated olefins.

33. Six of the structures are reported in this thesis, the other two are of complexes prepared by C. M. Nelson: Henling, L. M.; Day, M. D.; Nelson, C. M.; Bercaw, J. E. Unpublished results. A ninth structure, that of $Cp^*\{C_4H_3MeBNH(CHMe_2)_2\}HfICl$ (chap. 4), was omitted from this count due to the poor quality of the data set. The Hf-B distance found for this structure is 2.722(20) Å.

34. This does not necessarily preclude hyperconjugative interaction. In the O-exo isomer of $Cp^*_2Zr(CO)(C(O)Me)^+$, the acyl carbon and carbonyl carbon are ~ 2.73 Å apart, similar to what is found for **7**. However, the backbonding is weaker in this case, as ν(CO) is 2105 cm^{-1}.

35. *Introduction to Spectroscopy*, Pavia, D. I.; Lampman, G. M.; Kriz, G. S. Saunders; Fort Worth, **1979**, p. 108.

36 Groen, J. H.; Elsevier, C. J.; Vriese, K.; Smeets, W. J. J.; Spek, A. L. *Organometallics* **1995**, *15*, 3445.

37. (a) Erker, G.; Kropp, C.; Kruger, C.; Chiang, A.-P. *Chem. Ber.* **1982**, *115*, 2447. (b) Manriquez, J. M.; Fagan, P. J.; Marks, T. J.; Day, V.; Day, C. S. *J. Am. Chem. Soc.* **1978**, *100*, 7112. (c) Roddick, D. M.; Bercaw, J. E. *Chem. Ber.* **1989**, *122*, 1579.

38. (a) Hillhouse, G.L.; Bercaw, J.E. *J. Am. Chem. Soc.* **1984**, *106*, 5472. (b) Hillhouse, G.L.; Bulls A.R.; Santarsiero, B.D.; Bercaw, J.E. *Organometallics* **1988**, *7*, 1309. (c) Coughlin, E.B.; Bercaw, J.E. *Organometallics* **1992**, *11*, 465.

39. Ziegler, T; Tschinke, V.; Becke, A. *J. Am. Chem. Soc.* **1987**, *109*, 1351.

40. Mandich, M. L.; Halle, L. F.; Beauchamp, J. *J. Am. Chem. Soc.* **1984**, *106*, 4403.

41. Thermochemical measurements indicate that β-hydride elimination is endothermic for early transition metal alkyls, see Schock, L.; Marks, T. J. *J. Am. Chem. Soc.* **1988**, *110*, 7701.

42. 1-lithio-2-dimethylaminomethylbenzene has been used to prepare a number of transition metal complexes (a-c). Manzer appears to have been the first to use it to prepare early transition metal metallocene derivatives (d). (a) Cope, A. C.; Gourley, R. N. *J. Organomet. Chem.* **1967**, *8*, 527. (b) Koten, G. van; Noltes, J. G. *J. Organomet. Chem.* **1974**, *82*, C53. (c) Leusink, A. J.; Koten, G. van; Marsman, J. W.; Noltes, J. G.; *J. Organomet. Chem.* **1973**, *55*, 419. (d) Manzer, L. E. *J. Am. Chem. Soc.* **1978**, *100*, 8069.

43. Unpublished results, Wong-Foy, A. Another case is the putative hydride $Cp^*\{C_4H_4BN(CHMe_2)_2\}ZrH(L)$, which is apparently not stable even for minutes at room temperature Pastor, A. P. unpublished results.

44. Green, M. L. H. *J. Organomet. Chem.* **1995**, *500*, 127.

45. (a) Erker, G.; Engel, K.; Krüger, C.; Chiang, A.-P. *Chem. Ber.* **1982**, *115*, 3311. (b) Benn, R.; Schroth, G. *J. Organomet. Chem.* **1982**, *228*, 71. (c) Erker, G.; Engel, K.; Krüger, C.; Müller, G. *Organometallics* **1984**, *3*, 128.

46. *Inorganic Electronic Spectroscopy* A.B.P. Lever; Wiley, New York, **1968**, p. 225-232.

47. (a) Heinselman, K. S.; Hopkins, M. D. *J. Am. Chem. Soc.* **1995**, *117*, 12340. (b) Williams, D. S.; Thompson, D. W.; Korolev, A. V. *J. Am. Chem. Soc.* **1996**, *118*, 6526. (c) Paulson, S.; Sullivan, B. P.; Caspar, J. V. *J. Am. Chem. Soc.* **1989**, *114*, 6905. (d) Abrahamson, H. B.; Brandenburg, K. L.; Lucero, B.; Martin, M. E.; Dennis, E. *Organometallics* **1984**, *3*, 1379.

48. Pfenning, B.W.; Thompson, M.E.; Bocarsly, B.W. *J. Am. Chem. Soc.* **1989**, *111*, 8947. (b) Pfenning, B.W.; Thompson, M.E.; Bocarsly, B.W. *Organometallics* **1993**, *12*, 649.

49. Tsai, Z.; Brubaker, C. *J. Organomet. Chem.* **1979**, *166*, 199.

50. The CV showed an oxidation wave at -320 mV and a reduction at -2.12 V. Thus the difference $\Delta E^{1/2}$ of 1.8 V corresponds to an energy of 41.5 kcal/mol or 1.46 x 10^4 cm^{-1}. The visible transition is centered around 570 nm for an energy of 50 kcal/mol or 1.76 x 10^4 cm^{-1}. Quan, R. W. Ph. D. Thesis, Caltech, **1994**, p 106 (Note that in the reference cited, the energy value for the redox difference was apparently miscalculated and was given as 56 kcal/mol rather than 41.5 kcal/mol).

51. The LMCT for $(C_2B_9H_{11})_2Fe^{2-}$ appears at 229 nm compared to 200 nm for Cp_2Fe. Hawthorne, M. F.; Young, D. C.; Andrews, T. D..; Howe, D. V.; Pilling, R. L.; Pitts, A. D.; Reintjes, M.; Warren, L. F.; Wegner, P. A. *J. Am. Chem. Soc.* **1968**, *90*, 879.

52. Jordan has reported Hückel calculations for the zirconium dicarbollide complex, Crowther, D. J.; Jordan, R. F. *Makromol. Chem. Macromol. Symp.* **1993**, *66*, 121.

53. Lauher, J. W.; Hoffmann, R. *J. Am. Chem. Soc.* **1976**, *98*, 1729.

54. Eisch, J. J.; Galle, J. E.; Kozima, S. *J. Am. Chem. Soc.* **1986**, *108*, 379.

55. Hyla-Kryspin, I.; Gleiter, R.; Herberich, G. E.; Bernard, M. *Organometallics* **1994**, *13*, 1795.

56. Formation of triple-decker complexes of aminoboroles has been observed in early transition metal complexes as well, (a) Bazan, G. C.; Rodriguez, G. *Polyhedron*, **1995**, *14*, 93. (b) Wong-Foy, A.; Bercaw, J. E. unpublished results.

57. Nelson, C. M.; Bercaw, J. E. unpublished results.

58. *The Organometallic Chemistry of the Transition Metals*, Crabtree, R. H.; Wiley, New York, **1988**, p. 50-53.
59. Burger, B.J.; Bercaw, J.E. In *Experimental Organometallic Chemistry*; Wayda, A.L., Darensbourg, M.Y. Eds.; ACS Symposium Series 357; American Chemical Society, Washington, D.C. 1987
60. Marvich, R. H.; Brintzinger, H.H. *J. Am. Chem. Soc.* **1971**, *93*, 2046
61. Lund, E. C.; Livinghouse, T. *Organometallics* **1990**, *9*, 2426.

Chapter 4

Heterolytic Reactivity of Hafnium Pentamethylcyclopentadienyl Aminoborole Complexes Towards H-X Bonds

Abstract

The amphoteric complex $Cp^*\{\eta^5\text{-}C_4H_4BN(CHMe_2)_2\}HfCl\cdot LiCl$ heterolytically cleaves H-X bonds to form $Cp^*\{\eta^5\text{-}C_4H_4BNH(CHMe_2)_2\}HfCl(X)$ (X = Cl, CCR). Acetophenone reacts with $Cp^*\{\eta^5\text{-}C_4H_4BN(CHMe_2)_2\}HfCl\cdot LiCl$ to form $Cp^*\{\eta^5\text{-}C_4H_4BNH(CHMe_2)_2\}HfCl_2$ and $PhC(O)CH_2Li$. $Cp^*\{\eta^5\text{-}C_4H_4BNH(CHMe_2)_2\}Hf(CCTMS)_2$ is prepared from $Cp^*\{\eta^5\text{-}C_4H_4BN(CHMe_2)_2\}Hf(\eta^3\text{-}C_3H_5)$ and two equivalents of (trimethylsilyl)acetylene. Methyl iodide reacts with $Cp^*\{\eta^5\text{-}C_4H_4BN(CHMe_2)_2\}HfCl\cdot LiCl$ to form $Cp^*\{\eta^5\text{-}C_4H_3MeBNH(CHMe_2)_2\}HfClI$. Control experiments using deuterium labelled substrates show heterolysis occurs with no incorporation of deuterium into the 2,5 positions of the borole heterocycle. The X-ray structure determinations of $Cp^*\{\eta^5\text{-}C_4H_4BNH(CHMe_2)_2\}HfCl_2$, $Cp^*\{\eta^5\text{-}C_4H_4BNH(CHMe_2)_2\}HfCl(CCTMS)$, and $Cp^*\{\eta^5\text{-}C_4H_3MeBN(CHMe_2)_2\}HfClI$ are reported.

1. Introduction

The electrophilic reactivity of early transition metal metallocenes is well established. A relatively unexplored area is the chemistry of electrophilic metal complexes with ligands containing a Lewis basic site. Previous investigations of such complexes have found that the Lewis basic site typically undergoes three reactions: protonation, alkylation, and intra or intermolecular coordination.[1]

The protonation of basic centers appended to ancillary ligands is well precedented, with examples spanning the transition metals[1] and even including the s and p block elements.[2] In the protonated complexes the counterion may or may not coordinate to the metal, depending on factors such as the electrophilicity of the metal and the coordinating ability of the counterion. Alkylation of an appended basic site is also well precedented for nitrogen bases. In cases where the nitrogen base is in conjugation with the ancillary ligand, however, the base may be significantly less nucleophilic. For instance, Boche and coworkers noted that the amino groups of bis(dimethylamino)titanocene dichloride are not readily alkylated, consistent with strong interaction between the amino group and the Cp ligand.[3] Structural and spectroscopic evidence provide further support for strong π-donation from the amino group. Such π-interaction between substituents and ligand is frequently observed for heterocyclic ligands such as boratabenzenes and boroles.[4]

Coordination to a metal is perhaps the most commonly observed reaction for pendant nitrogen, oxygen and phosphorous bases. In many cases, intramolecular coordination has been employed as a means of stabilizing monomeric fragments which would otherwise oligomerize.[2] Complexes with appended phosphines are generally very good at intermolecular coordination, and in some cases have been employed as ligands in organometallic chemistry (e.g. ferrocenyl phosphines[5]).

As described in the previous chapter, we have been investigating mixed aminoborole/pentamethylcyclopentadienyl derivatives of zirconium and hafnium as metallocene analogues.[6] Aside from their potential similarity to d^0 metallocenes, these complexes are amphoteric molecules, that is, they possess sites of both Lewis acidic and basic reactivity. Floriani and coworkers have shown that "bifunctional" complexes of transition metals with porphyrinogen or Schiff-base type ligands may be employed as carriers for polar species (e.g. NaH, LiMe) and have investigated the reactivity of the coordinated alkyl and hydride groups.[7] Our interest is in the ability of the two sites of reactivity to act in a cooperative fashion to induce heterolysis of HX bonds.

2. Results and discussion

Treatment of a THF solution of $Cp^*\{\eta^5\text{-}C_4H_4BN(CHMe_2)_2\}HfCl\cdot LiCl$ with anhydrous HCl results in the disappearance of the deep red color and the formation of a new species, bright yellow $Cp^*\{\eta^5\text{-}C_4H_4BNH(CHMe_2)_2\}HfCl_2$ (**1**) (eq. 1). The protonated complex **1** displays the expected molecular mirror plane of symmetry in solution, but its ^1H NMR spectrum differs from those of the non-protonated aminoborole derivatives in that the methyl groups of the isopropyl substituents are now pairwise diastereotopic rather than equivalent. This is a direct consequence of the protonation of the amino group, since 180° rotation about the B-N bond no longer results in an equivalent conformation of the amino group. In the ^1H NMR, the amino hydrogen appears as a broad peak at 6.4 ppm, close to the shift of 6.5 ppm that Herberich has observed for the protonated aminoborole complex $[\{\eta^5\text{-}C_4H_4BNH(CHMe_2)_2\}Cr(CO)_4]BF_4$.

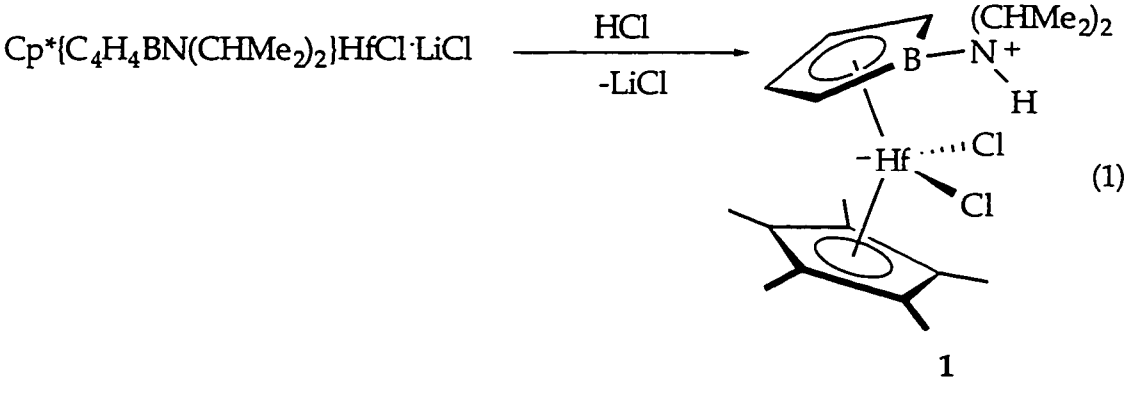

(1)

1

The color of **1** displays the expected blue shift compared to the starting complex. As discussed in the previous chapter, the colors of the aminoborole hafnium complexes are due to a borole to metal charge transfer transition, and the energy of the transition depends strongly on the boron-nitrogen interaction. Protonation of the nitrogen of the aminoborole eliminates the nitrogen lone pair-borole interaction, stabilizing the borole π-orbitals, and thus raising the energy of this transition.

Recrystallization of **1** from hot heptane resulted in the isolation of a 50% yield as small yellow crystals. An X-ray structure determination was undertaken and the results are shown in Figure 1. Selected bond distances and angles are listed in Table 1.

Table 1. Selected Distances (Å)* and Angles (°)* for

$Cp^*\{\eta^5\text{-}C_4H_4BNH(CHMe_2)_2\}HfCl_2$ (1).

Hf -Cp*	2.221	Hf -C1	2.471
Hf -Cl1	2.428(2)	Hf -C2	2.411
Hf -Cl2	2.458(2)	Hf -C3	2.420
B -C1	1.509(8)	Hf -C4	2.524
B -C4	1.476(9)	Hf -B	2.624(6)
HN_{ca}-Cl2	2.305(2)	HN_{pk}-Cl2	2.526(2)
B -N	1.580(8)	Cl1 -Hf -Cl2	94.1
C1 -C2	1.424(9)	Cp* -Hf -$Centroid_{Bo}$	132.6
C2 -C3	1.381(10)	C5 -N -B	116.7
C3 -C4	1.418(9)	C8 -N -B	112.9
N-Cl2	3.056(5)	C8 -N -C5	114.3

HN_{ca} = Calculated H position HN_{pk} = H position from peak in the difference map

The structure of $Cp^*\{\eta^5\text{-}C_4H_4BNH(CHMe_2)_2\}HfCl_2$ shows that the aminoborole ligand is η^5-coordinated, but in contrast to what has been found

previously, the nitrogen is pyramidal (sum of the angles about N = 344°) rather than planar, and the B-N distance is considerably longer. The Hf-B distance is somewhat shorter than was found for the non-protonated amino boroles, which is consistent with an expected increase in the strength of the boron-hafnium bond when there is no lone pair on nitrogen available to compete for the vacant p-orbital on boron. Unfortunately, the hydrogen located on the amino group could not be reliably located, but the difference map did show a region of positive density between Cl2 and N, consistent with the presence of this hydrogen. The position of the hydrogen shown in Figure 1 was determined by fixing the N-H distance at 0.95 Å. In Table 1, bond distances based on both the calculated position and the position determined from the difference map are reported.

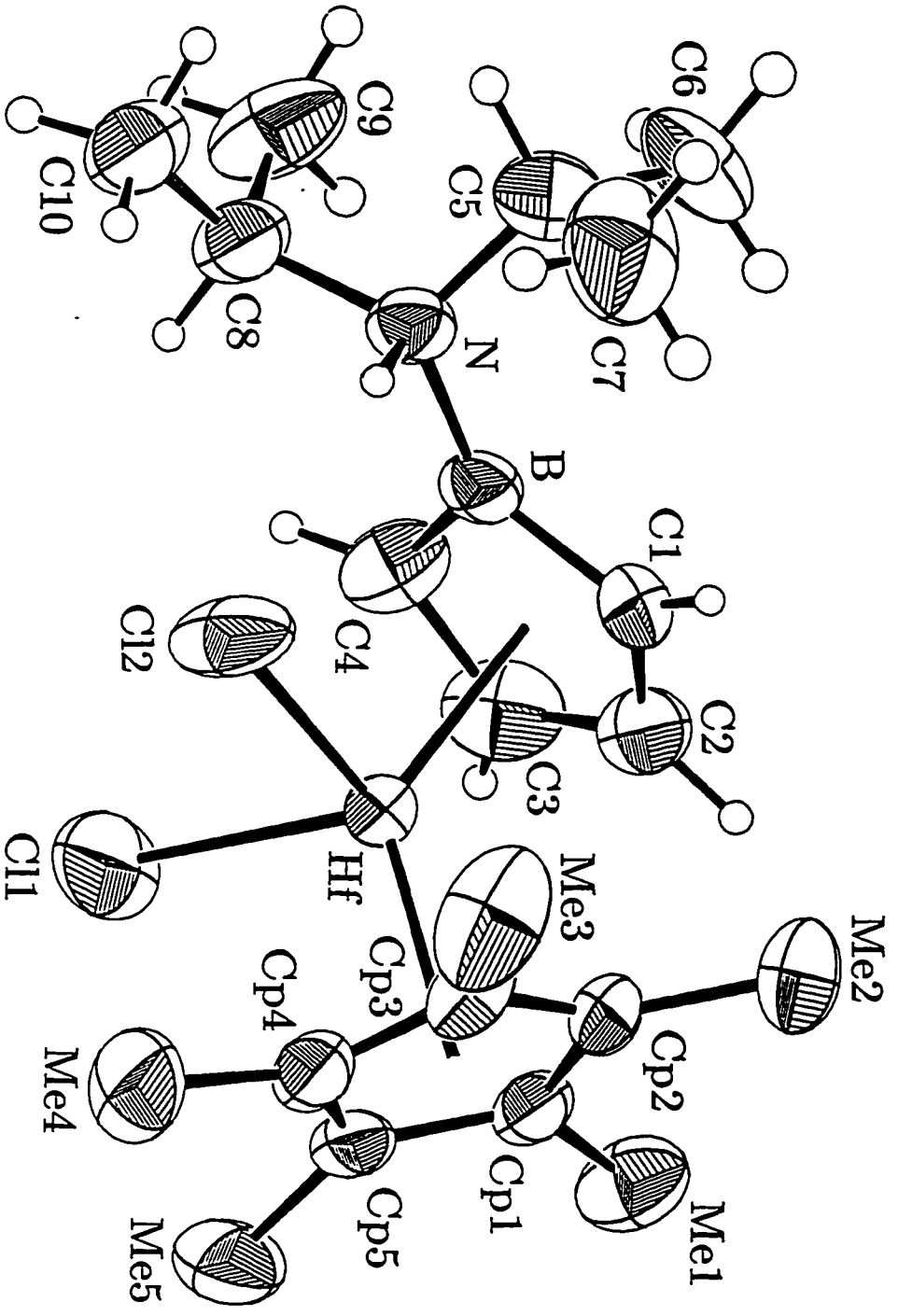

Figure 1: ORTEP Diagram of $Cp^*\{\eta^5\text{-}C_4H_4BNH(CHMe_2)_2\}HfCl_2$

The position of the amino group of the borole ligand almost directly over Cl2 (Cl2-Hf-B-N torsion angle of -2.2°(4)) suggests that the amino group is hydrogen bonded to this chloride. The bond distances from the two hydrogen positions to the chloride differ considerably, though both are somewhat closer than the estimated van der Waals contact of 2.75-2.95 Å.[8] Because of the difficulties in locating hydrogen atoms by X-ray diffraction, the distance between the donor and acceptor atoms is often used as a more reliable indicator of hydrogen bonding. The N-Cl2 distance of 3.056(5) Å is slightly less than the sum of the van der Waals radii (3.3 Å) of these two atoms, and is good evidence for the presence of a moderate-to-weak hydrogen bond between the amino hydrogen and Cl2. The small difference in the two hafnium chloride bond lengths is also consistent with a weak NH-Cl2 hydrogen bond.

The addition of acetophenone to $Cp^*\{\eta^5\text{-}C_4H_4BN(CHMe_2)_2\}HfCl\cdot LiCl$ in benzene-d_6 results in the precipitation of a colorless solid and the formation of a deep yellow solution. However, ^1H NMR clearly reveals that the product is not the anticipated enolate derivative, but rather $Cp^*\{\eta^5\text{-}C_4H_4BNH(CHMe_2)_2\}HfCl_2$ (eq. 2).

$$Cp^*\{C_4H_4BN(CHMe_2)_2\}HfCl\cdot LiCl + PhC(O)Me \xrightarrow{C_6D_6} \begin{matrix} Cp^*\{C_4H_4BNH(CHMe_2)_2\}HfCl_2\,(\mathbf{1}) \\ + \; LiCH_2C(O)Ph \end{matrix} \qquad (2)$$

This unexpected result shows that the heterolytic reactions of the aminoborole complexes are complicated by the extra equivalent of LiCl. It is unclear why the lithium enolate forms rather than the hafnium one, though the insolubility of the lithium enolate may drive the formation of this product.

The reactions of $Cp^*\{\eta^5\text{-}C_4H_4BN(CHMe_2)_2\}HfCl\cdot LiCl$ with a number of other acidic substrates (e.g. acetone, acetonitrile) were also investigated. Even under mild conditions and in a variety of solvents, mixtures of products resulted. Due to the complexity of the resulting NMR spectra, it was not possible to identify the products. However, it is likely that **1** is formed as one of the products in these reactions. Another complication may be the

generation of isomers of the expected products. For instance, in the reaction of Cp*{η^5-$C_4H_4BN(CHMe_2)_2$}HfCl·LiCl with acetone, a potential kinetic product is the C-bound enolate Cp*{η^5-$C_4H_4BNH(CHMe_2)_2$}HfCl($CH_2C(O)CH_3$). However, the thermodynamic product for the oxophilic hafnium complex would certainly be the O-bound enolate, Cp*{η^5-$C_4H_4BNH(CHMe_2)_2$}HfCl($OC(CH_2)CH_3$).[9] Such structural isomerism could help explain the number of observed products. Additionally, the distance of the amino group from the hafnium center (ca. 3.7 Å) may be a limitation on the kind of substrates that can undergo intramolecular activation.

In contrast to the reactions to the reactions with other acidic C-H bonds, the reaction with TMS-acetylene is quite clean. The reaction does require slightly more forcing conditions than those required for the reaction with HCl, however. Heating Cp*{η^5-$C_4H_4BN(CHMe_2)_2$}HfCl·LiCl and TMS-acetylene in toluene at 80°C for approximately one hour results in the formation of the acetylide product Cp*{η^5-$C_4H_4BNH(CHMe_2)_2$}HfCl(CCTMS) (**2**) (eq. 3).

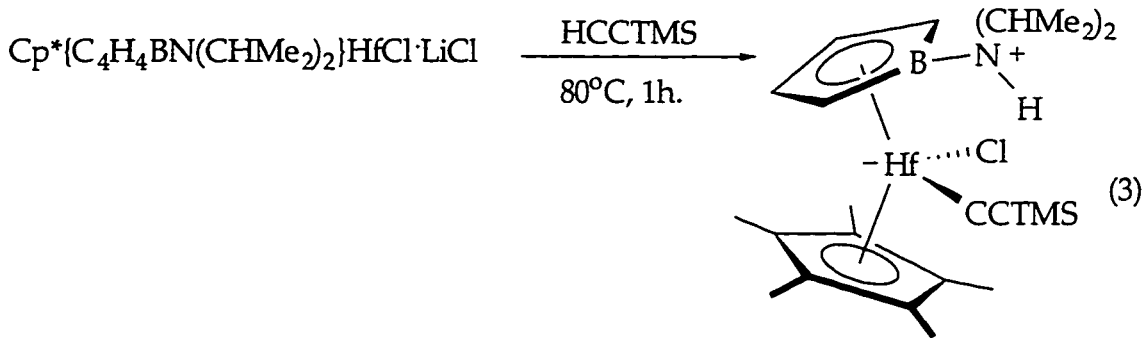

(3)

2

As the reaction proceeds the mostly toluene insoluble Cp*{η^5-$C_4H_4BN(CHMe_2)_2$}HfCl·LiCl complex gradually disappears, leaving a white solid (presumably LiCl) and an orange solution. Recrystallization of the crude product from hot heptane results in ~65% yield of yellow crystalline **2**. The solution NMR spectra of **2** are consistent with its formulation as a complex containing a σ-bonded acetylide and a protonated amino group. The N-H peak is found at 7.48 ppm, almost 1 ppm downfield of the analogous peak in **1**. The observed stretch at 2010 cm^{-1} in the IR spectrum of **2** is also

consistent with a σ-bonded acetylide.[10] One curious observation is that solutions of **2** are found to darken when exposed to direct sunlight.

In order to verify the bonding in complex **2**, we undertook a single crystal X-ray structure determination. An ORTEP plot with 30% thermal ellipsoids is shown in Figure 2, and bond distances and angles are listed in Table 2. Generally, the bond distances and angles are similar to those found in the structure of $Cp^*\{\eta^5\text{-}C_4H_4BNH(CHMe_2)_2\}HfCl_2$. In the structure determination, the amino hydrogen was located in the difference map, but this atom was set at a fixed distance of 0.95 Å, and was not included in the refinement. Additional support for the presence of a proton on the nitrogen comes from the B-N bond distance (1.571 Å vs. 1.43 Å for $Cp^*\{\eta^5\text{-}C_4H_4BN(CHMe_2)_2\}HfCl\cdot LiCl$), and the non-planar bond angles around the nitrogen ($\Sigma\angle N = 343^\circ$). One difference between the structure of **2** and that of **1** is that there is no evidence for an intramolecular hydrogen bond between the N-H moiety and the chloride in **2**.[11]

Table 2. Selected Distances (Å)* and Angles (°)* for $Cp^*\{\eta^5\text{-}C_4H_4BNH(CHMe_2)_2\}HfCl(CC(TMS))$ (**2**).

Hf -Cp*	2.214	Hf -C1	2.472(5)
Hf -Cl	2.432(2)	Hf -C2	2.388(6)
Hf -C11	2.237(6)	Hf -C3	2.446(6)
C11 -C12	1.196(8)	Hf -C4	2.519(5)
B -C1	1.482(8)	Hf -B	2.620(7)
B -C4	1.506(8)	Hf -C11 -C12	173.9
B -N	1.571(8)	Cp* -Hf -$Centroid_{Bo}$	133.7
C1 -C2	1.426(7)	C5 -N -B	112.7
C2 -C3	1.393(8)	C8 -N -B	117.6
C3 -C4	1.413(8)	C8 -N -C5	113.

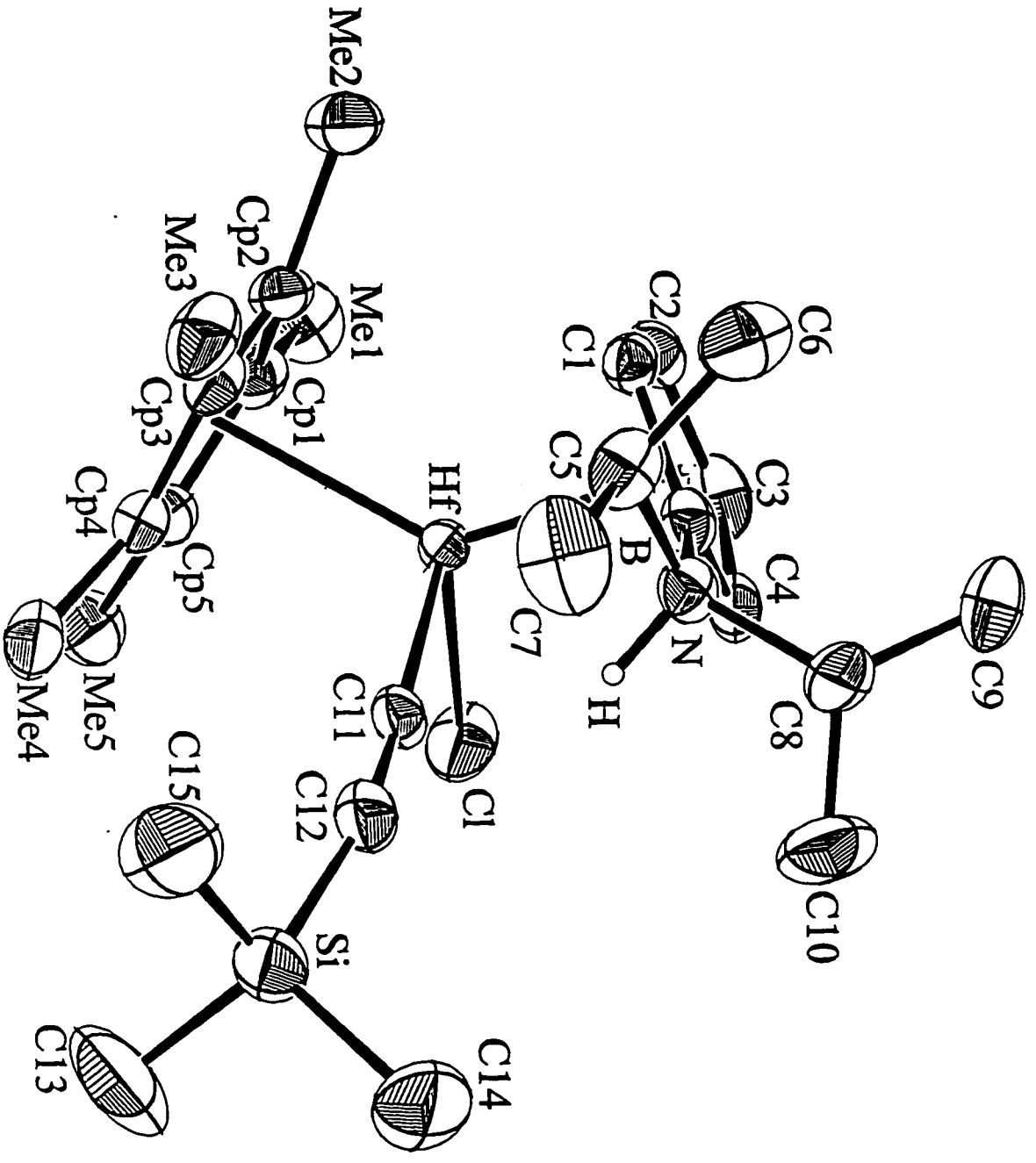

Figure 2: ORTEP Diagram of $Cp^*\{\eta^5\text{-}C_4H_4BNH(CHMe_2)_2\}HfCl(CC(TMS))$

Another important difference between **2** and **1** is that **2** can only be prepared in non-coordinating solvents. Thus, in contrast to the synthesis of $Cp^*\{\eta^5\text{-}C_4H_4BNH(CHMe_2)_2\}HfCl_2$, which is best carried out in THF, the synthesis of **2** must be carried out in toluene. Attempts to produce **2** in THF fail even if the reaction is maintained at 80°C for weeks. The most likely explanation for this difference is that heterolysis occurs from the coordinated acetylene, and that in THF solution, the acetylene is not able to compete effectively for the coordination site with the large excess of solvent. There is precedent for the deprotonation of coordinated acetylenes with amines.[12]

The hafnium chloride complex is not the only one capable of cleaving the C-H bond of TMS-acetylene. Treatment of $Cp^*\{\eta^5\text{-}C_4H_4BN(CHMe_2)_2\}Hf(\eta^3\text{-}C_3H_5)$ with two equivalents of TMS-acetylene result in the quantitative formation of orange-yellow $Cp^*\{\eta^5\text{-}C_4H_4BNH(CHMe_2)_2\}Hf(CCTMS)_2$, **3**, and propene (eq. 4). Complex **3** displays the expected molecular mirror plane of symmetry in both the ^1H and ^{13}C NMR spectrum. The presence of a proton on the amino group is indicated by the characteristically broad peak at ~7.4 ppm. The IR spectrum of **3** shows 2 stretches at 2025 and 2007 cm^{-1} for the ν(CC) modes of the acetylides.[13]

$$Cp^*\{C_4H_4BN(CHMe_2)_2\}Hf(\eta^3\text{-}C_3H_5) + 2\,HCCTMS \longrightarrow Cp^*\{C_4H_4BNH(CHMe_2)_2\}Hf(CC(TMS))_2 + C_3H_6 \quad (4)$$

3

When this reaction was monitored by ^1H NMR, it was observed that an other species was initially formed, and disappeared with concomitant formation of the final product over the course of 12 hours. Since coordination of the acetylene is expected to increase the acidity of the C-H bond, it is tempting to assign this species as an intermediate in the reaction, and this species will be referred to as the intermediate hereafter. However, mere observation of this species during the course of the reaction does not constitute proof that this species does in fact lie on the reaction coordinate (i.e. that it is a true intermediate), and the assignment of this species as an intermediate is strictly provisional. The discovery of this intermediate was

unexpected since, to the eye, the reaction appears to be quite rapid. The deep blue color of $Cp^*\{\eta^5\text{-}C_4H_4BN(CHMe_2)_2\}Hf(\eta^3\text{-}C_3H_5)$ is observed to fade in seconds to the orange-yellow color of the final product upon addition of the acetylene. Apparently the intermediate and the final product have very similar colors. The most reasonable intermediate is an acetylide-acetylene derivative, $Cp^*\{\eta^5\text{-}C_4H_4BN(CHMe_2)_2\}Hf(CCTMS)(\eta^2\text{-}HCCTMS)$ (Figure 3). η^2-Acetylenes can donate from 2 to 4 electrons, depending on whether one or both of the π-orbitals are involved in the bonding.[14] In this case, the orange-yellow color of the intermediate suggests that the acetylene ligand is acting as a 4 electron donor[15] and that the intermediate is a coordinatively saturated, 18 electron species with no low energy LUMO to act as an acceptor for the LMCT.[16]

$$Cp^*\{C_4H_4BN(CHMe_2)_2\}Hf(\eta^3\text{-}C_3H_5) \xrightarrow{2HCCTMS} Cp^*\{C_4H_4BN(CHMe_2)_2\}Hf(CCTMS)(\eta^2\text{-}HCCTMS)$$

$$\swarrow$$

3

Figure 3: Proposed Intermediate in TMS-Acetylene C-H Cleavage Reaction

The reactions of other terminal acetylenes, HCCR (R = Me, ^{t}Bu, Ph), with $Cp^*\{\eta^5\text{-}C_4H_4BN(CHMe_2)_2\}HfCl\cdot LiCl$ and $Cp^*\{\eta^5\text{-}C_4H_4BN(CHMe_2)_2\}Hf(\eta^3\text{-}C_3H_5)$ were not found to proceed cleanly, so they were not investigated further.

We were also interested in studying the reaction of the aminoborole complexes with C-X bonds rather than H-X bonds. Addition of MeI to $Cp^*\{\eta^5\text{-}C_4H_4BN(CHMe_2)_2\}HfCl\cdot LiCl$ results not in the alkylation of the amino group, as expected, but rather in formal electrophilic attack of the methyl group at the 2,5-position of the borole (eq. 5). The crude reaction mixture displays a mixture of species, in which **4** is the major product.[17]

$$Cp^*\{C_4H_4BN(CHMe_2)_2\}HfCl\cdot LiCl + MeI \longrightarrow Cp^*\{C_4H_3MeBNH(CHMe_2)_2\}HfClI + LiCl \quad (5)$$

4

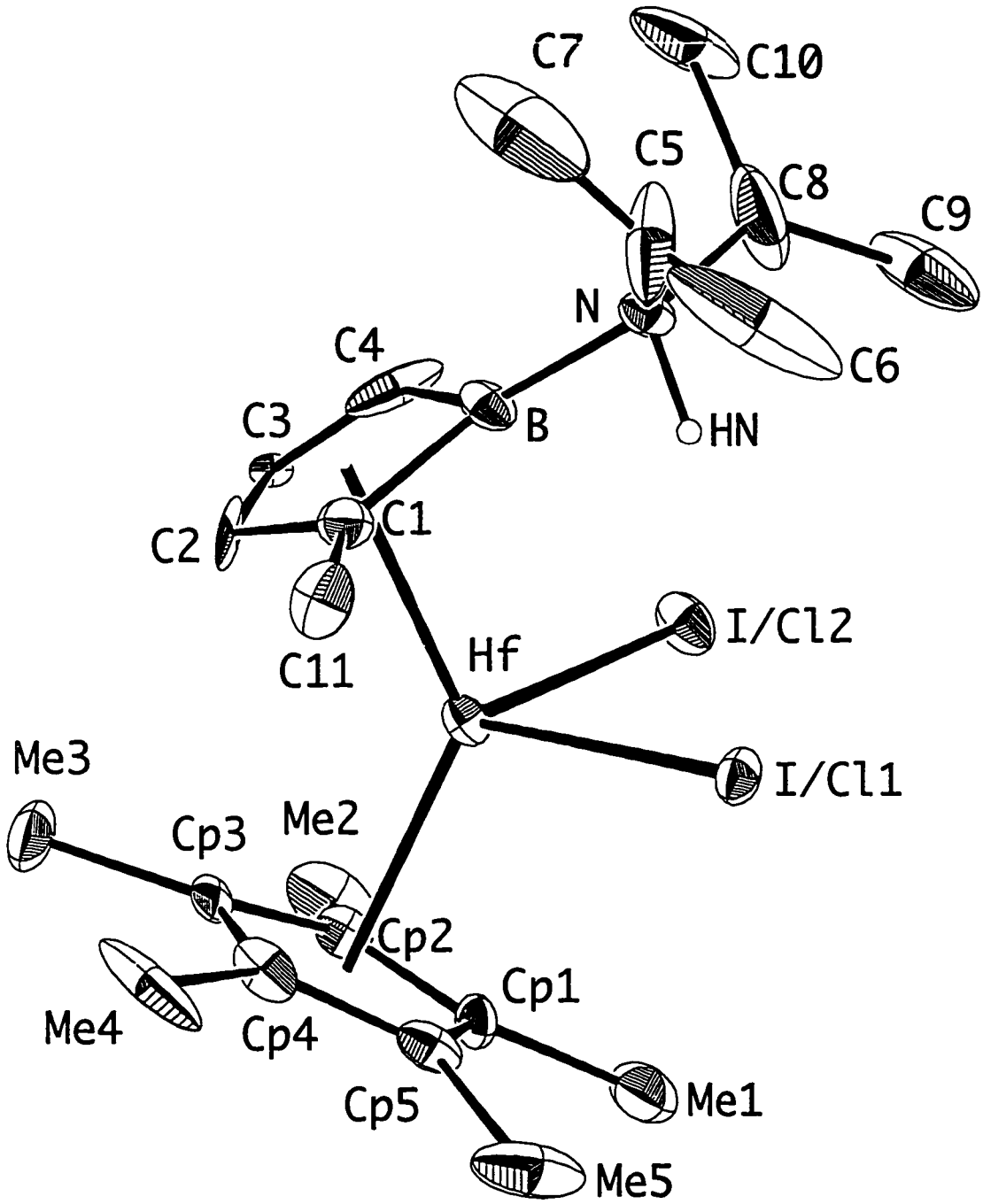

Figure 4: ORTEP Diagram of $Cp^*\{C_4H_3MeBNH(CHMe_2)_2\}HfClI$

Recrystallization of the product from toluene/petroleum ether resulted in the isolation of crystalline **4**. An X-ray structure determination was undertaken. Unfortunately, the crystal was disordered, so the resulting structure is not of a very high quality. An ORTEP diagram is shown in Figure 4. As the quality of the structure is poor, it will not be discussed in detail. The important feature of the structure is the location of the methyl on the 2-position of the heterocycle. Based on the bond angles at nitrogen, it appears that the amino group is protonated. Thus the complex has undergone alkylation of the 2-position and proton migration to the amino group.

While we were investigating the MeI reaction, Herberich, Gleiter, Zenneck and their coworkers reported a reaction between iron phenylborole complexes and MeI, in which the 2,5 positions of the borole were alkylated (eq. 6).[18] Their results, along with the isolation and characterization of **4**,[19] suggested to us the worrying possibility that the HX heterolytic reactions might proceed via initial protonation of the 2,5 position rather than via initial involvement of the amino group. Such a reaction, followed by an intra or intermolecular deprotonation of the intermediate by the amino group could then account for the products we observe (Figure 5).

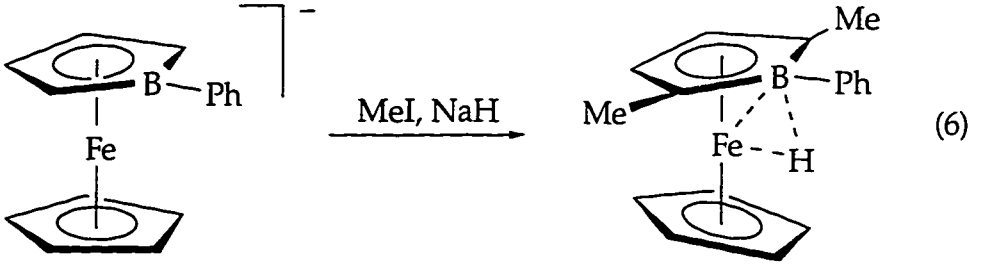

(6)

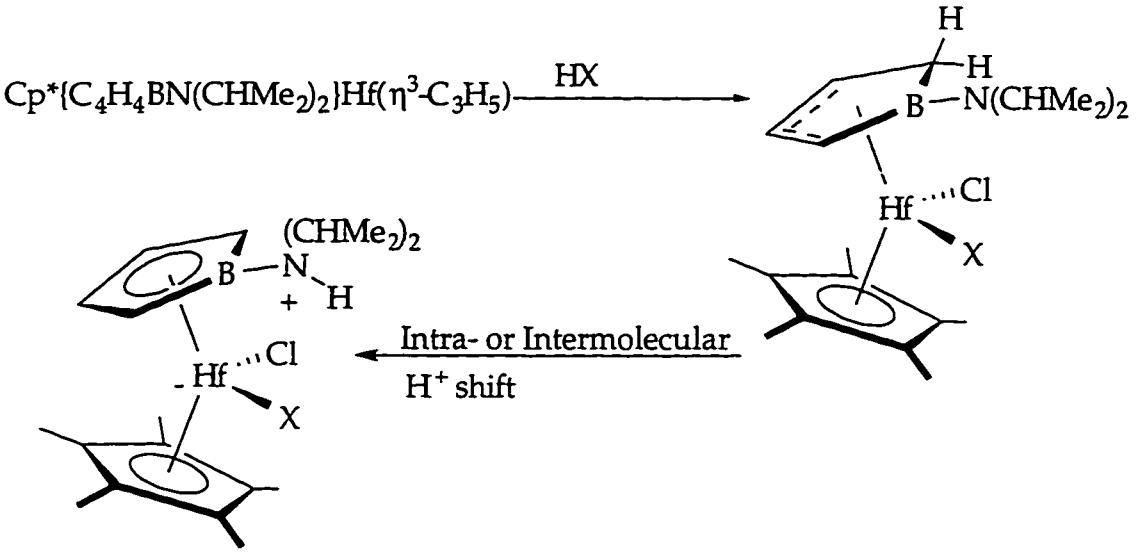

Figure 5: Possible Mechanism for Heterolysis Involving Initial Attack at 2,5 Position of Heterocycle

In order to test whether this mechanism might be operating, we undertook control experiments using the deuterium labelled substrates DCl and TMS-acetylene-d_1. The products were prepared in the same way as their protio isotopomers, and the products examined by ^1H and ^2H NMR (complex $Cp^*\{\eta^5\text{-}C_4H_4BND(CHMe_2)_2\}HfCl_2$ only) (eq. 7).

$$Cp^*\{C_4H_4BN(CHMe_2)_2\}HfCl{\cdot}LiCl + DX \xrightarrow{\text{-LiCl}} \underset{(X = Cl,\ CC(TMS))}{} \qquad (7)$$

$$Cp^*\{C_4H_4BND(CHMe_2)_2\}HfCl(X)$$
exclusive product

In both cases, in the ^1H NMR of the d_1-product, the peak assigned to the amino proton is completely absent, and the integrals of the peaks corresponding to the 2,5 positions of the borole are unchanged relative to what is found in the protio isotopomer. Thus, the controls exclude scrambling of the deuterium label into the borole.

In order to verify that the deuterium label had been incorporated into the product, the ^2H NMR of $Cp^*\{\eta^5\text{-}C_4H_4BND(CHMe_2)_2\}HfCl_2$ was

undertaken. In this spectrum, only one peak was observed, a broad singlet at 6.4 ppm, verifying the incorporation of deuterium onto the amino group of the product. Of course, these controls cannot be used to exclude a mechanism involving stereospecific protonation/deprotonation; that is, one in which the same proton that is added to the 2,5 position of the borole migrates to the amino group. Only mechanisms involving scrambling of the hydrogens in the intermediate are excluded. Herberich and coworkers, however, have also shown that the iron borole complex incorporates deuterium into the 2,5-positions instantaneously upon contact with D_2O. This result supports the notion that the presumed intermediate undergoes facile deprotonation from both faces; i.e. that deprotonation is not stereospecific. Thus, we feel that the mechanism involving direct protonation at the amino group is the more reasonable one.

3. Conclusions

The hafnium aminoborole complexes are found to heterolytically cleave several H-X bonds (X = Cl, CCTMS). Many of the other reactions with polar H-X bonds were found to proceed to a mixture of products. Addition of MeI to the aminoborole complex results in alkylation at the 2-position of the heterocycle. Herberich has found similar results for iron phenylborole complexes. Control experiments provide evidence against a mechanism involving initial attack at the 2,5-position of the borole in the heterolysis of the H-X substrates.

Currently, there does not appear to be any single explanation to account for why certain substrates react cleanly and others react to form mixtures. A more detailed understanding of the kinetics of the reactions would likely further the understanding of this issue. In this sense, the reaction in equation 4 is a good candidate for further investigation, since the intermediate can be observed by NMR.

4. Experimental

All manipulations were performed using glove box and high-vacuum line techniques[20]. Solvents were dried over Na/benzophenone and stored over Na/benzophenone (THF, ether) or titanocene[21] (toluene, petroleum

ether, heptane). NMR solvents: benzene-d_6 was dried over $LiAlH_4$ and then over sodium metal; THF-d_8 was purified by vacuum transfer from Na/benzophenone.

Argon was purified by passage over MnO on vermiculite and activated 4Å molecular sieves. TMS-acetylene (Aldrich) and MeI (Aldrich) were degassed and stored over activated molecular sieves. LiCCTMS was prepared by deprotonation of HCCTMS with ^{n}BuLi in petroleum ether. ^{n}BuLi (Aldrich), Acetophenone (Aldrich), HCl (Matheson), DCl (Cambridge Isotope Labs), D_2O (Cambridge Isotope Labs) were all used as received.

NMR spectra were carried out on a Bruker AM-500 spectrometer at 500 MHz for proton, 125.8 MHz for carbon, and 76.75 MHz for deuterium, a GE QE-300 spectrometer at 300 MHz for proton and 75.5 MHz for carbon. All shifts reported for proton, deuterium and carbon NMR were referenced to solvent. NMR tube reactions were carried out using J. Young-type Teflon-valved NMR tubes purchased from Wilmad. Infrared spectra were recorded on a Perkin-Elmer 1600 Series FTIR. Elemental analyses were carried out by Mr. Fenton Harvey at Caltech.

$Cp^*[C_4H_4BNH(CHMe_2)_2]HfCl_2$ (1)

A swivel frit assembly was charged with 1.25 g (2.26 mmol) of $Cp^*[C_4H_4BN(CHMe_2)_2]HfCl{\cdot}LiCl$. THF (50 mL) was condensed onto the solid. Using a 104 mL gas bulb, 402 torr HCl (1 eq.) was condensed into the solution at -78°C. Upon warming, the red solution rapidly changed color to yellow. The solution was stirred an additional two hours, and volatiles were removed. Toluene (50 mL) was condensed in, the solution filtered, and volatiles evaporated. Petroleum ether was condensed (40 mL) onto the residue, and the crude product isolated on the frit by cold filtration, yielding 0.96g (78%) of yellow powder. The crude product was recrystallized from hot heptane (8 mL), yielding 0.5 mg of $Cp^*[C_4H_4BNH(CHMe_2)_2]HfCl_2$ as small yellow cubic crystals.

^{1}H NMR (300 MHz, benzene-d_6): 6.38 (br, 1H, $HNCH(CH_3)_2$); 5.90 (m, 2H, H3, H4); 4.75 (m, 2H, H2, H5); 3.25 (pseudo sept., $^3J_{HH}$ = 7 Hz, 2H,

NC*H*(CH_3)$_2$); 2.15 (s, 15H, C_5(CH_3)$_5$); 0.97 (d, $^3J_{HH}$ = 7 Hz, 12H, HNCH(CH_3)$_2$); 0.92 (d, $^3J_{HH}$ = 7 Hz, 12H, HNCH(CH_3)$_2$). $^{13}C\{^1H\}$ NMR (75 MHz, benzene-d_6): 119.1 (s, C_5(CH_3)$_5$); 114.1 (s, C3,C4); 50.6 (s, NCH(CH_3)$_2$); 20.2 (s, NCH(CH_3)$_2$); 19.4 (s, NCH(CH_3)$_2$); 12.1 (s, C_5(CH_3)$_5$). UV-vis: Elemental analysis, calculated for $C_{20}H_{34}BCl_2HfN$: C 43.80; H 6.20; N 2.55. Found: C 42.80; H 6.06; N 2.37.

Cp*(η^5-C_4H_4BND(CH(Me)$_2$)$_2$)$HfCl_2$ (1-d_1)

A swivel frit assembly was charged with 250mg Cp*(η^5-C_4H_4BN(CH(Me)$_2$)$_2$)HfCl·LiCl (0.45 mmol). THF (20 mL) was condensed in at -78°C. The vacuum manifold was exposed to D_2O vapor from hot D_2O (5 mL) for 5 minutes to exchange acidic sites on the silica. The manifold was evacuated for 5 min. to remove the vapor. DCl (1 eq.) was added by gas bulb to the solution. Upon warming, the solution changed from red to yellow in color. Work up and recrystallization as for the HCl analogue. Isolated 90mg (37%).

^1H NMR (300 MHz, C_6D_6): 5.90 (m, 2H, H3, H4); 4.75 (m, 2H, H2, H5); 3.25 (sept., $^3J_{HH}$ = 7 Hz, 2H, 2 C*H*(CH_3)$_2$); 2.15 (s, 15H, C_5(CH_3)$_5$); 0.97 (d, $^3J_{HH}$ = 7 Hz, 6H, CH(C*H*$_3$)$_2$); 0.92 (d, $^3J_{HH}$ = 7 Hz, 6H, CH(C*H*$_3$)$_2$). ^2H NMR (76.75 MHz, C_6D_{12}): 6.4 (br, 1D, N*D*(CH(CH_3)$_2$)$_2$).

Cp*(η^5-C_4H_4BNH(CH(Me)$_2$)$_2$)HfCl(CC(TMS)) (2)

A medium-sized fine-porosity frit assembly with 100 mL flasks was loaded with 2.00 g (0.0036 moles) Cp*(η^5-C_4H_4BN(CH(Me)$_2$)$_2$)HfCl·LiCl in the dry box. The apparatus was evacuated on the high vacuum line and 40 mL toluene was condensed onto the solid to give a deep orange solution. Then 1.1 equivalents (trimethylsilyl)acetylene was added via 104 mL gas bulb (4 x 176 torr). The solution was heated to 80°C in an oil bath for 75 minutes, slowly changing from orange to yellow in color. The solution was cooled to room temperature, and the LiCl precipitate was allowed to settle for 30 minutes and filtered off. Volatiles were removed and then 30 mL petroleum

ether was added and removed *in vacuo* to facilitate removal of residual toluene. The crude product was recrystallized from 40mL hot heptane, yielding 1.49 g (67.7%) of Cp*(η^5-$C_4H_4BNH(CH(Me)_2)_2$)HfCl(CC(TMS)) as yellow-orange crystals.

^{1}H NMR (500 MHz, C_6D_6): 7.47 (s, br, 1H, N-*H*); 5.90 (m, 1H, H3, H4); 5.61 (m, 1H, H3, H4); 5.15 (m, 1H, H2, H5); 3.85 (m, 1H, H2, H5); 3.55 (psd. sept., $^3J_{HH}$ = 6.8 Hz, 1H, C*H*$(CH_3)_2$); 3.04 (psd. sept., $^3J_{HH}$ = 6.7 Hz, 1H, C*H*$(CH_3)_2$); 2.10 (s, 15H, $C_5(CH_3)_5$); 1.06 (m, 6H, CH(C*H*$_3)_2$); 0.98 (m, 6H, CH(C*H*$_3)_2$); 0.23 (s, 9H, CCSi(C*H*$_3)_3$). ^{13}C NMR (125.8 MHz, C_6D_6): 183.0 (s, *C*CTMS); 131.6 (s, C*C*TMS); 118.22 (s, *C*$_5(CH_3)_5$); 114.1 (d, $^1J_{CH}$ = 160 Hz, C3, C4); 110.4 (d, $^1J_{CH}$ = 163 Hz, C3, C4); 106.5 (d, br, C2, C5); 96.3 (d, br, C2, C5); 52.4 (d, $^1J_{CH}$ = 142 Hz, *C*H$(CH_3)_2$); 50.6 (d, $^1J_{CH}$ = 140 Hz, *C*H$(CH_3)_2$); 20.0-21.5 (overlapping, 2CH$(CH_3)_2$); 12.9 (q, $^1J_{CH}$ = 125 Hz, $C_5(CH_3)_5$); 1.37 (q, $^1J_{CH}$ = 119 Hz, CCSi$(CH_3)_3$). IR(Nujol): 2010 cm^{-1} ν(CC). Elemental analysis, calculated for $C_{25}H_{43}BClHfNSi$: C 49.21; H 7.05; N 2.29. Found: C 48.98; H 7.17; N 2.22.

Cp*(η^5-$C_4H_4BND(CH(Me)_2)_2$)HfCl(CC(TMS)) (2-*d*$_1$)

TMS-acetylene-*d*$_1$ was prepared by treatment of LiCCTMS with D_2O and distillation of the acetylene from the reaction solvent (toluene). Preparation of Cp*(η^5-$C_4H_4BND(CH(Me)_2)_2$)HfCl(CC(TMS)) was analogous to that of the protio isotopomer.

^{1}H NMR (300 MHz, C_6D_6): 5.90 (m, 1H, H3, H4); 5.61 (m, 1H, H3, H4); 5.15 (m, 1H, H2, H5); 3.85 (m, 1H, H2, H5); 3.55 (psd. sept., $^3J_{HH}$ = 7 Hz, 1H, C*H*$(CH_3)_2$); 3.04 (psd. sept., $^3J_{HH}$ = 7 Hz, 1H, C*H*$(CH_3)_2$); 2.10 (s, 15H, $C_5(CH_3)_5$); 1.06 (d, $^3J_{HH}$ = 7 Hz, 3H, CH(C*H*$_3)_2$); 1.05 (d, $^3J_{HH}$ = 7 Hz, 3H, CH(C*H*$_3)_2$), 0.98 (d, $^3J_{HH}$ = 7 Hz, 3H, CH(C*H*$_3)_2$); 0.97 (d, $^3J_{HH}$ = 7 Hz, 3H, CH(C*H*$_3)_2$); 0.23 (s, 9H, CCSi(C*H*$_3)_3$).

Cp*(η^5-$C_4H_4BNH(CH(Me)_2)_2$)Hf(CC(TMS))$_2$ (3)

A J. Young-type NMR tube was charged with 50 mg (.097 mmol) $Cp^*(\eta^5\text{-}C_4H_4BN(CH(Me)_2)_2)Hf(\eta^3\text{-}C_3H_5)$ and 0.75 mL C_6D_6. On the vacuum line, 2.0 equivalents TMS-acetylene was added via a gas bulb. Upon thawing, the solution changed color from blue to orange-yellow. Volatiles were evaporated, and fresh C_6D_6 added (0.75 mL). The reaction was complete in 6h.

^1H NMR (300 MHz, C_6D_6): 7.4 (br, 1H, N-*H*); 5.57 (m, 2H, H3, H4); 4.84 (m, 2H, H2, H5); 3.42 (psd. sept., $^3J_{HH}$ = 6.6 Hz, 2H, C*H*$(CH_3)_2$); 2.17 (s, 15H, $C_5(CH_3)_5$); 1.14 (d, $^3J_{HH}$ = 6.6 Hz, 6H, CH(C*H*$_3)_2$); 1.02 (d, $^3J_{HH}$ = 6.6 Hz, 6H, CH(C*H*$_3)_2$); 0.22 (s, 18H, (CC(Si(C*H*$_3)_3)_2$). $^{13}C\{^1H\}$ NMR (75.5 MHz, C_6D_6): 183.54 (s, *C*C(Si$(CH_3)_3)_2$); 128.92 (s, C*C*(Si$(CH_3)_3)_2$); 117.1 (s, *C*$_5(CH_3)_5$); 109.96 (s, C3, C4); 102 (br, C2, C5); 50.9 (s, *C*H$(CH_3)_2$); 20.76 (s, CH(*C*H$_3)_2$); 20.68 (s, CH(*C*H$_3)_2$); 12.74 (s, C_5(*C*H$_3)_5$); 0.937 (s, CC(Si(*C*H$_3)_3)_2$). IR (Nujol): 2025 cm^{-1} (w, ν(CC)); 2007 cm^{-1} (m, ν(CC)).

$Cp^*\{\eta^5\text{-}C_4H_4BN(CHMe_2)_2\}Hf(CCTMS)(\eta^2\text{-}HCCTMS)$

The intermediate is observed along with **3** shortly after addition of the acetylene to the allyl. After 12 hours, only product remains.

^1H NMR (300 MHz, C_6D_6): 8.5 (s, 1H, *H*CCTMS); 5.5-5.6 (mult., overlapping, 2H, H3, H4); 4.35 (m, 1H, H2, H5); 3.78 (psd. sept., $^3J_{HH}$ = 6.6 Hz, 1H, C*H*$(CH_3)_2$); 3.7 (m, 1H, H2, H5); 3.23 (psd. sept., $^3J_{HH}$ = 6.6 Hz, 1H, C*H*$(CH_3)_2$); 1.92 (s, 15H, $C_5(CH_3)_5$); 1.61 (d, $^3J_{HH}$ = 6.6 Hz, 3H, CH(C*H*$_3)_2$); 1.40 (d, $^3J_{HH}$ = 6.6 Hz, 3H, CH(C*H*$_3)_2$); 1.30 (d, $^3J_{HH}$ = 6.6 Hz, 3H, CH(C*H*$_3)_2$); 0.95 (d, $^3J_{HH}$ = 6.6 Hz, 6H, CH(C*H*$_3)_2$); 0.27 (s, 9H, (CC(Si(C*H*$_3)_3)$)); 0.10 (s, 9H, (HCC(Si(C*H*$_3)_3$)).

$Cp^*(\eta^5\text{-}C_4H_3MeBNH(CH(Me)_2)_2)HfClI$ (4)

A small frit was charged with 0.50g (9.0 mmol) $Cp^*[C_4H_4BN(CHMe_2)_2]HfCl\cdot LiCl$. The solid was dissolved in THF (50 mL). Using a gas bulb, 1.0 eq. of MeI was added at -78°C. The red solution turned yellow over the course of one hour at RT. Volatiles were evaporated and toluene (30 mL) was condensed in. The solution was allowed to settle for 1h.,

and then was filtered by gravity. Volatiles evaporated. X-ray quality crystals were grown by slow diffusion of toluene into a pentane solution at -20°C.

^{1}H NMR (300 MHz, C_6D_6): 5.42 (m, 1H, H3 or H4); 5.25 (m, 1H, H2 or H5); 3.75 (m, 1H, H2 or H5); 3.40 (sept., 1H, NC*H*$(CH_3)_2$); 3.05 (sept., 1H, NC*H*$(CH_3)_2$); 1.95 (s, 15H, $C_5(CH_3)_5$); 1.3-0.8 (m, 12H, N$(CH(CH_3)_2)_2$). Elemental analysis, calculated for $C_{21}H_{36}BClHfI$: C 38.58; H 5.51; N 2.14. Found: C 39.88; H 5.61; N 1.84.

5. References and Notes

1. Jutzi, P.; Siemelimg, U. *J. Organomet. Chem.*, **1995**, *500*, 175 and references therein.
2. Jutzi, P.; Dahlhaus, J. *Coord. Chem. Rev.*, **1994**, *137*, 179 and references therein.
3. Stahl, K.-P.; Boche, G.; Massa, W. *J. Organomet. Chem.*, **1984**, *277*, 113.
4. Boratabenzenes, see (a) Herberich, G.E.; Ohst, H. *Adv. Organomet. Chem.*, **1986**, *25*, 199 and references therein. (b) Herberich, G.E.; Schmidt, B.; Englert, U.; Wagner, T. *Organometallics*, **1993**, *12*, 2891. (c) Herberich, G.E.; Schmidt, B.; Englert, U. *Organometallics*, **1995**, *14*, 471. (d) Ashe, A.J.; Kampf, J. W.; Muller, C.; Schneider, M. *Organometallics*, **1996**, *15*, 387. Boroles, see (e) Herberich, G.E.; Hostalek, M.; Laven, R.; Boese, R. *Angew. Chem. Int. Ed. Engl.*, **1990**, *29*, 317. (f) Herberich, G.E.; Hessner, B.; Ohst, H.; Rapp, I.A. *J. Organomet. Chem.*, **1988**, *348*, 305. (g) Herberich, G.E.; Negele, M.; Ohst, H. *Chem. Ber.*, **1991**, *124*, 25. (h) Bazan, G.C.; Donnelly, S.J.; Rodriguez, G. *J. Am. Chem. Soc.* **1995**, *117*, 2671.
5. (a) Cullen, W.R.; Woollins, J. D. *Coord. Chem. Rev.*, **1982**, *39*, 1 and references therein. (b) Hayashi, T.; Kumada, M. *Acc. Chem. Res.*, **1982**, *15*, 395. (c) Hayashi, T.; Konishi, M.; Ito, H.; Kumada, M. *J. Am. Chem. Soc.* **1984**, *106*, 4962.
6. (a) Pastor, A.; Kiely, A.F.; Henling, L.M.; Day, M.W.; Bercaw, J.E. *J. Organomet. Chem.*, in press. (b) Quan, R.W.; Bazan, G.C.; Kiely, A.F.; Schaefer, W.P.; Bercaw, J.E. *J. Am. Chem. Soc.* **1994**, *116*, 4489.
7. (a) Jacoby, D.; Floriani, C.; Chiesi-Villa, A.; Rizzoli, C. *J. Am. Chem. Soc.* **1993**, *115*, 3595. (b) Jacoby, D.; Isoz, S.; Floriani, C.; Chiesi-Villa, A.; Rizzoli, C. *J. Am. Chem. Soc.* **1995**, *117*, 2805. (c) Gallo, E.; Solari, E.; Floriani, C.; Chiesi-Villa, A.; Rizzoli, C. *Organometallics*, **1995**, *14*, 2156. (d) De Angelis, S.; Solari, E.; Floriani, C.; Chiesi-Villa, A.; Rizzoli, C. *Organometallics*, **1995**, *14*, 4505. (e) Jacoby, D.; Isoz, S.; Floriani, C.; Schenk, K.; Chiesi-Villa, A.; Rizzoli, C. *Organometallics*, **1995**, *14*, 4816.

8. Hibbert, F.; Emsley, J. *Adv. Phys. Org. Chem.* **1990**, *26*, 255 and references therein.
9. So far, all the group IV enolates that have been characterized have been O-bound. see (a) Veya, P.; Floriani, C.; Chiesi-Villa, A.; Rizzoli, C. *Organometallics*, **1993**, *12*, 4892. (b) Veya, P.; Floriani, C.; Chiesi-Villa, A.; Rizzoli, C. *Organometallics*, **1994**, *13*, 213. (c) Cozzi, P. G.; Floriani, C.; Chiesi-Villa, A.; Rizzoli, C. *Organometallics*, **1994**, *13*, 2131 and references therein.
10. Lang, H.; Herres, M.; Zsolnai, L.; Imhof, W. *J. Organomet. Chem.*, **1991**, *409*, C7-C11.
11. It has recently been found by solution molecular weight measurment that **2** is apparently a dimer in bezene solution. Work in progress, Nelson, C. M.
12. Cassar, L. *J. Organomet. Chem.*, **1975**, *93*, 253.
13. The appearance of two stretching modes is consistent with the complex having C_s symmetry. For acetylides, all the IR-active modes are not necessarily observed. For a review of metal-acetylides, see Manna, J. K.; John, K. D.; Hopkins, M. D. *Adv. Organomet. Chem.* **1995**, *38*, 79.
14. *Principles and Applications of Organotransition Metal Chemistry*, Collman, J. P.; Hegedus, L. S.; Norton, J. R.; Finke, R. G. University Science, Mill Valley, **1987**, p 156-157.
15. Qualitative correlations between the ^{1}H NMR chemical shifts of terminal acetylenes and their donor character have been observed, with downfield shifts indicating greater donation. These correlations are based on group VI complexes, so it is unclear how well they apply in this case. The acetylene C-H shift of 8.5 ppm is intermediate between what is observed for 2 (7-8 ppm) and 4 electron (12-14 ppm) donors. see Templeton, J. L.; Ward, B. C.; Chen, G. J.; McDonald, J. W.; Newton, W . E. *Inorg. Chem.* **1981**, *20*, 1248 and references therein.
16. If the acetylene is coordinated as shown, then the π-donor orbital of the acetylene is in the plane of the metallocene wedge, and should be able to interact with the vacant metal orbital. See chapter 3, section 2c for details on metallocene frontier orbitals.
17. Addition of MeI to Cp*{η^5-$C_4H_4BN(CHMe_2)_2$}HfI·LiI results in a much purer product, suggesting that most of the impurities in crude 4 are

species with all the possible combinations of halides coordinated to the metal. Wong-Foy, A. unpublished results.

18. Herberich, G.E.; Carstensen, T.; Koffer, D. P. J.; Klaff, N.; Boesse, R.; Stephan, M.; Meth, H.; Zenneck, U. *Organometallics*, **1994**, *13*, 619.
19. Reaction of ICH_2Ph with $Cp^*\{\eta^5\text{-}C_4H_4BN(CHMe_2)_2\}ZrCl\cdot LiCl$ results in a new species whose ^1H and ^{13}C NMR spectra are consistent with its formulation as the product resulting from alkylation of the 2 position of the borole. Pastor, A; Bercaw, J. E. unpublished results.
20. Burger, B.J.; Bercaw, J.E. In *Experimental Organometallic Chemistry*; Wayda, A.L., Darensbourg, M.Y. Eds.; ACS Symposium Series 357; American Chemical Society, Washington, D.C. 1987
21. Marvich, R.H.; Brintzinger, H.H. *J. Am. Chem. Soc.* **1971**, *93*, 2046

Appendix A: Crystal Stucture Data for PPN[(P_3O_9)Ru(C_6H_6)]

Table 1. Crystal and Intensity Collection Data for PPN[(P_3O_9)Ru(C_6H_6)]

Formula: $C_{42}H_{38}NO_{10}P_5Ru$ Formula Weight: 955.18

Color: Yellow Habit: Bladed

Crystal size: 0.186 X 0.256 X 0.480mm

Space group: $P2_1/c$ (#14)

a = 9.024(1)Å

b = 16.926(4)Å B = 93.31(1)°

c = 26.819(6)Å

V = 4089.5(14)Å^3

ρ_{calc} = 1.580g/cm^{-1}

μ = 6.259 cm^{-1} (μr_{max} = 0.18)

CAD-4 diffractometer

λ = 0.7107Å Graphite monochrometer

2θ range: 2-50°

T = 223K

Number of independant reflections: 7186

Number with $F_o^2 > 0$: 6869

Number with $F_o^2 > 3\sigma$: 5754

Goodness of fit for merging data: 1.01

Final goodness of fit: 1.68 for 7186 reflections and 684 parameters

Final R-index: .0382

Final R-index : .0286 for reflections with $F_o^2 > 3\sigma(F_o^2)$

Table 2. Complete Bond Distances and Angles for PPN[(P_3O_9)Ru(C_6H_6)]

	Distance(Å)		Distance(Å)
Ru –O1	2.124(2)	P5 –C51	1.792(2)
Ru –O4	2.120(2)	P5 –C61	1.793(2)
Ru –O7	2.127(2)	C11 –C12	1.390(3)
Ru –CB	1.630	C11 –C16	1.393(3)
Ru –C1	2.142(4)	C12 –C13	1.374(4)
Ru –C2	2.137(4)	C12 –H12	0.88(2)
Ru –C3	2.129(5)	C13 –C14	1.371(4)
Ru –C4	2.133(5)	C13 –H13	0.90(3)
Ru –C5	2.128(5)	C14 –C15	1.377(4)
Ru –C6	2.139(4)	C14 –H14	0.88(3)
P1 –O1	1.508(2)	C15 –C16	1.370(4)
P2 –O4	1.507(2)	C15 –H15	0.93(3)
P3 –O7	1.509(2)	C16 –H16	0.93(2)
P1 –O3	1.615(2)	C21 –C22	1.393(4)
P1 –O9	1.611(2)	C21 –C26	1.385(4)
P2 –O3	1.608(2)	C22 –C23	1.384(4)
P2 –O6	1.610(2)	C22 –H22	0.91(3)
P3 –O6	1.616(2)	C23 –C24	1.375(4)
P3 –O9	1.610(2)	C23 –H23	0.89(3)
P1 –O2	1.450(2)	C24 –C25	1.368(4)
P2 –O5	1.459(2)	C24 –H24	0.94(3)
P3 –O8	1.448(2)	C25 –C26	1.384(4)
C1 –C2	1.335(6)	C25 –H25	0.86(3)
C1 –C6	1.341(6)	C26 –H26	0.88(2)
C1 –H1	0.99(4)	C31 –C32	1.391(3)
C2 –C3	1.395(6)	C31 –C36	1.393(4)
C2 –H2	0.88(3)	C32 –C33	1.380(4)
C3 –C4	1.419(7)	C32 –H32	0.94(2)
C3 –H3	0.77(4)	C33 –C34	1.367(4)
C4 –C5	1.422(7)	C33 –H33	0.87(3)
C4 –H4	0.68(4)	C34 –C35	1.377(4)
C5 –C6	1.355(7)	C34 –H34	0.92(3)
C5 –H5	0.83(4)	C35 –C36	1.376(4)
C6 –H6	1.01(4)	C35 –H35	0.90(3)
N –P4	1.578(2)	C36 –H36	0.89(3)
N –P5	1.575(2)	C41 –C42	1.398(4)
P4 –C11	1.794(2)	C41 –C46	1.387(3)
P4 –C21	1.804(2)	C42 –C43	1.384(4)
P4 –C31	1.797(2)	C42 –H42	0.90(2)
P5 –C41	1.807(2)	C43 –C44	1.361(4)

Table 2. Complete Bond Distances and Angles for PPN[(P_3O_9)Ru(C_6H_6)]

	Distance(Å)		Angle(°)	
C43 –H43	0.85(3)	O1 –Ru –O4	87.2(1)
C44 –C45	1.374(4)	O4 –Ru –O7	85.4(1)
C44 –H44	0.91(3)	O7 –Ru –O1	84.9(1)
C45 –C46	1.379(4)	CB –Ru –O1	129.7
C45 –H45	0.89(3)	CB –Ru –O4	125.6
C46 –H46	0.93(3)	CB –Ru –O7	129.2
C51 –C52	1.392(3)	Ru –O1 –P1	127.1(1)
C51 –C56	1.383(3)	Ru –O4 –P2	126.2(1)
C52 –C53	1.371(4)	Ru –O7 –P3	127.3(1)
C52 –H52	0.87(2)	Ru –O1 –O3	99.9(1)
C53 –C54	1.373(4)	Ru –O1 –O9	101.4(1)
C53 –H53	0.89(3)	Ru –O4 –O3	100.0(1)
C54 –C55	1.374(4)	Ru –O4 –O6	101.1(1)
C54 –H54	0.88(3)	Ru –O7 –O6	100.9(1)
C55 –C56	1.383(4)	Ru –O7 –O9	101.0(1)
C55 –H55	0.92(3)	Ru –O1 –O2	156.7(1)
C56 –H56	0.93(2)	Ru –O4 –O5	156.4(1)
C61 –C62	1.387(3)	Ru –O7 –O8	157.1(1)
C61 –C66	1.385(3)	O2 –P1 –O1	119.3(1)
C62 –C63	1.379(4)	O5 –P2 –O4	118.3(1)
C62 –H62	0.88(2)	O8 –P3 –O7	119.1(1)
C63 –C64	1.374(4)	O3 –P1 –O1	107.6(1)
C63 –H63	0.92(3)	O9 –P1 –O1	107.0(1)
C64 –C65	1.372(4)	O9 –P1 –O3	99.8(1)
C64 –H64	0.91(3)	O5 –P2 –O3	109.9(1)
C65 –C66	1.377(4)	O6 –P2 –O3	101.2(1)
C65 –H65	0.89(2)	O6 –P2 –O5	110.3(1)
C66 –H66	0.88(2)	O7 –P3 –O6	107.2(1)
W –HW1	0.83(3)	O9 –P3 –O6	100.2(1)
W –HW2	0.76(3)	O9 –P3 –O7	107.6(1)
W –O5	2.862(3)	O3 –P1 –O2	110.2(1)
W –O1	3.114(3)	O9 –P1 –O2	111.1(1)
HW1 –O5	2.06(3)	O3 –P2 –O4	108.1(1)
HW2 –O1	2.37(3)	O6 –P2 –O4	107.6(1)
		O6 –P3 –O8	110.3(1)
		O9 –P3 –O8	110.8(1)
		P2 –O3 –P1	123.3(1)
		P3 –O6 –P2	122.3(1)
		P3 –O9 –P1	123.6(1)
		C6 –C1 –C2	122.0(4)

Table 2. Complete Bond Distances and Angles for PPN[(P_3O_9)Ru(C_6H_6)]

			Angle(°)				Angle(°)
H1	-C1	-C2	114.2(24)	H14	-C14	-C13	120.3(18)
H1	-C1	-C6	123.1(24)	H14	-C14	-C15	119.7(18)
C3	-C2	-C1	120.7(4)	C16	-C15	-C14	120.1(3)
H2	-C2	-C1	122.0(22)	H15	-C15	-C14	120.0(16)
H2	-C2	-C3	117.0(22)	H15	-C15	-C16	119.9(16)
C4	-C3	-C2	118.4(4)	C15	-C16	-C11	120.3(2)
H3	-C3	-C2	115.7(28)	H16	-C16	-C11	119.6(14)
H3	-C3	-C4	125.6(28)	H16	-C16	-C15	120.1(14)
C5	-C4	-C3	118.1(5)	C22	-C21	-P4	123.3(2)
H4	-C4	-C3	130.4(30)	C26	-C21	-P4	117.3(2)
H4	-C4	-C5	111.5(30)	C26	-C21	-C22	119.3(2)
C6	-C5	-C4	119.5(5)	C23	-C22	-C21	119.9(3)
H5	-C5	-C4	119.1(25)	H22	-C22	-C21	121.4(16)
H5	-C5	-C6	121.0(25)	H22	-C22	-C23	118.7(16)
C5	-C6	-C1	121.2(4)	C24	-C23	-C22	120.2(3)
H6	-C6	-C1	125.3(20)	H23	-C23	-C22	120.4(19)
H6	-C6	-C5	112.7(20)	H23	-C23	-C24	119.4(19)
P5	-N	-P4	142.1(1)	C25	-C24	-C23	120.2(3)
C11	-P4	-N	116.1(1)	H24	-C24	-C23	120.8(16)
C21	-P4	-N	107.1(1)	H24	-C24	-C25	119.0(16)
C31	-P4	-N	110.7(1)	C26	-C25	-C24	120.4(3)
C21	-P4	-C11	108.8(1)	H25	-C25	-C24	124.9(17)
C31	-P4	-C11	108.3(1)	H25	-C25	-C26	114.7(17)
C31	-P4	-C21	105.3(1)	C25	-C26	-C21	120.1(2)
C41	-P5	-N	111.4(1)	H26	-C26	-C21	119.2(15)
C51	-P5	-N	113.8(1)	H26	-C26	-C25	120.8(15)
C61	-P5	-N	108.6(1)	C32	-C31	-P4	118.5(2)
C51	-P5	-C41	107.5(1)	C36	-C31	-P4	122.6(2)
C61	-P5	-C41	106.9(1)	C36	-C31	-C32	118.8(2)
C61	-P5	-C51	108.4(1)	C33	-C32	-C31	120.2(2)
C12	-C11	-P4	120.7(2)	H32	-C32	-C31	118.5(14)
C16	-C11	-P4	120.1(2)	H32	-C32	-C33	121.3(14)
C16	-C11	-C12	119.1(2)	C34	-C33	-C32	120.4(3)
C13	-C12	-C11	119.8(2)	H33	-C33	-C32	119.8(17)
H12	-C12	-C11	119.9(15)	H33	-C33	-C34	119.8(17)
H12	-C12	-C13	120.3(15)	C35	-C34	-C33	120.0(3)
C14	-C13	-C12	120.6(3)	H34	-C34	-C33	120.1(17)
H13	-C13	-C12	121.0(16)	H34	-C34	-C35	119.9(17)
H13	-C13	-C14	118.3(16)	C36	-C35	-C34	120.4(3)
C15	-C14	-C13	120.1(3)	H35	-C35	-C34	120.1(18)

Table 2. Complete Bond Distances and Angles for PPN[(P_3O_9)Ru(C_6H_6)]

	Angle(°)		Angle(°)
H35 –C35 –C36	119.5(18)	C62 –C61 –P5	121.2(2)
C35 –C36 –C31	120.2(3)	C66 –C61 –P5	119.3(2)
H36 –C36 –C31	119.7(17)	C66 –C61 –C62	119.5(2)
H36 –C36 –C35	120.1(17)	C63 –C62 –C61	119.7(2)
C42 –C41 –P5	119.5(2)	H62 –C62 –C61	120.6(15)
C46 –C41 –P5	121.5(2)	H62 –C62 –C63	119.7(15)
C46 –C41 –C42	118.9(2)	C64 –C63 –C62	120.5(3)
C43 –C42 –C41	119.6(2)	H63 –C63 –C62	119.7(15)
H42 –C42 –C41	118.4(16)	H63 –C63 –C64	119.7(15)
H42 –C42 –C43	121.9(16)	C65 –C64 –C63	119.9(3)
C44 –C43 –C42	120.9(3)	H64 –C64 –C63	120.4(16)
H43 –C43 –C42	115.9(18)	H64 –C64 –C65	119.7(16)
H43 –C43 –C44	123.2(18)	C66 –C65 –C64	120.4(3)
C45 –C44 –C43	119.8(3)	H65 –C65 –C64	119.4(16)
H44 –C44 –C43	118.2(17)	H65 –C65 –C66	120.1(16)
H44 –C44 –C45	122.0(17)	C65 –C66 –C61	120.0(2)
C46 –C45 –C44	120.5(3)	H66 –C66 –C61	118.5(14)
H45 –C45 –C44	120.1(17)	H66 –C66 –C65	121.4(15)
H45 –C45 –C46	119.3(17)	HW2 –W –HW1	107.2(31)
C45 –C46 –C41	120.2(2)	O5 –HW1 –W	160.7(27)
H46 –C46 –C41	118.1(16)	O1 –HW2 –W	167.4(31)
H46 –C46 –C45	121.7(16)		
C52 –C51 –P5	119.0(2)		
C56 –C51 –P5	121.7(2)		
C56 –C51 –C52	118.8(2)		
C53 –C52 –C51	120.7(2)		
H52 –C52 –C51	117.7(15)		
H52 –C52 –C53	121.6(15)		
C54 –C53 –C52	120.1(3)		
H53 –C53 –C52	120.2(17)		
H53 –C53 –C54	119.5(17)		
C55 –C54 –C53	119.8(3)		
H54 –C54 –C53	118.8(16)		
H54 –C54 –C55	121.3(16)		
C56 –C55 –C54	120.5(3)		
H55 –C55 –C54	118.0(16)		
H55 –C55 –C56	121.4(16)		
C55 –C56 –C51	120.0(2)		
H56 –C56 –C51	121.8(14)		
H56 –C56 –C55	118.2(14)		

Appendix B: Crystal Structure Data for $Cp^*\{C_4H_4BN(CHMe_2)_2\}HfCl\cdot LiCl(Et_2O)_2$

Table 1. Crystal and Intensity Collection Data for $Cp^*\{C_4H_4BN(CHMe_2)_2\}HfCl\cdot LiCl(Et_2O)_2$

Formula: $C_{28}H_{53}BCl_2HfLiNO_2$ Formula Weight: 702.88

Color: Purple Habit: Irregular Plate

Crystal size: 0.008 X 0.48 X 0.4760mm

Space group: $P2_1/n$ (#14)

a = 10.987(4)Å

b = 21.362(7)Å $\beta = 95.85(2)^o$

c = 14.480(3)Å

V = 3380.8(19)Å^3

$\rho_{calc} = 1.380 g/cm^{-1}$

$\mu = 32.38\ cm^{-1}$

CAD-4 diffractometer

$\lambda = 0.7107$Å Graphite monochrometer

2θ range: 2-50^o

T = 296K

Number of independant reflections: 5940

Number with $F_o^2 > 0$: 5296

Number with $F_o^2 > 3\sigma$: 3580

Goodness of fit for merging data: 1.02

Final goodness of fit: 1.52 for 5939 reflections and 325 parameters

Final R-index: .006

Final R-index : .0042 for reflections with $F_o^2 > 3\sigma(F_o^2)$

Table 2. Complete Bond Distances and Angles for $Cp^*\{C_4H_4BN(CHMe_2)_2\}HfCl\cdot LiCl(Et_2O)_2$

		Distance(Å)			Distance(Å)
Hf	–Cp	2.219	Cp5	–Me5	1.504(11)
Hf	–Cb	2.132	C1	–C2	1.390(11)
Hf	–Cl1	2.496(2)	C1	–B	1.522(10)
Hf	–Cl2	2.531(2)	C2	–C3	1.382(12)
Hf	–Cp1	2.530(8)	C3	–C4	1.442(11)
Hf	–Cp2	2.525(8)	C4	–B	1.530(10)
Hf	–Cp3	2.538(8)	B	–N	1.435(9)
Hf	–Cp4	2.520(8)	N	–C5	1.421(10)
Hf	–Cp5	2.493(7)	N	–C8	1.465(10)
Hf	–C1	2.360(7)	C5	–C6	1.476(13)
Hf	–C2	2.358(8)	C5	–C7	1.467(13)
Hf	–C3	2.418(8)	C8	–C9	1.431(13)
Hf	–C4	2.498(7)	C8	–C10	1.454(13)
Hf	–B	2.693(8)	C11	–H11A	0.938
Cl1	–Li	2.417(13)	C11	–H11B	0.940
Cl2	–Li	2.410(13)	C12	–H12A	0.953
Li	–O1	1.921(14)	C12	–H12B	0.932
Li	–O2	1.962(14)	C12	–H12C	0.945
O1	–C11	1.480(13)	C13	–H13A	0.929
O1	–C13	1.342(16)	C13	–H13B	0.959
C11	–C12	1.458(17)	C14	–H14A	0.952
C13	–C14	1.357(19)	C14	–H14B	0.935
O2	–C15	1.38(3)	C14	–H14C	0.948
O2	–C17	1.42(3)	C15	–H15A	0.935
C15	–C16	0.99(4)	C15	–H15B	0.988
C17	–C18	0.99(3)	C16	–H16A	1.016
Cp1	–Cp2	1.400(11)	C16	–H16B	0.949
Cp1	–Cp5	1.396(10)	C16	–H16C	0.883
Cp1	–Me1	1.523(12)	C17	–H17A	1.072
Cp2	–Cp3	1.391(11)	C17	–H17B	0.892
Cp2	–Me2	1.504(13)	C18	–H18A	0.985
Cp3	–Cp4	1.402(11)	C18	–H18B	0.963
Cp3	–Me3	1.521(12)	C18	–H18C	0.891
Cp4	–Cp5	1.410(10)	Me1	–HC1A	0.941
Cp4	–Me4	1.502(12)	Me1	–HC1B	0.949

Table 2. Complete Bond Distances and Angles for $Cp^*\{C_4H_4BN(CHMe_2)_2\}HfCl\cdot LiCl(Et_2O)_2$

	Distance(Å)		Distance(Å)
Me1 –HC1C	0.949	C6 –H6C	0.943
Me1 –HC1D	0.951	C7 –H7A	0.957
Me1 –HC1E	0.943	C7 –H7B	0.946
Me1 –HC1F	0.945	C7 –H7C	0.935
Me2 –HC2A	0.938	C8 –H8	0.947
Me2 –HC2B	0.944	C9 –H9A	0.942
Me2 –HC2C	0.953	C9 –H9B	0.936
Me2 –HC2D	0.951	C9 –H9C	0.959
Me2 –HC2E	0.948	C10 –H10A	0.947
Me2 –HC2F	0.936	C10 –H10B	0.955
Me3 –HC3A	0.937	C10 –H10C	0.940
Me3 –HC3B	0.947		
Me3 –HC3C	0.956		
Me3 –HC3D	0.955		
Me3 –HC3E	0.947		
Me3 –HC3F	0.937		
Me4 –HC4A	0.943		
Me4 –HC4B	0.951		
Me4 –HC4C	0.946		
Me4 –HC4D	0.951		
Me4 –HC4E	0.943		
Me4 –HC4F	0.947		
Me5 –HC5A	0.941		
Me5 –HC5B	0.948		
Me5 –HC5C	0.953		
Me5 –HC5D	0.954		
Me5 –HC5E	0.947		
Me5 –HC5F	0.941		
C1 –H1	0.951		
C2 –H2	0.949		
C3 –H3	0.947		
C4 –H4	0.947		
C5 –H5	0.952		
C6 –H6A	0.954		
C6 –H6B	0.945		

Table 2. Complete Bond Distances and Angles for
$Cp^*\{C_4H_4BN(CHMe_2)_2\}HfCl\cdot LiCl(Et_2O)_2$

			Angle(°)				Angle(°)
Cl1	-Hf	-Cl2	87.7(1)	C3	-C2	-C1	110.8(7)
Cl1	-Hf	-Cp	108.8	C4	-C3	-C2	109.0(7)
Cl1	-Hf	-Cb	106.5	B	-C4	-C3	108.0(6)
Cl2	-Hf	-Cp	105.2	C4	-B	-C1	100.5(6)
Cl2	-Hf	-Cb	106.3	N	-B	-C1	130.9(6)
Cp	-Hf	-Cb	133.0	N	-B	-C4	128.5(6)
Hf	-Cl1	-Li	90.1(3)	C5	-N	-B	123.4(6)
Hf	-Cl2	-Li	89.4(3)	C8	-N	-B	120.7(6)
Cl1	-Li	-O1	113.9(6)	C8	-N	-C5	115.6(6)
Cl1	-Li	-O2	111.7(6)	C6	-C5	-N	116.7(7)
Cl2	-Li	-O1	119.8(6)	C7	-C5	-N	117.4(7)
Cl2	-Li	-O2	112.2(6)	C7	-C5	-C6	118.2(8)
O1	-Li	-O2	106.6(6)	C9	-C8	-N	118.4(7)
C13	-O1	-C11	112.2(9)	C10	-C8	-N	117.3(7)
C12	-C11	-O1	111.5(9)	C10	-C8	-C9	117.8(8)
C14	-C13	-O1	122.4(12)	H11A	-C11	-O1	107.3
C17	-O2	-C15	115.8(15)	H11B	-C11	-O1	107.3
C16	-C15	-O2	140.2(28)	H11A	-C11	-C12	109.5
C18	-C17	-O2	147.2(26)	H11B	-C11	-C12	109.9
Cp5	-Cp1	-Cp2	108.5(7)	H11B	-C11	-H11A	111.4
Me1	-Cp1	-Cp2	124.2(7)	H12A	-C12	-C11	106.7
Me1	-Cp1	-Cp5	126.8(7)	H12B	-C12	-C11	109.4
Cp3	-Cp2	-Cp1	108.1(7)	H12C	-C12	-C11	108.6
Me2	-Cp2	-Cp1	125.4(8)	H12B	-C12	-H12A	110.8
Me2	-Cp2	-Cp3	125.4(8)	H12C	-C12	-H12A	109.7
Cp4	-Cp3	-Cp2	108.1(7)	H12C	-C12	-H12B	111.5
Me3	-Cp3	-Cp2	124.9(7)	H13A	-C13	-O1	105.1
Me3	-Cp3	-Cp4	126.7(7)	H13B	-C13	-O1	103.3
Cp5	-Cp4	-Cp3	108.0(7)	H13A	-C13	-C14	108.3
Me4	-Cp4	-Cp3	126.1(7)	H13B	-C13	-C14	107.0
Me4	-Cp4	-Cp5	125.6(7)	H13B	-C13	-H13A	110.5
Cp4	-Cp5	-Cp1	107.3(6)	H14A	-C14	-C13	107.2
Me5	-Cp5	-Cp1	126.6(7)	H14B	-C14	-C13	109.1
Me5	-Cp5	-Cp4	125.8(7)	H14C	-C14	-C13	109.5
B	-C1	-C2	109.3(6)	H14B	-C14	-H14A	110.6

Table 2. Complete Bond Distances and Angles for
$Cp^*\{C_4H_4BN(CHMe_2)_2\}HfCl\cdot LiCl(Et_2O)_2$

	Angle(°)			Angle(°)	
H14C	-C14 -H14A	109.4	HC1F	-Me1 -HC1E	110.6
H14C	-C14 -H14B	110.9	HC2A	-Me2 -Cp2	109.0
H15A	-C15 -O2	99.7	HC2B	-Me2 -Cp2	108.6
H15B	-C15 -O2	97.0	HC2C	-Me2 -Cp2	108.2
H15A	-C15 -C16	108.4	HC2D	-Me2 -Cp2	108.3
H15B	-C15 -C16	100.6	HC2E	-Me2 -Cp2	108.5
H15B	-C15 -H15A	107.6	HC2F	-Me2 -Cp2	109.1
H16A	-C16 -C15	103.8	HC2B	-Me2 -HC2A	111.0
H16B	-C16 -C15	106.7	HC2C	-Me2 -HC2A	110.2
H16C	-C16 -C15	115.8	HC2C	-Me2 -HC2B	109.7
H16B	-C16 -H16A	104.3	HC2E	-Me2 -HC2D	109.6
H16C	-C16 -H16A	109.4	HC2F	-Me2 -HC2D	110.6
H16C	-C16 -H16B	115.7	HC2F	-Me2 -HC2E	110.8
H17A	-C17 -O2	89.4	HC3A	-Me3 -Cp3	109.4
H17B	-C17 -O2	97.2	HC3B	-Me3 -Cp3	108.8
H17A	-C17 -C18	95.4	HC3C	-Me3 -Cp3	108.3
H17B	-C17 -C18	112.9	HC3D	-Me3 -Cp3	108.3
H17B	-C17 -H17A	104.0	HC3E	-Me3 -Cp3	108.8
H18A	-C18 -C17	106.2	HC3F	-Me3 -Cp3	109.4
H18B	-C18 -C17	100.6	HC3B	-Me3 -HC3A	110.9
H18C	-C18 -C17	118.3	HC3C	-Me3 -HC3A	110.1
H18B	-C18 -H18A	105.6	HC3C	-Me3 -HC3B	109.2
H18C	-C18 -H18A	111.4	HC3E	-Me3 -HC3D	109.2
H18C	-C18 -H18B	113.6	HC3F	-Me3 -HC3D	110.1
HC1A	-Me1 -Cp1	109.0	HC3F	-Me3 -HC3E	110.8
HC1B	-Me1 -Cp1	108.8	HC4A	-Me4 -Cp4	109.1
HC1C	-Me1 -Cp1	108.7	HC4B	-Me4 -Cp4	108.7
HC1D	-Me1 -Cp1	108.6	HC4C	-Me4 -Cp4	109.0
HC1E	-Me1 -Cp1	108.9	HC4D	-Me4 -Cp4	108.8
HC1F	-Me1 -Cp1	108.9	HC4E	-Me4 -Cp4	109.1
HC1B	-Me1 -HC1A	110.3	HC4F	-Me4 -Cp4	108.9
HC1C	-Me1 -HC1A	110.3	HC4B	-Me4 -HC4A	110.0
HC1C	-Me1 -HC1B	109.7	HC4C	-Me4 -HC4A	110.4
HC1E	-Me1 -HC1D	109.9	HC4C	-Me4 -HC4B	109.7
HC1F	-Me1 -HC1D	109.8	HC4E	-Me4 -HC4D	110.0

Table 2. Complete Bond Distances and Angles for
$Cp^*\{C_4H_4BN(CHMe_2)_2\}HfCl\cdot LiCl(Et_2O)_2$

			Angle(°)				Angle(°)
HC4F	-Me4	-HC4D	109.7	H7C	-C7	-H7A	110.2
HC4F	-Me4	-HC4E	110.3	H7C	-C7	-H7B	111.2
HC5A	-Me5	-Cp5	109.4	H8	-C8	-N	98.1
HC5B	-Me5	-Cp5	108.9	H8	-C8	-C9	99.0
HC5C	-Me5	-Cp5	108.7	H8	-C8	-C10	98.7
HC5D	-Me5	-Cp5	108.7	H9A	-C9	-C8	108.8
HC5E	-Me5	-Cp5	109.0	H9B	-C9	-C8	109.4
HC5F	-Me5	-Cp5	109.3	H9C	-C9	-C8	107.8
HC5B	-Me5	-HC5A	110.4	H9B	-C9	-H9A	111.4
HC5C	-Me5	-HC5A	110.0	H9C	-C9	-H9A	109.4
HC5C	-Me5	-HC5B	109.4	H9C	-C9	-H9B	109.9
HC5E	-Me5	-HC5D	109.4	H10A	-C10	-C8	108.7
HC5F	-Me5	-HC5D	109.9	H10B	-C10	-C8	108.6
HC5F	-Me5	-HC5E	110.5	H10C	-C10	-C8	109.6
H1	-C1	-C2	125.4	H10B	-C10	-H10A	109.4
H1	-C1	-B	125.3	H10C	-C10	-H10A	110.7
H2	-C2	-C1	124.4	H10C	-C10	-H10B	109.9
H2	-C2	-C3	124.8				
H3	-C3	-C2	125.7				
H3	-C3	-C4	125.3				
H4	-C4	-C3	126.2				
H4	-C4	-B	125.8				
H5	-C5	-N	98.8				
H5	-C5	-C6	100.1				
H5	-C5	-C7	99.1				
H6A	-C6	-C5	108.5				
H6B	-C6	-C5	109.1				
H6C	-C6	-C5	109.4				
H6B	-C6	-H6A	109.5				
H6C	-C6	-H6A	109.7				
H6C	-C6	-H6B	110.5				
H7A	-C7	-C5	108.0				
H7B	-C7	-C5	108.9				
H7C	-C7	-C5	109.4				
H7B	-C7	-H7A	109.2				

Appendix C: Crystal Structure Data for $[Cp^*\{C_4H_4BN(CHMe_2)_2\}HfCl_2Li]_2$

Table 1. Crystal and Intensity Collection Data for $[Cp^*\{C_4H_4BN(CHMe_2)_2\}HfCl_2Li]_2$

Formula: $C_{20}H_{33}BCl_2HfNLi$	Formula weight: 554.64
Crystal color: Red/orange dichroic	Habit: tabular
Crystal size: $0.18 \times 0.19 \times 0.31$ mm	$\rho_{calc} = 1.650$ g cm^{-3}
Crystal System: Monoclinic	Space group: $P2_1/c$ (#14)
$a = 8.606(4)$Å	
$b = 24.694(7)$Å	$\beta = 108.99(4)°$
$c = 11.111(5)$Å	
V = 2232.8(16)Å^3	$Z = 4$
Lattice parameters: 25 reflections,	$10 \leq \theta \leq 13$
$\mu = 49.07$ cm^{-1} ($\mu r_{max} = 1.00$)	Transmission coeff. $= 0.78 - 1.14$
CAD-4 diffractometer	ω scan
MoKα, $\lambda = 0.7107$Å	Graphite monochromator
2θ range: 3°–50°	$0 \leq h \leq 10, -29 \leq k \leq 29, -13 \leq l \leq 13$
T = 160K	
Number of reflections measured: 9460	Number of independent reflections: 3919
Number with $F_o^2 > 0$: 3735	Number with $F_o^2 > 3\sigma(F_o^2)$: 3295
Standard reflections: 3 every 1 hr	Linear decay: 1.5 %
GOF_{merge}: 1.32 for 3391 multiples	R_{merge}: 0.025 for 2422 duplicates
Number used in refinement: 3919	Criterion: All reflections used

Final R: 0.024 for 3295 reflections with $F_o^2 > 3\sigma(F_o^2)$

Final R: 0.030 for 3735 reflections with $F_o^2 > 0$

Final weighted R: 0.051

Final goodness of fit: 1.53 for 334 parameters and 3919 reflections

$(\Delta/\sigma)_{max}$ in final least squares cycle: 0.02

$\Delta\rho_{max}$ 1.02 eÅ^{-3}, $\Delta\rho_{min}$ -.94 eÅ^{-3} in final difference map

Table 2. Complete Bond Distances and Angles for $[Cp^*\{C_4H_4BN(CHMe_2)_2\}HfCl_2Li]_2$

	Distance(Å)		Distance(Å)
Hf –Cl1	2.510(1)	C9 –H9a	0.95(5)
Hf –Cl2	2.492(1)	C9 –H9b	1.01(5)
Hf –Cp*	2.207	C9 –H9c	1.00(5)
Hf –CpB	2.138	C10 –H10a	0.99(5)
Hf –B	2.654(5)	C10 –H10b	0.96(5)
Hf –C1	2.421(5)	C10 –H10c	0.97(5)
Hf –C2	2.372(5)	C11 –C12	1.416(6)
Hf –C3	2.417(5)	C11 –C15	1.404(6)
Hf –C4	2.501(5)	C11 –C16	1.511(8)
Hf –C11	2.534(5)	C12 –C13	1.408(6)
Hf –C12	2.475(5)	C12 –C17	1.509(8)
Hf –C13	2.509(5)	C13 –C14	1.426(6)
Hf –C14	2.503(4)	C13 –C18	1.488(8)
Hf –C15	2.542(5)	C14 –C15	1.407(6)
B –C1	1.524(7)	C14 –C19	1.511(8)
B –C4	1.513(7)	C15 –C20	1.496(7)
B –N	1.509(6)	C16 –H16a	0.99(6)
C1 –C2	1.434(7)	C16 –H16b	0.89(6)
C1 –H1	0.93(5)	C16 –H16c	0.95(6)
C2 –C3	1.411(7)	C17 –H17a	0.89(6)
C2 –H2	0.96(5)	C17 –H17b	0.98(6)
C3 –C4	1.437(7)	C17 –H17c	0.99(6)
C3 –H3	0.99(5)	C18 –H18a	0.86(6)
C4 –H4	0.97(4)	C18 –H18b	0.94(6)
N –C5	1.503(6)	C18 –H18c	1.04(6)
N –C8	1.499(5)	C19 –H19a	0.98(5)
C5 –C6	1.522(7)	C19 –H19b	0.86(6)
C5 –C7	1.522(7)	C19 –H19c	1.02(6)
C5 –H5	1.05(4)	C20 –H20a	0.94(5)
C6 –H6a	0.97(5)	C20 –H20b	1.17(5)
C6 –H6b	1.07(5)	C20 –H20c	0.95(5)
C6 –H6c	0.98(5)	Cl1 –Li	2.378(8)
C7 –H7a	0.96(5)	Cl1 –Li^i	2.693(8)
C7 –H7b	0.99(5)	Cl2 –Li^i	2.450(8)
C7 –H7c	0.87(5)	Li –N	2.068(8)
C8 –C9	1.527(7)	Li $\cdots$ Li^i	3.407(11)
C8 –C10	1.516(7)		
C8 –H8	1.01(4)		

Table 2. Complete Bond Distances and Angles for $[Cp^*\{C_4H_4BN(CHMe_2)_2\}HfCl_2Li]_2$

			Angle(°)				Angle(°)
Cp*	-Hf	-CpB	132.0	H7c	-C7	-C5	111.7(33)
Cp*	-Hf	-Cl1	107.8	H7b	-C7	-H7a	107.3(41)
Cp*	-Hf	-Cl2	107.9	H7c	-C7	-H7a	110.9(45)
CpB	-Hf	-Cl1	105.9	H7c	-C7	-H7b	109.1(44)
CpB	-Hf	-Cl2	106.5	C9	-C8	-N	114.6(4)
Cl1	-Hf	-Cl2	87.96(3)	C10	-C8	-N	110.4(4)
C4	-B	-C1	103.2(4)	H8	-C8	-N	106.4(25)
N	-B	-C1	129.5(4)	C10	-C8	-C9	108.8(4)
N	-B	-C4	127.2(4)	H8	-C8	-C9	109.2(25)
C2	-C1	-B	107.6(4)	H8	-C8	-C10	107.2(25)
H1	-C1	-B	133.3(28)	H9a	-C9	-C8	108.9(29)
H1	-C1	-C2	118.7(28)	H9b	-C9	-C8	111.9(27)
C3	-C2	-C1	110.6(4)	H9c	-C9	-C8	115.1(28)
H2	-C2	-C1	122.6(28)	H9b	-C9	-H9a	112.6(40)
H2	-C2	-C3	126.8(28)	H9c	-C9	-H9a	103.2(40)
C4	-C3	-C2	108.9(4)	H9c	-C9	-H9b	104.9(39)
H3	-C3	-C2	123.5(27)	H10a	-C10	-C8	110.9(27)
H3	-C3	-C4	127.5(27)	H10b	-C10	-C8	111.9(28)
C3	-C4	-B	108.8(4)	H10c	-C10	-C8	112.3(28)
H4	-C4	-B	129.6(26)	H10b	-C10	-H10a	107.2(39)
H4	-C4	-C3	121.2(26)	H10c	-C10	-H10a	109.4(38)
C5	-N	-B	114.2(3)	H10c	-C10	-H10b	104.8(39)
C8	-N	-B	113.0(3)	C15	-C11	-C12	107.9(4)
C8	-N	-C5	112.9(3)	C16	-C11	-C12	125.6(4)
C6	-C5	-N	115.4(4)	C16	-C11	-C15	126.1(4)
C7	-C5	-N	111.4(4)	C13	-C12	-C11	108.5(4)
H5	-C5	-N	107.9(24)	C17	-C12	-C11	125.7(5)
C7	-C5	-C6	110.0(4)	C17	-C12	-C13	125.4(5)
H5	-C5	-C6	105.7(24)	C14	-C13	-C12	107.0(4)
H5	-C5	-C7	105.8(24)	C18	-C13	-C12	126.8(4)
H6a	-C6	-C5	107.4(30)	C18	-C13	-C14	124.9(4)
H6b	-C6	-C5	111.8(26)	C15	-C14	-C13	108.3(4)
H6c	-C6	-C5	111.8(29)	C19	-C14	-C13	125.2(4)
H6b	-C6	-H6a	101.8(39)	C19	-C14	-C15	126.2(4)
H6c	-C6	-H6a	108.4(41)	C14	-C15	-C11	108.2(4)
H6c	-C6	-H6b	114.8(39)	C20	-C15	-C11	126.3(4)
H7a	-C7	-C5	108.1(30)	C20	-C15	-C14	125.1(4)
H7b	-C7	-C5	109.7(29)	H16a	-C16	-C11	111.7(32)

Table 2. Complete Bond Distances and Angles for $[Cp^*\{C_4H_4BN(CHMe_2)_2\}HfCl_2Li]_2$

			Angle(°)				Angle(°)
H16b	–C16	–C11	110.0(37)	B	–N	–Li	98.1(3)
H16c	–C16	–C11	107.0(35)	C5	–N	–Li	111.4(3)
H16b	–C16	–H16a	92.9(49)	C8	–N	–Li	105.9(3)
H16c	–C16	–H16a	107.9(47)				
H16c	–C16	–H16b	126.4(51)				
H17a	–C17	–C12	111.5(38)				
H17b	–C17	–C12	100.9(35)				
H17c	–C17	–C12	110.0(34)				
H17b	–C17	–H17a	100.0(51)				
H17c	–C17	–H17a	88.5(51)				
H17c	–C17	–H17b	142.2(49)				
H18a	–C18	–C13	114.6(39)				
H18b	–C18	–C13	114.7(37)				
H18c	–C18	–C13	112.8(32)				
H18b	–C18	–H18a	108.9(53)				
H18c	–C18	–H18a	108.0(50)				
H18c	–C18	–H18b	96.2(48)				
H19a	–C19	–C14	103.8(32)				
H19b	–C19	–C14	113.1(39)				
H19c	–C19	–C14	115.3(31)				
H19b	–C19	–H19a	101.5(50)				
H19c	–C19	–H19a	111.6(44)				
H19c	–C19	–H19b	110.4(50)				
H20a	–C20	–C15	113.2(33)				
H20b	–C20	–C15	113.1(26)				
H20c	–C20	–C15	109.5(32)				
H20b	–C20	–H20a	99.2(42)				
H20c	–C20	–H20a	105.5(46)				
H20c	–C20	–H20b	115.8(41)				
Li	–Cl1^i	–Hf^i	90.0(2)				
Li	–Cl1^i	–Li^i	84.2(3)				
Li	–Cl2^i	–Hf^i	96.3(2)				
Cl1^i	–Li	–Cl1	95.8(3)				
Cl2^i	–Li	–Cl1	111.1(3)				
N	–Li	–Cl1	98.1(3)				
Cl2^i	–Li	–Cl1^i	84.8(2)				
N	–Li	–Cl1^i	136.3(4)				
N	–Li	–Cl2^i	126.9(4)				

Symmetry code (i) $1-x, 1-y, 1-z$

Appendix D: Crystal Structure Data for $Cp^*\{C_4H_4BN(CHMe_2)_2\}Hf(\eta^3\text{-}C_3H_5)$

Table 1. Crystal and Intensity Collection Data for
$Cp^*\{C_4H_4BN(CHMe_2)_2\}Hf(\eta^3\text{-}C_3H_5)$

Formula: $C_{23}H_{38}BNHf$	Formula weight: 517.86
Crystal color: Dark blue	Habit: Prismatic
Crystal size: 0.12 × 0.23 × 0.44 mm	$\rho_{calc} = 1.506$ g cm^{-3}
Crystal System: Triclinic	Space group: $P\bar{1}$ (#2)
$a = 8.959(3)$Å	$\alpha = 88.55(4)°$
$b = 9.538(3)$Å	$\beta = 86.15(4)°$
$c = 13.911(7)$Å	$\gamma = 74.36(3)°$
V = 1142.1(8)Å^3	$Z = 2$
Lattice parameters: 25 reflections,	$11 \leq \theta \leq 13$
$\mu = 45.32$ cm^{-1} ($\mu r_{max} = 1.16$)	Transmission coeff. $= 0.67 - 1.22, \psi$-scan
CAD-4 diffractometer	ω scan
MoKα, $\lambda = 0.7107$Å	Graphite monochromator
2θ range: 2°–45°	$-9 \leq h \leq 9, -10 \leq k \leq -10, -15 \leq l \leq -15$
T = 295K	
Number of reflections measured: 6709	Number of independent reflections: 2978
Number with $F_o^2 > 0$: 2840	Number with $F_o^2 > 3\sigma(F_o^2)$: 2382
Standard reflections: 3 every 150 min	Linear decay: 4.3%
GOF_{merge}: 1.10 for 2975 multiples	R_{merge}: 0.034 for 2247 duplicates
Number used in refinement: 2978	Criterion: All reflections used

Final R: 0.031 for 2382 reflections with $F_o^2 > 3\sigma(F_o^2)$

Final R: 0.043 for 2840 reflections with $F_o^2 > 0$

Final weighted R: 0.057 for 2978 reflections

Final goodness of fit: 1.36 for 235 parameters and 2978 reflections

$(\Delta/\sigma)_{max}$ in final least squares cycle: 0.03

$\Delta\rho_{max}$: 1.5 eÅ^{-3}, $\Delta\rho_{min}$: -.69 eÅ^{-3} in final difference map

Table 2. Complete Bond Distances and Angles for
$Cp^*\{C_4H_4BN(CHMe_2)_2\}Hf(\eta^3\text{-}C_3H_5)$

	Distance(Å)		Distance(Å)
Hf –CpB	2.119	Me5 –HMe5b	0.948
Hf –Cp*	2.185	Me5 –HMe5c	0.947
Hf –C11	2.460(10)	B –C1	1.559(12)
Hf –C12	2.423(10)	B –C4	1.572(12)
Hf –C13	2.451(10)	B –N	1.414(10)
Hf –Cp1	2.479(7)	C1 –C2	1.411(11)
Hf –Cp2	2.466(7)	C1 –H1	0.950
Hf –Cp3	2.526(7)	C2 –C3	1.392(12)
Hf –Cp4	2.535(8)	C2 –H2	0.950
Hf –Cp5	2.454(7)	C3 –C4	1.424(11)
Hf –C1	2.428(8)	C3 –H3	0.950
Hf –C2	2.365(8)	C4 –H4	0.950
Hf –C3	2.374(8)	N –C5	1.454(10)
Hf –C4	2.421(8)	N –C8	1.487(10)
Hf –B	2.691(9)	C5 –C6	1.497(12)
Cp1 –Cp2	1.413(10)	C5 –C7	1.493(13)
Cp1 –Cp5	1.413(10)	C5 –H5	0.950
Cp1 –Me1	1.519(11)	C6 –H6a	0.950
Cp2 –Cp3	1.410(10)	C6 –H6b	0.950
Cp2 –Me2	1.507(11)	C6 –H6c	0.950
Cp3 –Cp4	1.395(10)	C7 –H7a	0.950
Cp3 –Me3	1.518(11)	C7 –H7b	0.950
Cp4 –Cp5	1.415(11)	C7 –H7c	0.950
Cp4 –Me4	1.516(11)	C8 –C9	1.537(13)
Cp5 –Me5	1.499(12)	C8 –C10	1.492(13)
Me1 –HMe1a	0.948	C8 –H8	0.950
Me1 –HMe1b	0.949	C9 –H9a	0.950
Me1 –HMe1c	0.948	C9 –H9b	0.950
Me2 –HMe2a	0.949	C9 –H9c	0.950
Me2 –HMe2b	0.948	C10 –H10a	0.950
Me2 –HMe2c	0.950	C10 –H10b	0.950
Me3 –HMe3a	0.948	C10 –H10c	0.950
Me3 –HMe3b	0.948	C11 –C12	1.364(14)
Me3 –HMe3c	0.948	C11 –H11a	0.950
Me4 –HMe4a	0.948	C11 –H11b	0.950
Me4 –HMe4b	0.949	C12 –C13	1.369(14)
Me4 –HMe4c	0.948	C12 –H12	0.950
Me5 –HMe5a	0.949	C13 –H13a	0.950

Table 2. Complete Bond Distances and Angles for
$Cp^*\{C_4H_4BN(CHMe_2)_2\}Hf(\eta^3\text{-}C_3H_5)$

Distance(Å)		Angle(°)			
C13 –H13b	0.950	C11	–Hf	–C12	32.4(3)
		C12	–Hf	–C13	32.6(3)
		C11	–Hf	–C13	58.9(3)
		Cp*	–Hf	–CpB	134.9
		Cp*	–Hf	–C11	113.0
		Cp*	–Hf	–C12	101.9
		Cp*	–Hf	–C13	112.6
		CpB	–Hf	–C11	105.4
		CpB	–Hf	–C12	123.2
		CpB	–Hf	–C13	106.9
		Cp5	–Cp1	–Cp2	108.1(6)
		Me1	–Cp1	–Cp2	124.4(7)
		Me1	–Cp1	–Cp5	126.9(7)
		Cp3	–Cp2	–Cp1	107.1(6)
		Me2	–Cp2	–Cp1	127.2(6)
		Me2	–Cp2	–Cp3	125.4(6)
		Cp4	–Cp3	–Cp2	109.1(6)
		Me3	–Cp3	–Cp2	124.1(6)
		Me3	–Cp3	–Cp4	126.3(7)
		Cp5	–Cp4	–Cp3	107.8(6)
		Me4	–Cp4	–Cp3	126.5(7)
		Me4	–Cp4	–Cp5	125.4(7)
		Cp4	–Cp5	–Cp1	107.7(6)
		Me5	–Cp5	–Cp1	125.9(7)
		Me5	–Cp5	–Cp4	125.9(7)
		HMe1a	–Me1	–Cp1	108.4
		HMe1b	–Me1	–Cp1	108.4
		HMe1c	–Me1	–Cp1	108.4
		HMe1b	–Me1	–HMe1a	110.4
		HMe1c	–Me1	–HMe1a	110.6
		HMe1c	–Me1	–HMe1b	110.5
		HMe2a	–Me2	–Cp2	108.4
		HMe2b	–Me2	–Cp2	108.4
		HMe2c	–Me2	–Cp2	108.5
		HMe2b	–Me2	–HMe2a	110.5
		HMe2c	–Me2	–HMe2a	110.4
		HMe2c	–Me2	–HMe2b	110.5
		HMe3a	–Me3	–Cp3	108.3

Table 2. Complete Bond Distances and Angles for
$Cp^*\{C_4H_4BN(CHMe_2)_2\}Hf(\eta^3\text{-}C_3H_5)$

			Angle(°)				Angle(°)
HMe3b	–Me3	–Cp3	108.4	C7	–C5	–C6	112.2(7)
HMe3c	–Me3	–Cp3	108.3	H5	–C5	–C6	105.6
HMe3b	–Me3	–HMe3a	110.6	H5	–C5	–C7	106.4
HMe3c	–Me3	–HMe3a	110.6	H6a	–C6	–C5	109.5
HMe3c	–Me3	–HMe3b	110.6	H6b	–C6	–C5	109.5
HMe4a	–Me4	–Cp4	108.4	H6c	–C6	–C5	109.5
HMe4b	–Me4	–Cp4	108.4	H6b	–C6	–H6a	109.5
HMe4c	–Me4	–Cp4	108.4	H6c	–C6	–H6a	109.5
HMe4b	–Me4	–HMe4a	110.6	H6c	–C6	–H6b	109.5
HMe4c	–Me4	–HMe4a	110.6	H7a	–C7	–C5	109.5
HMe4c	–Me4	–HMe4b	110.5	H7b	–C7	–C5	109.5
HMe5a	–Me5	–Cp5	108.3	H7c	–C7	–C5	109.5
HMe5b	–Me5	–Cp5	108.4	H7b	–C7	–H7a	109.5
HMe5c	–Me5	–Cp5	108.4	H7c	–C7	–H7a	109.5
HMe5b	–Me5	–HMe5a	110.5	H7c	–C7	–H7b	109.5
HMe5c	–Me5	–HMe5a	110.5	C9	–C8	–N	112.2(7)
HMe5c	–Me5	–HMe5b	110.7	C10	–C8	–N	114.3(7)
C4	–B	–C1	100.3(6)	H8	–C8	–N	105.7
N	–B	–C1	130.9(7)	C10	–C8	–C9	114.1(7)
N	–B	–C4	128.8(7)	H8	–C8	–C9	106.0
C2	–C1	–B	108.3(7)	H8	–C8	–C10	103.4
H1	–C1	–B	125.8	H9a	–C9	–C8	109.5
H1	–C1	–C2	125.8	H9b	–C9	–C8	109.5
C3	–C2	–C1	110.9(7)	H9c	–C9	–C8	109.5
H2	–C2	–C1	124.6	H9b	–C9	–H9a	109.5
H2	–C2	–C3	124.6	H9c	–C9	–H9a	109.5
C4	–C3	–C2	110.9(7)	H9c	–C9	–H9b	109.5
H3	–C3	–C2	124.5	H10a	–C10	–C8	109.5
H3	–C3	–C4	124.5	H10b	–C10	–C8	109.5
C3	–C4	–B	107.2(7)	H10c	–C10	–C8	109.5
H4	–C4	–B	126.4	H10b	–C10	–H10a	109.5
H4	–C4	–C3	126.4	H10c	–C10	–H10a	109.5
C5	–N	–B	124.3(6)	H10c	–C10	–H10b	109.5
C8	–N	–B	118.4(6)	Hf	–C11	–C12	72.3(6)
C8	–N	–C5	114.9(6)	H11a	–C11	–C12	120.0
C6	–C5	–N	114.2(7)	H11b	–C11	–C12	120.0
C7	–C5	–N	113.5(7)	H11b	–C11	–H11a	120.0
H5	–C5	–N	103.9	Hf	–C12	–C11	75.3(6)

Table 2. Complete Bond Distances and Angles for $Cp^*\{C_4H_4BN(CHMe_2)_2\}Hf(\eta^3\text{-}C_3H_5)$

			Angle(°)
Hf	-C12	-C13	74.8(6)
C13	-C12	-C11	124.1(9)
H12	-C12	-C11	117.9
H12	-C12	-C13	117.9
Hf	-C13	-C12	72.6(6)
H13a	-C13	-C12	120.0
H13b	-C13	-C12	120.0
H13b	-C13	-H13a	120.0

Appendix E:

Crystal Structure Data for $Cp^*\{C_4H_4BN(CHMe_2)_2\}Hf(\eta^3\text{-}C_3H_5)(CO)$

Table 1. Crystal and Intensity Collection Data for
$Cp^*\{C_4H_4BN(CHMe_2)_2\}Hf(\eta^3\text{-}C_3H_5)(CO)$

Formula: $C_{24}H_{38}BHfNO$ Formula Weight: 545.85

Color: Orange Habit: Flat Rod

Crystal size: 0.6 X 0.4 X 0.2 mm

Space group: $P2_1/n$ (#14)

a = 13.838(5)Å

b = 8.3770(10)Å $\beta = 99.36(3)^o$

c = 21.185(7)Å

V = 2423.1(12)Å^3

$\rho_{calc} = 1.496$ g/cm^{-1}

$\mu = 43.18$ cm^{-1}

CAD-4 diffractometer

$\lambda = 0.7107$Å Graphite monochrometer

2θ range: 3.2-50°

T = 296K

Number of independant reflections: 9165

Number with $F_o^2 > 0$: 5296

Number with $F_o^2 > 3\sigma$: 3580

Goodness of fit for merging data: 1.16

Final goodness of fit: 1.177 for 4243 reflections and 253 parameters

Final R-index: .1041

Final R-index : .0525 for reflections with $F_o^2 > 3\sigma(F_o^2)$

Table 2. Complete Bond Distances and Angles for
$Cp^*\{C_4H_4BN(CHMe_2)_2\}Hf(\eta^3\text{-}C_3H_5)(CO)$

Hf-C(54)	2.143(12)
Hf-C(22)	2.351(8)
Hf-C(21)	2.456(7)
Hf-C(23)	2.438(7)
Hf-C(52)	2.512(10)
Hf-C(2)	2.497(9)
Hf-C(53)	2.492(10)
Hf-C(51)	2.509(10)
Hf-C(4)	2.529(9)
Hf-C(1)	2.530(8)
Hf-C(3)	2.533(9)
Hf-C(24)	2.547(8)
B-N	1.435(13)
B-C(21)	1.548(13)
B-C(24)	1.584(14)
N-C(41)	1.440(11)
N-C(31)	1.488(12)
O(54)-C(54)	1.172(12)
C(1)-C(2)	1.426(12)
C(1)-C(5)	1.422(12)
C(1)-C(6)	1.511(12)
C(2)-C(3)	1.407(12)
C(2)-C(7)	1.505(12)
C(3)-C(4)	1.393(13)
C(3)-C(8)	1.509(12)
C(4)-C(5)	1.385(13)
C(4)-C(9)	1.522(12)
C(5)-C(10)	1.518(13)
C(21)-C(22)	1.439(11)
C(22)-C(23)	1.389(12)
C(23)-C(24)	1.418(11)
C(31)-C(32)	1.514(13)
C(31)-C(33)	1.536(13)
C(41)-C(42)	1.498(13)
C(41)-C(43)	1.536(14)
C(51)-C(52)	1.37(2)
C(52)-C(53)	1.379(14)

C(54)-Hf-C(22)	116.5(3)
C(54)-Hf-C(21)	83.2(3)
C(22)-Hf-C(21)	34.7(3)
C(54)-Hf-C(23)	115.6(3)
C(22)-Hf-C(23)	33.6(3)
C(21)-Hf-C(23)	56.7(3)
C(54)-Hf-C(52)	96.6(5)
C(22)-Hf-C(52)	113.4(4)
C(21)-Hf-C(52)	131.0(3)
C(23)-Hf-C(52)	80.5(4)
C(54)-Hf-C(2)	78.7(4)
C(22)-Hf-C(2)	100.3(3)
C(21)-Hf-C(2)	84.3(3)
C(23)-Hf-C(2)	133.9(3)
C(52)-Hf-C(2)	144.0(4)
C(54)-Hf-C(53)	69.6(4)
C(22)-Hf-C(53)	140.9(4)
C(21)-Hf-C(53)	138.5(3)
C(23)-Hf-C(53)	107.4(4)
C(52)-Hf-C(53)	32.0(3)
C(2)-Hf-C(53)	118.5(4)
C(54)-Hf-C(51)	127.4(4)
C(22)-Hf-C(51)	99.9(3)
C(21)-Hf-C(51)	131.8(3)

Table 2. Complete Bond Distances and Angles for
$Cp^*\{C_4H_4BN(CHMe_2)_2\}Hf(\eta^3\text{-}C_3H_5)(CO)$

C(23)-Hf-C(51)	75.5(3)
C(52)-Hf-C(51)	31.7(3)
C(2)-Hf-C(51)	132.4(3)
C(53)-Hf-C(51)	58.5(4)
C(54)-Hf-C(4)	127.9(3)
C(22)-Hf-C(4)	93.3(3)
C(21)-Hf-C(4)	107.9(3)
C(23)-Hf-C(4)	112.5(3)
C(52)-Hf-C(4)	110.1(4)
C(2)-Hf-C(4)	53.3(3)
C(53)-Hf-C(4)	113.5(4)
C(51)-Hf-C(4)	83.0(4)
C(54)-Hf-C(1)	75.7(4)
C(22)-Hf-C(1)	131.6(3)
C(21)-Hf-C(1)	116.1(3)
C(23)-Hf-C(1)	163.6(3)
C(52)-Hf-C(1)	111.1(4)
C(2)-Hf-C(1)	32.9(3)
C(53)-Hf-C(1)	87.5(4)
C(51)-Hf-C(1)	108.0(3)
C(4)-Hf-C(1)	53.3(3)
C(54)-Hf-C(3)	110.0(4)
C(22)-Hf-C(3)	78.9(3)
C(21)-Hf-C(3)	80.1(3)
C(23)-Hf-C(3)	109.7(3)
C(52)-Hf-C(3)	142.0(4)
C(2)-Hf-C(3)	32.5(3)
C(53)-Hf-C(3)	137.9(3)
C(51)-Hf-C(3)	113.4(4)
C(4)-Hf-C(3)	31.9(3)
C(1)-Hf-C(3)	54.0(3)
C(54)-Hf-C(24)	84.0(3)
C(22)-Hf-C(24)	56.2(3)
C(21)-Hf-C(24)	57.4(3)
C(23)-Hf-C(24)	33.0(3)
C(52)-Hf-C(24)	73.8(4)
C(2)-Hf-C(24)	139.6(3)
C(53)-Hf-C(24)	88.2(4)
C(51)-Hf-C(24)	86.7(3)
C(4)-Hf-C(24)	145.4(3)
C(1)-Hf-C(24)	159.5(3)
C(3)-Hf-C(24)	133.8(3)
N-B-C(21)	129.1(9)
N-B-C(24)	130.6(9)
C(21)-B-C(24)	100.1(8)
N-B-Hf	140.4(7)
C(21)-B-Hf	60.4(4)
C(24)-B-Hf	63.6(5)
B-N-C(41)	118.1(9)
B-N-C(31)	123.2(8)
C(41)-N-C(31)	117.5(9)
C(2)-C(1)-C(5)	106.5(9)
C(2)-C(1)-C(6)	126.6(10)
C(5)-C(1)-C(6)	125.9(9)
C(2)-C(1)-Hf	72.3(5)
C(5)-C(1)-Hf	74.3(5)
C(6)-C(1)-Hf	127.4(7)
C(3)-C(2)-C(1)	108.4(9)
C(3)-C(2)-C(7)	126.2(10)
C(1)-C(2)-C(7)	124.1(9)
C(3)-C(2)-Hf	75.2(5)
C(1)-C(2)-Hf	74.8(5)
C(7)-C(2)-Hf	126.6(7)
C(4)-C(3)-C(2)	107.2(9)
C(4)-C(3)-C(8)	126.9(10)
C(2)-C(3)-C(8)	125.0(10)

Table 2. Complete Bond Distances and Angles for
$Cp^*\{C_4H_4BN(CHMe_2)_2\}Hf(\eta^3\text{-}C_3H_5)(CO)$

C(4)-C(3)-Hf	73.9(6)
C(2)-C(3)-Hf	72.4(5)
C(8)-C(3)-Hf	127.6(6)
C(3)-C(4)-C(5)	110.0(9)
C(3)-C(4)-C(9)	124.8(11)
C(5)-C(4)-C(9)	124.8(10)
C(3)-C(4)-Hf	74.2(6)
C(5)-C(4)-Hf	74.8(6)
C(9)-C(4)-Hf	124.0(6)
C(4)-C(5)-C(1)	107.9(9)
C(4)-C(5)-C(10)	127.9(10)
C(1)-C(5)-C(10)	123.2(9)
C(4)-C(5)-Hf	73.5(5)
C(1)-C(5)-Hf	73.2(5)
C(10)-C(5)-Hf	128.2(6)
C(22)-C(21)-B	108.1(8)
C(22)-C(21)-Hf	68.7(4)
B-C(21)-Hf	86.4(5)
C(23)-C(22)-C(21)	110.6(8)
C(23)-C(22)-Hf	76.6(5)
C(21)-C(22)-Hf	76.6(4)
C(22)-C(23)-C(24)	110.9(9)
C(22)-C(23)-Hf	69.7(5)
C(24)-C(23)-Hf	77.7(5)
C(23)-C(24)-B	107.5(10)
C(23)-C(24)-Hf	69.3(4)
B-C(24)-Hf	82.5(5)
N-C(31)-C(32)	112.7(9)
N-C(31)-C(33)	111.9(9)
C(32)-C(31)-C(33)	112.7(9)
N-C(41)-C(42)	114.9(10)
N-C(41)-C(43)	112.8(9)
C(42)-C(41)-C(43)	110.1(10)
C(52)-C(51)-Hf	74.3(6)
C(51)-C(52)-C(53)	125.2(12)
C(51)-C(52)-Hf	74.0(6)
C(53)-C(52)-Hf	73.2(6)
C(52)-C(53)-Hf	74.8(6)
O(54)-C(54)-Hf	176.4(10)

Symmetry transformations used to generate equivalent atoms:

Appendix F: Crystal Structure Data for $Cp^*\{C_4H_4BNH(CHMe_2)_2\}HfCl_2$

Table 1. Crystal and Intensity Collection Data for $Cp^*\{C_4H_4BNH(CHMe_2)_2\}HfCl_2$

Formula: $C_{25}H_{32}BCl_2HfN$ Formula Weight: 498.65

Color: Orange Habit: Monoclinic Pyramid

Crystal size: 0.23 X 0.26 X 0.34 mm

Space group: $P2_1/n$ (#14)

a = 12.073(3)Å

b = 15.295(4)Å $\beta = 95.58(2)^o$

c = 12.314(3)Å

V = 2263.1(10)Å^3

$\rho_{calc} = 1.46$ g/cm^{-1}

$\mu = 48.02$ cm^{-1}

CAD-4 diffractometer

$\lambda = 0.7107$Å Graphite monochrometer

2θ range: 2-58°

T = 295K

Number of independant reflections: 6012

Number with $F_o^2 > 0$: 5363

Number with $F_o^2 > 3\sigma$: 3522

Goodness of fit for merging data: 1.06

Final goodness of fit: 1.15 for 6012 reflections and 226 parameters

Final R-index: .071

Final R-index : .037 for reflections with $F_o^2 > 3\sigma(F_o^2)$

Table 2. Complete Bond Distances and Angles for $Cp^*\{C_4H_4BNH(CHMe_2)_2\}HfCl_2$

	Distance(Å)		Distance(Å)
Hf –Cl1	2.428(2)	Me2 –HC2D	0.974
Hf –Cl2	2.458(2)	Me2 –HC2E	0.960
Hf –Cp*	2.221	Me2 –HC2F	0.974
Hf –CpB	2.169	Me3 –HC3A	0.979
Cp1 –Cp2	1.424(8)	Me3 –HC3B	0.967
Cp1 –Cp5	1.415(8)	Me3 –HC3C	0.969
Cp1 –Me1	1.505(8)	Me3 –HC3D	0.975
Cp2 –Cp3	1.406(8)	Me3 –HC3E	0.965
Cp2 –Me2	1.491(8)	Me3 –HC3F	0.975
Cp3 –Cp4	1.409(8)	Me4 –HC4A	0.967
Cp3 –Me3	1.484(9)	Me4 –HC4B	0.956
Cp4 –Cp5	1.408(8)	Me4 –HC4C	0.963
Cp4 –Me4	1.513(9)	Me4 –HC4D	0.968
Cp5 –Me5	1.507(9)	Me4 –HC4E	0.962
C1 –C2	1.424(9)	Me4 –HC4F	0.957
C1 –B	1.509(8)	Me5 –HC5A	0.971
C2 –C3	1.381(10)	Me5 –HC5B	0.963
C3 –C4	1.418(9)	Me5 –HC5C	0.948
C4 –B	1.476(9)	C1 –H1	0.950
B –N	1.580(8)	C2 –H2	0.953
N –C5	1.509(9)	C3 –H3	0.951
N –C8	1.526(8)	C4 –H4	0.951
C5 –C6	1.515(11)	N –HN	0.951
C5 –C7	1.500(11)	C5 –H5	0.948
C8 –C9	1.516(10)	C6 –H6A	0.947
C8 –C10	1.496(9)	C6 –H6B	0.951
Me1 –HC1A	0.975	C6 –H6C	0.950
Me1 –HC1B	0.950	C7 –H7A	0.951
Me1 –HC1C	0.963	C7 –H7B	0.948
Me1 –HC1D	0.975	C7 –H7C	0.953
Me1 –HC1E	0.962	C8 –H8	0.951
Me1 –HC1F	0.951	C9 –H9A	0.950
Me2 –HC2A	0.965	C9 –H9B	0.954
Me2 –HC2B	0.965	C9 –H9C	0.946
Me2 –HC2C	0.979	C10 –H10A	0.949

Table 2. Complete Bond Distances and Angles for $Cp^*\{C_4H_4BNH(CHMe_2)_2\}HfCl_2$

Distance(Å)		Angle(°)	
C10 –H10B	0.945	Cl1 –Hf –Cl2	94.1(1)
C10 –H10C	0.953	Cp* –Hf –CpB	132.6
		Cp* –Hf –Cl1	106.4
		Cp* –Hf –Cl2	105.3
		CpB –Hf –Cl1	107.1
		CpB –Hf –Cl2	104.7
		Cp5 –Cp1 –Cp2	106.9(5)
		Me1 –Cp1 –Cp2	127.3(5)
		Me1 –Cp1 –Cp5	124.9(5)
		Cp3 –Cp2 –Cp1	108.3(5)
		Me2 –Cp2 –Cp1	125.5(5)
		Me2 –Cp2 –Cp3	125.3(5)
		Cp4 –Cp3 –Cp2	108.2(5)
		Me3 –Cp3 –Cp2	126.4(5)
		Me3 –Cp3 –Cp4	125.0(5)
		Cp5 –Cp4 –Cp3	107.9(5)
		Me4 –Cp4 –Cp3	126.8(5)
		Me4 –Cp4 –Cp5	125.2(5)
		Cp4 –Cp5 –Cp1	108.6(5)
		Me5 –Cp5 –Cp1	125.8(5)
		Me5 –Cp5 –Cp4	125.0(5)
		B –C1 –C2	105.1(5)
		C3 –C2 –C1	111.1(6)
		C4 –C3 –C2	110.4(6)
		B –C4 –C3	106.8(5)
		C4 –B –C1	106.2(5)
		N –B –C1	125.9(5)
		N –B –C4	127.3(5)
		C5 –N –B	116.7(5)
		C8 –N –B	112.9(4)
		C8 –N –C5	114.3(5)
		C6 –C5 –N	113.5(6)
		C7 –C5 –N	110.2(6)
		C7 –C5 –C6	111.3(6)
		C9 –C8 –N	113.0(5)

Table 2. Complete Bond Distances and Angles for $Cp^*\{C_4H_4BNH(CHMe_2)_2\}HfCl_2$

			Angle(°)				Angle(°)
C10	-C8	-N	111.6(5)	HC3E	-Me3	-HC3D	106.9
C10	-C8	-C9	113.7(5)	HC3F	-Me3	-HC3D	106.1
HC1A	-Me1	-Cp1	110.8	HC3F	-Me3	-HC3E	107.0
HC1B	-Me1	-Cp1	110.9	HC4A	-Me4	-Cp4	110.5
HC1C	-Me1	-Cp1	110.6	HC4B	-Me4	-Cp4	110.7
HC1D	-Me1	-Cp1	110.7	HC4C	-Me4	-Cp4	110.9
HC1E	-Me1	-Cp1	110.9	HC4D	-Me4	-Cp4	110.8
HC1F	-Me1	-Cp1	110.8	HC4E	-Me4	-Cp4	110.5
HC1B	-Me1	-HC1A	108.1	HC4F	-Me4	-Cp4	110.9
HC1C	-Me1	-HC1A	107.1	HC4B	-Me4	-HC4A	108.3
HC1C	-Me1	-HC1B	109.2	HC4C	-Me4	-HC4A	107.7
HC1E	-Me1	-HC1D	107.1	HC4C	-Me4	-HC4B	108.6
HC1F	-Me1	-HC1D	108.0	HC4E	-Me4	-HC4D	107.7
HC1F	-Me1	-HC1E	109.2	HC4F	-Me4	-HC4D	108.2
HC2A	-Me2	-Cp2	111.8	HC4F	-Me4	-HC4E	108.7
HC2B	-Me2	-Cp2	112.5	HC5A	-Me5	-Cp5	109.9
HC2C	-Me2	-Cp2	111.3	HC5B	-Me5	-Cp5	110.4
HC2D	-Me2	-Cp2	111.2	HC5C	-Me5	-Cp5	111.0
HC2E	-Me2	-Cp2	112.4	HC5B	-Me5	-HC5A	107.4
HC2F	-Me2	-Cp2	111.9	HC5C	-Me5	-HC5A	108.6
HC2B	-Me2	-HC2A	107.8	HC5C	-Me5	-HC5B	109.3
HC2C	-Me2	-HC2A	106.6	H1	-C1	-C2	127.6
HC2C	-Me2	-HC2B	106.6	H1	-C1	-B	127.4
HC2E	-Me2	-HC2D	107.3	H2	-C2	-C1	124.7
HC2F	-Me2	-HC2D	106.2	H2	-C2	-C3	124.2
HC2F	-Me2	-HC2E	107.4	H3	-C3	-C2	125.3
HC3A	-Me3	-Cp3	111.4	H3	-C3	-C4	124.3
HC3B	-Me3	-Cp3	112.5	H4	-C4	-C3	126.8
HC3C	-Me3	-Cp3	112.5	H4	-C4	-B	126.4
HC3D	-Me3	-Cp3	111.6	HN	-N	-B	103.1
HC3E	-Me3	-Cp3	112.9	HN	-N	-C5	101.3
HC3F	-Me3	-Cp3	111.9	HN	-N	-C8	106.5
HC3B	-Me3	-HC3A	106.5	H5	-C5	-N	106.5
HC3C	-Me3	-HC3A	106.3	H5	-C5	-C6	105.7
HC3C	-Me3	-HC3B	107.2	H5	-C5	-C7	109.3

Table 2. Complete Bond Distances and Angles for $Cp^*\{C_4H_4BNH(CHMe_2)_2\}HfCl_2$

Angle(°)

H6A	-C6	-C5	109.5
H6B	-C6	-C5	109.2
H6C	-C6	-C5	109.4
H6B	-C6	-H6A	109.6
H6C	-C6	-H6A	109.7
H6C	-C6	-H6B	109.3
H7A	-C7	-C5	109.5
H7B	-C7	-C5	109.8
H7C	-C7	-C5	109.3
H7B	-C7	-H7A	109.6
H7C	-C7	-H7A	109.2
H7C	-C7	-H7B	109.4
H8	-C8	-N	106.7
H8	-C8	-C9	104.9
H8	-C8	-C10	106.2
H9A	-C9	-C8	109.4
H9B	-C9	-C8	109.2
H9C	-C9	-C8	109.7
H9B	-C9	-H9A	109.2
H9C	-C9	-H9A	109.9
H9C	-C9	-H9B	109.5
H10A	-C10	-C8	109.4
H10B	-C10	-C8	109.5
H10C	-C10	-C8	109.0
H10B	-C10	-H10A	110.0
H10C	-C10	-H10A	109.2
H10C	-C10	-H10B	109.6

Appendix G: Crystal Structure Data for $Cp^*\{C_4H_4BNH(CHMe_2)_2\}HfCl(CCTMS)$

Formula: $C_{25}H_{43}BClHfNSi$	Formula weight: 610.46
Crystal color: Yellow	Habit: Lozenge
Crystal size: 0.30 × 0.37 × 0.63 mm	$\rho_{calc} = 1.393$ g cm^{-3}
Crystal System: Monoclinic	Space group: $P2_1/n$ (#14)
$a = 8.237(2)$Å	
$b = 12.210(3)$Å	$\beta = 97.68(2)°$
$c = 29.204(5)$Å	
V = 2910.8(11)Å^3	$Z = 4$
Lattice parameters: 25 reflections,	$12 \leq \theta \leq 18$
$\mu = 36.96$ cm^{-1} ($\mu r_{max} = 1.46$)	Transmission coeff. = 0.90 − 1.10, ψ-scan
CAD-4 diffractometer	ω scan
MoKα, $\lambda = 0.7107$Å	Graphite monochromator
2θ range: 3°–50°	$-9 \leq h \leq 9$, $0 \leq k \leq 14$, $-34 \leq l \leq -34$
T = 295K	
Number of reflections measured: 11116	Number of independent reflections: 5128
Number with $F_o^2 > 0$: 4717	Number with $F_o^2 > 3\sigma(F_o^2)$: 3620
Standard reflections: 3 every 75 min	Linear decay: 8.9%
GOF_{merge}: 1.17 for 5117 multiples	R_{merge}: 0.031 for 4339 duplicates
Number used in refinement: 5128	Criterion: All reflections used

Final R: 0.030 for 3620 reflections with $F_o^2 > 3\sigma(F_o^2)$

Final R: 0.048 for 4717 reflections with $F_o^2 > 0$

Final weighted R: 0.062 for 5128 reflections

Final goodness of fit: 1.42 for 271 parameters and 5128 reflections

$(\Delta/\sigma)_{max}$ in final least squares cycle: 0.06

$\Delta\rho_{max}$: 0.63 eÅ^{-3}, $\Delta\rho_{min}$: -0.51 eÅ^{-3} in final difference map

Table 2. Complete Bond Distances and Angles for $Cp^*\{C_4H_4BNH(CHMe_2)_2\}HfCl(CCTMS)$

	Distance(Å)		Distance(Å)
Hf –C11	2.237(6)	Me5 –HM5c	0.948
Hf –Cl	2.432(2)	B –C1	1.482(8)
Hf –C*	2.166	B –C4	1.506(8)
Hf –Cp*	2.214	B –N	1.571(8)
Hf –Cp1	2.495(6)	C1 –C2	1.426(7)
Hf –Cp2	2.508(5)	C1 –H1	0.950
Hf –Cp3	2.511(5)	C2 –C3	1.393(8)
Hf –Cp4	2.540(6)	C2 –H2	0.950
Hf –Cp5	2.531(5)	C3 –C4	1.413(8)
Hf –C1	2.472(5)	C3 –H3	0.950
Hf –C2	2.388(6)	C4 –H4	0.950
Hf –C3	2.446(6)	N –C5	1.522(8)
Hf –C4	2.519(5)	N –C8	1.522(7)
Hf –B	2.620(7)	N –HN	0.950
Cp1 –Cp2	1.413(8)	C5 –C6	1.500(9)
Cp1 –Cp5	1.405(8)	C5 –C7	1.534(10)
Cp1 –Me1	1.504(9)	C5 –H5	0.950
Cp2 –Cp3	1.391(8)	C6 –H6a	0.950
Cp2 –Me2	1.512(8)	C6 –H6b	0.950
Cp3 –Cp4	1.439(8)	C6 –H6c	0.950
Cp3 –Me3	1.504(9)	C7 –H7a	0.950
Cp4 –Cp5	1.395(8)	C7 –H7b	0.950
Cp4 –Me4	1.509(9)	C7 –H7c	0.950
Cp5 –Me5	1.515(8)	C8 –C9	1.514(9)
Me1 –HM1a	0.950	C8 –C10	1.494(10)
Me1 –HM1b	0.947	C8 –H8	0.950
Me1 –HM1c	0.949	C9 –H9a	0.950
Me2 –HM2a	0.949	C9 –H9b	0.950
Me2 –HM2b	0.949	C9 –H9c	0.950
Me2 –HM2c	0.948	C10 –H10a	0.950
Me3 –HM3a	0.947	C10 –H10b	0.950
Me3 –HM3b	0.949	C10 –H10c	0.950
Me3 –HM3c	0.949	C11 –C12	1.196(8)
Me4 –HM4a	0.951	C12 –Si	1.840(7)
Me4 –HM4b	0.951	Si –C13	1.866(10)
Me4 –HM4c	0.944	Si –C14	1.852(9)
Me5 –HM5a	0.949	Si –C15	1.856(10)
Me5 –HM5b	0.947	C13 –H13a	0.950

Table 2. Complete Bond Distances and Angles for $Cp^*\{C_4H_4BNH(CHMe_2)_2\}HfCl(CCTMS)$

Distance(Å)		Angle(°)			
C13 –H13b	0.950	Cl	–Hf	–C11	97.5(1)
C13 –H13c	0.950	Cp*	–Hf	–C*	133.7
C14 –H14a	0.950	Cp*	–Hf	–Cl	107.3
C14 –H14b	0.950	Cp*	–Hf	–C11	104.5
C14 –H14c	0.950	C*	–Hf	–Cl	106.9
C15 –H15a	0.950	C*	–Hf	–C11	101.0
C15 –H15b	0.950	Cp5	–Cp1	–Cp2	107.4(5)
C15 –H15c	0.950	Me1	–Cp1	–Cp2	126.3(5)
		Me1	–Cp1	–Cp5	126.0(5)
		Cp3	–Cp2	–Cp1	108.8(5)
		Me2	–Cp2	–Cp1	124.5(5)
		Me2	–Cp2	–Cp3	125.9(5)
		Cp4	–Cp3	–Cp2	107.5(5)
		Me3	–Cp3	–Cp2	127.8(5)
		Me3	–Cp3	–Cp4	124.4(5)
		Cp5	–Cp4	–Cp3	107.3(5)
		Me4	–Cp4	–Cp3	126.1(5)
		Me4	–Cp4	–Cp5	126.1(5)
		Cp4	–Cp5	–Cp1	108.9(5)
		Me5	–Cp5	–Cp1	126.1(5)
		Me5	–Cp5	–Cp4	124.5(5)
		HM1a	–Me1	–Cp1	108.3
		HM1b	–Me1	–Cp1	108.5
		HM1c	–Me1	–Cp1	108.4
		HM1b	–Me1	–HM1a	110.6
		HM1c	–Me1	–HM1a	110.3
		HM1c	–Me1	–HM1b	110.6
		HM2a	–Me2	–Cp2	108.4
		HM2b	–Me2	–Cp2	108.4
		HM2c	–Me2	–Cp2	108.4
		HM2b	–Me2	–HM2a	110.5
		HM2c	–Me2	–HM2a	110.5
		HM2c	–Me2	–HM2b	110.5
		HM3a	–Me3	–Cp3	108.4
		HM3b	–Me3	–Cp3	108.3
		HM3c	–Me3	–Cp3	108.4
		HM3b	–Me3	–HM3a	110.6
		HM3c	–Me3	–HM3a	110.6

Table 2. Complete Bond Distances and Angles for $Cp^*\{C_4H_4BNH(CHMe_2)_2\}HfCl(CCTMS)$

			Angle(°)				Angle(°)
HM3c	-Me3	-HM3b	110.4	C7	-C5	-C6	111.8(6)
HM4a	-Me4	-Cp4	108.4	H5	-C5	-C6	105.8
HM4b	-Me4	-Cp4	108.4	H5	-C5	-C7	108.3
HM4c	-Me4	-Cp4	108.6	H6a	-C6	-C5	109.5
HM4b	-Me4	-HM4a	110.1	H6b	-C6	-C5	109.5
HM4c	-Me4	-HM4a	110.5	H6c	-C6	-C5	109.5
HM4c	-Me4	-HM4b	110.8	H6b	-C6	-H6a	109.5
HM5a	-Me5	-Cp5	108.4	H6c	-C6	-H6a	109.5
HM5b	-Me5	-Cp5	108.4	H6c	-C6	-H6b	109.5
HM5c	-Me5	-Cp5	108.4	H7a	-C7	-C5	109.5
HM5b	-Me5	-HM5a	110.6	H7b	-C7	-C5	109.5
HM5c	-Me5	-HM5a	110.5	H7c	-C7	-C5	109.5
HM5c	-Me5	-HM5b	110.5	H7b	-C7	-H7a	109.5
C4	-B	-C1	104.9(5)	H7c	-C7	-H7a	109.5
N	-B	-C1	127.1(5)	H7c	-C7	-H7b	109.5
N	-B	-C4	127.8(5)	C9	-C8	-N	111.7(5)
Hf	-B	-N	123.4(4)	C10	-C8	-N	109.9(5)
C2	-C1	-B	107.2(5)	H8	-C8	-N	108.0
H1	-C1	-B	126.4	C10	-C8	-C9	110.4(5)
H1	-C1	-C2	126.4	H8	-C8	-C9	107.4
C3	-C2	-C1	110.3(5)	H8	-C8	-C10	109.4
H2	-C2	-C1	124.8	H9a	-C9	-C8	109.5
H2	-C2	-C3	124.8	H9b	-C9	-C8	109.5
C4	-C3	-C2	109.8(5)	H9c	-C9	-C8	109.5
H3	-C3	-C2	125.1	H9b	-C9	-H9a	109.5
H3	-C3	-C4	125.1	H9c	-C9	-H9a	109.5
C3	-C4	-B	107.3(5)	H9c	-C9	-H9b	109.5
H4	-C4	-B	126.3	H10a	-C10	-C8	109.5
H4	-C4	-C3	126.3	H10b	-C10	-C8	109.5
C5	-N	-B	112.7(4)	H10c	-C10	-C8	109.5
C8	-N	-B	117.6(4)	H10b	-C10	-H10a	109.5
HN	-N	-B	102.2	H10c	-C10	-H10a	109.5
C8	-N	-C5	113.5(4)	H10c	-C10	-H10b	109.5
HN	-N	-C5	107.7	Hf	-C11	-C12	173.9(5)
HN	-N	-C8	101.2	Si	-C12	-C11	167.6(6)
C6	-C5	-N	112.8(5)	C13	-Si	-C12	108.5(4)
C7	-C5	-N	110.6(5)	C14	-Si	-C12	111.6(4)
H5	-C5	-N	107.2	C15	-Si	-C12	106.8(4)

Table 2. Complete Bond Distances and Angles for $Cp^*\{C_4H_4BNH(CHMe_2)_2\}HfCl(CCTMS)$

Angle(°)

C14	–Si	–C13	108.7(4)
C15	–Si	–C13	110.9(4)
C15	–Si	–C14	110.3(4)
H13a	–C13	–Si	109.5
H13b	–C13	–Si	109.5
H13c	–C13	–Si	109.5
H13b	–C13	–H13a	109.5
H13c	–C13	–H13a	109.5
H13c	–C13	–H13b	109.5
H14a	–C14	–Si	109.5
H14b	–C14	–Si	109.5
H14c	–C14	–Si	109.5
H14b	–C14	–H14a	109.5
H14c	–C14	–H14a	109.5
H14c	–C14	–H14b	109.5
H15a	–C15	–Si	109.5
H15b	–C15	–Si	109.5
H15c	–C15	–Si	109.5
H15b	–C15	–H15a	109.5
H15c	–C15	–H15a	109.5
H15c	–C15	–H15b	109.5

Appendix H: $Cp^*\{C_4H_3MeBNH(CHMe_2)_2\}HfClI$

Table 1. Crystal and Intensity Collection Data for $Cp^*\{C_4H_3MeBNH(CHMe_2)_2\}HfClI$

Formula: $C_{21}H_{36}BClHfIN$ Formula Weight: 654.18

Color: red-orange Habit: Prismatic

Crystal size: 0.22 X 0.25 X 0.26 mm

Space group: $P2_1/c$ (#14)

a = 15.396(7)Å

b = 14.432(5)Å $\beta = 108.92(3)^o$

c = 11.643(4)Å

V = 2447(2)Å^3

$\rho_{calc} = 1.78$ g/cm^{-1}

$\mu = 55.90$ cm^{-1}

CAD-4 diffractometer

$\lambda = 0.7107$Å Graphite monochrometer

2θ range: 2-45^o

T = 295K

Number of independant reflections: 3193

Number with $F_o^2 > 0$: 2954

Number with $F_o^2 > 3\sigma$: 1918

Goodness of fit for merging data: 1.00

Final goodness of fit: 1.80 for 3193 reflections and 237 parameters

Final R-index: .103

Final R-index : .061 for reflections with $F_o^2 > 3\sigma(F_o^2)$

Table 2. Complete Bond Distances and Angles for $Cp^*\{C_4H_3MeBNH(CHMe_2)_2\}HfClI$

		Distance(Å)			Distance(Å)
Hf	–Cp*	2.204	Me5	–HMe5c	0.946
Hf	–CpB	2.261	N	–B	1.50(2)
Hf	–I/Cl1	2.769(2)	N	–C5	1.41(4)
Hf	–I/Cl2	2.740(2)	N	–C8	1.47(4)
Hf	–Cp1	2.507(18)	N	–HN	0.952
Hf	–Cp2	2.497(17)	B	–C1	1.52(3)
Hf	–Cp3	2.483(17)	B	–C4	1.59(3)
Hf	–Cp4	2.484(20)	C1	–C2	1.44(3)
Hf	–Cp5	2.504(19)	C1	–C11	1.57(2)
Hf	–C1	2.572(17)	C2	–C3	1.18(3)
Hf	–C2	2.414(24)	C2	–HC2	0.950
Hf	–C3	2.419(18)	C3	–C4	1.14(3)
Hf	–C4	2.580(22)	C3	–HC3	0.948
Hf	–B	2.722(20)	C4	–HC4	0.950
Cp1	–Cp2	1.37(3)	C5	–C6	1.37(5)
Cp1	–Cp5	1.30(3)	C5	–C7	1.35(6)
Cp1	–Me1	1.53(3)	C5	–HC5	0.942
Cp2	–Cp3	1.38(2)	C6	–H6a	0.947
Cp2	–Me2	1.51(3)	C6	–H6b	0.953
Cp3	–Cp4	1.42(3)	C6	–H6c	0.952
Cp3	–Me3	1.48(3)	C7	–H7a	0.919
Cp4	–Cp5	1.41(3)	C7	–H7b	0.959
Cp4	–Me4	1.51(3)	C7	–H7c	0.990
Cp5	–Me5	1.57(3)	C8	–C9	1.32(5)
Me1	–HMe1a	0.949	C8	–C10	1.53(4)
Me1	–HMe1b	0.949	C8	–HC8	1.086
Me1	–HMe1c	0.948	C9	–H9a	0.938
Me2	–HMe2a	0.951	C9	–H9b	0.986
Me2	–HMe2b	0.947	C9	–H9c	0.950
Me2	–HMe2c	0.947	C10	–H10a	0.954
Me3	–HMe3a	0.944	C10	–H10b	0.938
Me3	–HMe3b	0.953	C10	–H10c	0.950
Me3	–HMe3c	0.951	C11	–H11a	0.948
Me4	–HMe4a	0.949	C11	–H11b	0.950
Me4	–HMe4b	0.952	C11	–H11c	0.951
Me4	–HMe4c	0.949			
Me5	–HMe5a	0.949			
Me5	–HMe5b	0.951			

Table 2. Complete Bond Distances and Angles for
$Cp^*\{C_4H_3MeBNH(CHMe_2)_2\}HfClI$

			Angle(°)				Angle(°)
Cp*	-Hf	-CpB	131.3	HMe3c	-Me3	-HMe3b	109.8
Cp*	-Hf	-I/Cl1	109.7	HMe4a	-Me4	-Cp4	108.8
Cp*	-Hf	-I/Cl2	107.2	HMe4b	-Me4	-Cp4	108.6
CpB	-Hf	-I/Cl1	103.4	HMe4c	-Me4	-Cp4	108.7
CpB	-Hf	-I/Cl2	104.6	HMe4b	-Me4	-HMe4a	110.1
I/Cl1	-Hf	-I/Cl2	94.7(1)	HMe4c	-Me4	-HMe4a	110.4
Cp5	-Cp1	-Cp2	108.6(17)	HMe4c	-Me4	-HMe4b	110.2
Me1	-Cp1	-Cp2	124.8(16)	HMe5a	-Me5	-Cp5	108.5
Me1	-Cp1	-Cp5	126.4(17)	HMe5b	-Me5	-Cp5	108.3
Cp3	-Cp2	-Cp1	108.8(16)	HMe5c	-Me5	-Cp5	108.5
Me2	-Cp2	-Cp1	125.6(16)	HMe5b	-Me5	-HMe5a	110.2
Me2	-Cp2	-Cp3	125.0(16)	HMe5c	-Me5	-HMe5a	110.7
Cp4	-Cp3	-Cp2	107.2(16)	HMe5c	-Me5	-HMe5b	110.5
Me3	-Cp3	-Cp2	127.2(17)	C5	-N	-B	123.6(18)
Me3	-Cp3	-Cp4	124.4(17)	C8	-N	-B	116.9(17)
Cp5	-Cp4	-Cp3	104.2(16)	HN	-N	-B	80.7
Me4	-Cp4	-Cp3	125.0(18)	C8	-N	-C5	112.5(21)
Me4	-Cp4	-Cp5	129.9(19)	HN	-N	-C5	110.4
Cp4	-Cp5	-Cp1	111.2(17)	HN	-N	-C8	105.9
Me5	-Cp5	-Cp1	125.7(18)	C1	-B	-N	133.3(16)
Me5	-Cp5	-Cp4	122.4(17)	C4	-B	-N	131.7(17)
HMe1a	-Me1	-Cp1	108.5	C4	-B	-C1	94.5(15)
HMe1b	-Me1	-Cp1	108.5	C2	-C1	-B	99.4(16)
HMe1c	-Me1	-Cp1	108.3	C11	-C1	-B	130.8(15)
HMe1b	-Me1	-HMe1a	110.4	C11	-C1	-C2	129.6(16)
HMe1c	-Me1	-HMe1a	110.5	C3	-C2	-C1	119.8(21)
HMe1c	-Me1	-HMe1b	110.5	HC2	-C2	-C1	120.1
HMe2a	-Me2	-Cp2	108.3	HC2	-C2	-C3	120.1
HMe2b	-Me2	-Cp2	108.4	C4	-C3	-C2	108.9(22)
HMe2c	-Me2	-Cp2	108.5	HC3	-C3	-C2	125.4
HMe2b	-Me2	-HMe2a	110.4	HC3	-C3	-C4	125.7
HMe2c	-Me2	-HMe2a	110.4	C3	-C4	-B	116.4(20)
HMe2c	-Me2	-HMe2b	110.8	HC4	-C4	-B	121.7
HMe3a	-Me3	-Cp3	108.8	HC4	-C4	-C3	121.8
HMe3b	-Me3	-Cp3	108.5	C6	-C5	-N	118.1(29)
HMe3c	-Me3	-Cp3	108.5	C7	-C5	-N	117.6(33)
HMe3b	-Me3	-HMe3a	110.5	HC5	-C5	-N	120.1
HMe3c	-Me3	-HMe3a	110.7	C7	-C5	-C6	122.6(36)

Table 2. Complete Bond Distances and Angles for $Cp^*\{C_4H_3MeBNH(CHMe_2)_2\}HfClI$

Angle(°)

HC5	-C5	-C6	75.8
HC5	-C5	-C7	88.3
H6a	-C6	-C5	109.2
H6b	-C6	-C5	108.5
H6c	-C6	-C5	108.8
H6b	-C6	-H6a	110.2
H6c	-C6	-H6a	110.4
H6c	-C6	-H6b	109.8
H7a	-C7	-C5	112.3
H7b	-C7	-C5	109.5
H7c	-C7	-C5	107.1
H7b	-C7	-H7a	112.2
H7c	-C7	-H7a	109.4
H7c	-C7	-H7b	106.2
C9	-C8	-N	117.8(27)
C10	-C8	-N	115.2(24)
HC8	-C8	-N	120.3
C10	-C8	-C9	125.9(29)
HC8	-C8	-C9	79.8
HC8	-C8	-C10	65.3
H9a	-C9	-C8	104.3
H9b	-C9	-C8	112.6
H9c	-C9	-C8	113.0
H9b	-C9	-H9a	108.2
H9c	-C9	-H9a	111.3
H9c	-C9	-H9b	107.3
H10a	-C10	-C8	113.8
H10b	-C10	-C8	107.1
H10c	-C10	-C8	103.4
H10b	-C10	-H10a	111.0
H10c	-C10	-H10a	109.9
H10c	-C10	-H10b	111.4
H11a	-C11	-C1	108.7
H11b	-C11	-C1	108.5
H11c	-C11	-C1	108.5
H11b	-C11	-H11a	110.5
H11c	-C11	-H11a	110.4
H11c	-C11	-H11b	110.2